eLife

Reviewed Preprint
v2 • March 20, 2025
Revised by authors

Reviewed Preprint
v1 • November 18, 2024

Neuroscience

An antisense oligonucleotide-based strategy to ameliorate cognitive dysfunction in the 22q11.2 Deletion Syndrome

Pratibha Thakur, Martin Lackinger, Anastasia Diamantopoulou, Sneha Rao, Yijing Chen, Khakima Khalizova, Annie Ferng, Curt Mazur, Holly Kordasiewicz, Robert J Shprintzen, Sander Markx, Bin Xu, Joseph A Gogos

Mortimer B. Zuckerman Mind Brain and Behavior Institute, Columbia University, New York, United States • Stavros Niarchos Foundation Center for Precision Psychiatry and Mental Health, Columbia University, New York, United States • Department of Genetics and Development, Columbia University Irvine Medical Center, New York, United States • Ionis Pharmaceuticals, Inc., Carlsbad, United States • The Virtual Center for Velo-Cardio-Facial-Syndrome, Inc • Department of Psychiatry, Vagelos College of Physicians & Surgeons, Columbia University, New York, United States • Department of Physiology and Cellular Biophysics, College of Physicians and Surgeons, Columbia University, New York, United States • Department of Neuroscience, Columbia University, New York, United States

eLife Assessment

This is an **important** study that establishes how anti-sense oligonucleotides degrading a specific target protein called EMC10 can rescue neuronal function in models of chromosome 22.11.2 deletions. The authors use human iPSC-derived neurons and a mouse model to provide **compelling** data for the rescue of cellular and cognitive features of 22.11.2 phenotypes upon ASO regulation of EMC10. These pre-clinical data are of interest because they support reduction of ECM10 as a promising therapeutic strategy.

https://doi.org/10.7554/eLife.103328.2.sa2

Abstract

Adults and children with the 22q11.2 Deletion Syndrome demonstrate cognitive, social and emotional impairments and high risk for schizophrenia. Work in mouse model of the 22q11.2 deletion provided compelling evidence for abnormal expression and processing of microRNAs. A major transcriptional effect of the microRNA dysregulation is up-regulation of *Emc10*, a component of the ER membrane complex, which promotes membrane insertion of a subset of polytopic and tail-anchored membrane proteins. We previously uncovered a key contribution of EMC10 in mediating the behavioral phenotypes observed in 22q11.2 deletion mouse models. Here we show that expression and processing of miRNAs is abnormal and *EMC10* expression is elevated in neurons derived from 22q11.2 deletion carriers. Reduction of *EMC10 levels* restores defects in neurite outgrowth and calcium signaling in patient neurons. Furthermore, antisense oligonucleotide administration and normalization of *Emc10*

in the adult mouse brain not only alleviates cognitive deficits in social and spatial memory but remarkably sustains these improvements for over two months post injection, indicating its therapeutic potential. Broadly, our study integrates findings from both animal models and human neurons to elucidate the translational potential of modulating *EMC10* levels and downstream targets as a specific venue to ameliorate disease progression in 22q11.2 Deletion Syndrome.

Introduction

Adults and children with the 22q11.2 Deletion Syndrome (22q11.2DS) demonstrate cognitive, social and emotional impairments (1–3). 22q11.2 deletions are also one of the strongest genetic risk factors for schizophrenia (SCZ) (4). There are currently no targeted therapies that address the underlying molecular mechanisms of 22q11.2DS. Previous work in a model of the 22q11.2 deletion, carrying a hemizygous 1.3-Mb deficiency on mouse chromosome 16 [*Df(16)A*], which is syntenic to the 1.5Mb 22q11.2 deletion [*Df(16)A*$^{+/-}$mice] revealed a distinct behavioral and cognitive profile (5, 6). Molecular analysis of the *Df(16)A*$^{+/-}$ strain provided compelling evidence for abnormal processing of brain enriched microRNAs (miRNAs) (5, 7). The *Df(16)A*$^{+/-}$ related miRNA dysregulation is due to (i) hemizygosity of *Dgcr8*, a component of the "microprocessor" complex that is essential for miRNA production (8) and (ii) hemizygosity of miRNA genes residing within the deletion, including *mir185*. Reduction of miR-185 levels and to a lesser degree of miRNAs residing outside the deletion {such as miR-485 (7)} result in a de-repression of *Mirta22/Emc10* gene (herein after referred to as *Emc10*), whose expression is under the repressive control of *miRNAs* (7). Indeed, comprehensive RNA profiling of *Df(16)A*$^{+/-}$ mice found that postnatal elevation in the expression of *Emc10* gene represents a key transcriptional effect of the 22q11.2 deletion (7). Increased brain expression of *Emc10* is recapitulated in *Df(16)A*$^{+/-}$ primary neurons (9) as well as in mouse models of the more common 3Mb 22q11.2 deletion (10). Other miRNA targets are dysregulated, but their levels of change are subtler and more variable. *Emc10* encodes for a component of the ER membrane complex (EMC), which promotes membrane insertion and maturation of a subset of polytopic and tail-anchored membrane proteins including neurotransmitter receptors, channels, and transporters (11–18). *Emc10* is a prenatally biased gene with high expression in embryonic life that gradually subsides after birth (7), a developmental pattern of expression conserved between mice, humans and nonhuman primates (19). *Emc10* Loss-of-Function (LoF) mutation that leads to reduction of *Emc10* levels rescues key cellular, cognitive and behavioral alterations in the *Df(16)A*$^{+/-}$ mice (19). However, whether similar beneficial effects could be achieved in human neurons and whether Emc10 normalization in the adult brain could reverse established cognitive deficits remained unknown.

Here we show that 22q11.2 deletion results in abnormal processing of miRNAs in human neurons and in turn drives misexpression of *EMC10* as previously described in animal models (5). Human *EMC10* expression is elevated in neurons derived from 22q11.2 deletion carriers and reversal of *EMC10* expression leads to restoration of key morphological and functional alterations linked to 22q11.2 deletions, supporting normalization of *EMC10* expression as a disease-modifying intervention. Toward this end, we also show that antisense oligonucleotide (ASO)-mediated *Emc10* normalization in the adult mouse brain is effective at reversing cognitive alterations. Improvements in cognition are sustained for over two months post ASO administration, underscoring the potential of this approach for providing durable therapeutic benefits. The observations that ASO-mediated Emc10 reduction in adult mouse brain rescues cognitive deficits linked to 22q11.2 deletion strongly support a key contribution of Emc10 and Emc10-dependent membrane protein trafficking in mediating the effects of 22q11.2 deletions on cognitive function and pave the way towards translating these observations into potential disease-modifying therapeutic interventions.

Results

To investigate whether miRNA dysregulation and upregulation of *EMC10* is also prominent in cortical neurons from patients carrying 22q11.2 deletions (**Fig. 1A**), we used hiPSC lines obtained from three independent 22q11.2DS/SCZ donors carrying a 3Mb deletion and diagnosed with SCZ, along with matched healthy controls (**Supplementary Table 1**) to ensure the robustness and generalizability of our findings across different genetic backgrounds. The first patient/control pair is derived from dizygotic twins discordant for the 22q11.2DS and SCZ [Q6 (22q11.2) and Q5 (Ctrl)] (**Fig. S1A-D**). The second patient/control pair is derived from siblings [Q1 (22q11.2) and Q2 (Ctrl)] while the third patient/control pair is a case and age/sex matched unrelated control pair from the NIMH Repository and Genomic Resource [QR27 (22q11.2) and QR20 (Ctrl)].

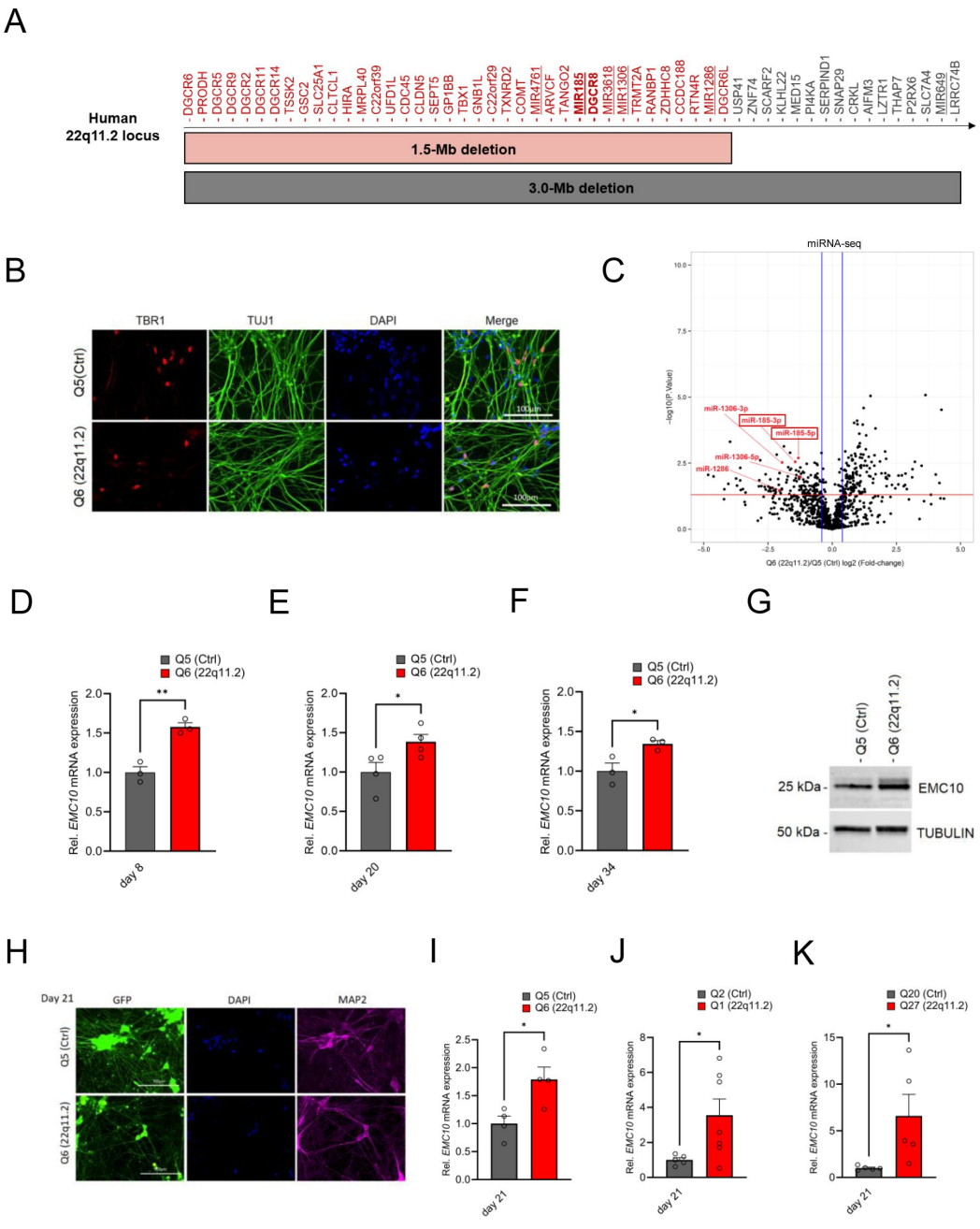

Fig. 1.

EMC10 is robustly upregulated in hiPSC-derived neurons from 22q11.2 deletion carriers.

(A) Schematic diagram depicting the human chromosome 22q11.2 region. Bright grey and red horizontal bars indicate the two most common hemizygous genomic deletions found in the 22q11.2 deletion syndrome. The location of the coding genes and non-coding RNAs (miRNAs, underlined) are shown for chromosome 22q11.2. The microprocessor *DGCR8* (DiGeorge Syndrome Critical Region Gene 8) and *mir185* are shown in bold. **(B)** Cortical marker TBR1 and pan-neuronal marker TUJ1 expression in cortical neurons as detected by immunocytochemistry at day 13 of differentiation. TBR1 (red), TUJ1 (green) and DAPI (blue) expression are shown. Scale bars: 100 μm. **(C)** Volcano plot showing differentially expressed miRNAs (DEmiRs) in cortical neurons at day 8 of differentiation. Significant DEmiRs (P value < 5%) are shown above red line; Q5 (Ctrl) n=3, Q6 (22q11.2) n=3. 153/133 miRNAs were significantly up- and downregulated in Q6 (22q11.2) hiPSC-derived cortical neurons, respectively. 22q11.2 deletion region residing miRNAs miR-185, miR-1286 and miR-1306 are highlighted. **(D-F)** Consistent upregulation of *EMC10* mRNA in Q6 (22q11.2) line derived cortical neurons as assayed by qRT-PCR at **(D)** day 8 (P= 0.031; Q5: n=3, Q6: n=3), **(E)** day 20 (P= 0.0478; Q5: n=4, Q6: n=4) and **(F)** day 34 (P= 0.0358; Q5: n=3, Q6: n=3) of differentiation. **(G)** Western blot analysis showing upregulated EMC10 protein levels in Q6 (22q11.2) line derived cortical neurons at day 8 of differentiation. Tubulin was probed as a loading control. **(H)** Immunofluorescence images of NGN2 generated cells. Representative images of NGN2-iNs at DIV21 from Q5 (Ctrl) and Q6 (22q11.2) hiPSC lines identified via EGFP fluorescence and immunostained for neuronal dendrite marker MAP2 and the nuclear marker DAPI. Scale bars=100 μm. **(I-K)** qRT-PCR assay of *EMC10* mRNA expression level in NGN2-iNs at DIV21. **(I)** Upregulation of *EMC10* mRNA in Q6 (22q11.2) line derived neurons compared to the healthy control line Q5 (P=0.0222). Q5 (Ctrl) n=4, Q6 (22q11.2) n=4. **(J)** Upregulation of *EMC10* mRNA in Q1 (22q11.2) patient line compared to healthy control line Q2 (P=0.0441). Q2 (Ctrl) n=5 and Q1 (22q11.2) n=7. **(K)** Upregulation of *EMC10* mRNA in QR27 (22q11.2) patient line compared to healthy control line QR20 (P=0.0414). QR20 (Ctrl) n=5 and QR27 (22q11.2) n=5. Data are presented as mean ±SEM, unpaired two-tailed t-test, *P<0.05, **P<0.01.

We examined whether 22q11.2 deletion results in abnormal processing of miRNAs in human neurons as we have previously described in animal models (5). We performed parallel small RNA/miRNA sequencing on DIV8 differentiated human cortical neurons from the sibling (Q5/Q6) pair derived using an approach that combines small-molecule inhibitors to repress SMAD and WNT signaling pathways to promote CNS fate (20). This protocol has been extensively validated and is known to robustly generate cortical neurons while actively suppressing glial differentiation. We confirmed the efficiency of differentiation using immunohistochemistry (IHC) and gene expression assays, which indicated the anticipated increase of TUJ1/TBR1 positive derived neurons and downregulation of embryonic stem cell marker *OCT4* (**Fig. 1B** and **Fig. S1E-G**). We identified a number of mature miRNAs dysregulated in response to the 22q11.2 deletion (**Fig. 1C**, **Fig. S2A, B**, Supplementary Table S2). As a validation of our approach, we observed the expected downregulation of miRNAs miR-185, miR-1286 and miR-1306 that reside in the 22q11.2 locus (three other predicted 22q11.2 miRNAs, miR-649, miR-3618 and miR-4761 were not detected in DIV8 neurons) (**Fig. S2A**). Among miRNAs located outside the 22q11.2 region, we note downregulation of miRNAs such as miR-137, as well as miR-134 and several other members form the largest placental mammal-specific miRNA gene cluster miR379-410 (**Fig. S2B**) that have been previously implicated in neuronal development, differentiation and function (5, 21–29). We used the miRNA-target interaction network tool miRNet 2.0 (30) to perform target enrichment and network analysis for the dysregulated miRNAs and performed GO term enrichment analysis on this target interaction network. Affected biological processes were prominently centered on cell division and intracellular protein transport (**Fig. S3A**) whereas cellular components were associated with the nucleus and the perinuclear region (endoplasmic reticulum and Golgi apparatus) of the cytoplasm (**Fig. S3B**).

In addition to 22q11.2 deletion region miRNAs, lower abundance of miRNAs in cases is likely due to haploinsufficiency of the *DGCR8* gene and is expected to result in upregulation of target genes. To identify candidate miRNA target genes we performed an unbiased evaluation of the transcriptional responses using bulk RNA sequencing on RNA collected from DIV8 differentiated cortical neurons derived from the patient (Q6) and the corresponding healthy dizygotic twin (Q5) line (**Fig. S4A**). We observed the expected downregulation of genes within the 22q11.2 locus in patient neurons (Supplementary Table 3). Further, RNA and protein expression characterization confirmed the reductions in the abundance of the 22q11.2 locus residing genes *DGCR8* and *RANBP1* (**Fig. S4B, C**). Among the differentially expressed genes (DEGs) 2094 were downregulated and 1937 were upregulated. As expected EMC10 expression was elevated in patient neurons while expression of other EMC subunits (*EMC1-4, EMC6-9*) detected in our DIV8 sequencing data did not show significant differences. GO term enrichment analysis on downregulated DEGs identified significantly altered biological processes centered on neurogenesis, neuronal development, and differentiation (**Fig. S4D**). Among the upregulated DEGs, the GO terms enriched were related to neuronal development as well as neuronal cilia assembly and structure (**Fig. S4E**).

Intersection of predicted targets of downregulated miRNAs and up-regulated DEGs identified 774 predicted targets of downregulated miRNAs (**Fig. S4F**, Supplementary Table 4) including *EMC10*. Notably, functional annotation revealed that predicted targets of downregulated miRNAs include genes that modulate neuronal development and are associated with GO terms such as endoplasmic reticulum and endomembrane system of neurons (**Fig. S4G, H**).

qRT-PCR assays confirmed a robust and significant upregulation of *EMC10* levels in RNA extracted from cortical neurons derived from hiPSCs of the Q5/Q6 pair through SMAD/WNT signaling inhibition, at three distinct stages of in vitro maturation (**Fig. 1D-F**). Additionally, this upregulation was confirmed in protein extracts from cortical neurons at day 8 of differentiation (**Fig. 1G**). To examine whether transcriptional *EMC10* upregulation is independent of the neuronal derivation method, we generated neurons via inducible expression of Neurogenin-2 (NGN2), a widely used protocol that generates a robust population of excitatory neurons (NGN2-iNs) within 3 weeks (31–34). MAP2 staining was used to demonstrate the successful neuronal differentiation of the hiPSC lines (**Fig. 1H**). qRT-PCR assay of *EMC10* mRNA expression level in NGN2-iNs at DIV21 confirmed transcriptional *EMC10* upregulation in three independent pairs of patient and sex-/age matched healthy control lines (**Fig. 1I-K**). Taken together our results highlight a reproducible and robust upregulation of *EMC10* in neurons derived from patients with 22q11.2 deletions, which is independent of the derivation method. It is noteworthy that in addition to monolayer cultures, *EMC10* shows significant upregulation along the excitatory neuron lineage (radial glia, intermediate progenitors and excitatory neurons) but not in astrocytes, choroid or interneuron lineage cells, in patient forebrain organoids generated by the same hiPSCs lines used in the present study (35).

We have previously shown that upregulation of the murine orthologue of *Emc10* is primarily due to downregulation of miR-185 and to a lesser degree of miR-485 (7). Both conserved and non-conserved binding sites at the 3'UTR of human *EMC10* are predicted in silico for both miRNAs (**Fig. S5A**). Consistently, the observed upregulation in the levels of *EMC10* gene is accompanied by a robust reciprocal decrease in the levels of the miRNA precursor of miR-185 at DIV8 as indicated both by our miRNA sequencing analysis (**Fig. 2A**, Supplementary Table 2) and follow up qRT-PCR assays (**Fig. 2A**). The miRNA precursor of miR-485 exhibited a modest but non-significant reduction in abundance (**Fig. 2B**), consistent with our miRNA sequencing profile (**Fig. S2B**). This may be attributed to the early developmental stage of the neurons, as miR-485 expression increase during neuronal maturation (36, 37). Collectively, these findings demonstrate a strong inverse correlation between EMC10 upregulation and miR-185 downregulation, while suggesting that miR-485 may play a less prominent role at this early stage of neuronal development. Notably, overexpression of miR-185 and miR-485 using miRNA mimics in human

cortical neurons at DIV10 resulted in reduction of *EMC10* expression levels in both the healthy control (Q5, **Fig. 2C**) and patient line (Q6, **Fig. 2D**). Furthermore, inhibition of endogenous miR-185 and miR-485 in the control line by using specific miRNA inhibitors increased *EMC10* expression level (**Fig. 2E**) confirming the predicted conserved functionality of miR-185 and miR-485 miRNA binding sites in *EMC10*. It is worth noting that in addition to miR-185, non-conserved binding sites at the 3'UTR of human *EMC10* are predicted *in silico* for two additional downregulated miRNAs residing within the 22q11.2 locus, miR-1286 and miR-1306 (**Supplementary Table 5**). The functionality of these miRNA binding sites in *EMC10* and whether they contribute to the observed elevation of its expression in human neurons remains to be determined. Taken together our results confirm that miRNA dysregulation emerges in human neurons as a result of the 22q11.2 deletion and in turn drives misexpression of genes primarily involved in intracellular membrane and protein trafficking-related processes required for neuronal development and maturation. Among them, *EMC10* represents a major downstream effector of the 22q11.2-linked miRNA dysregulation.

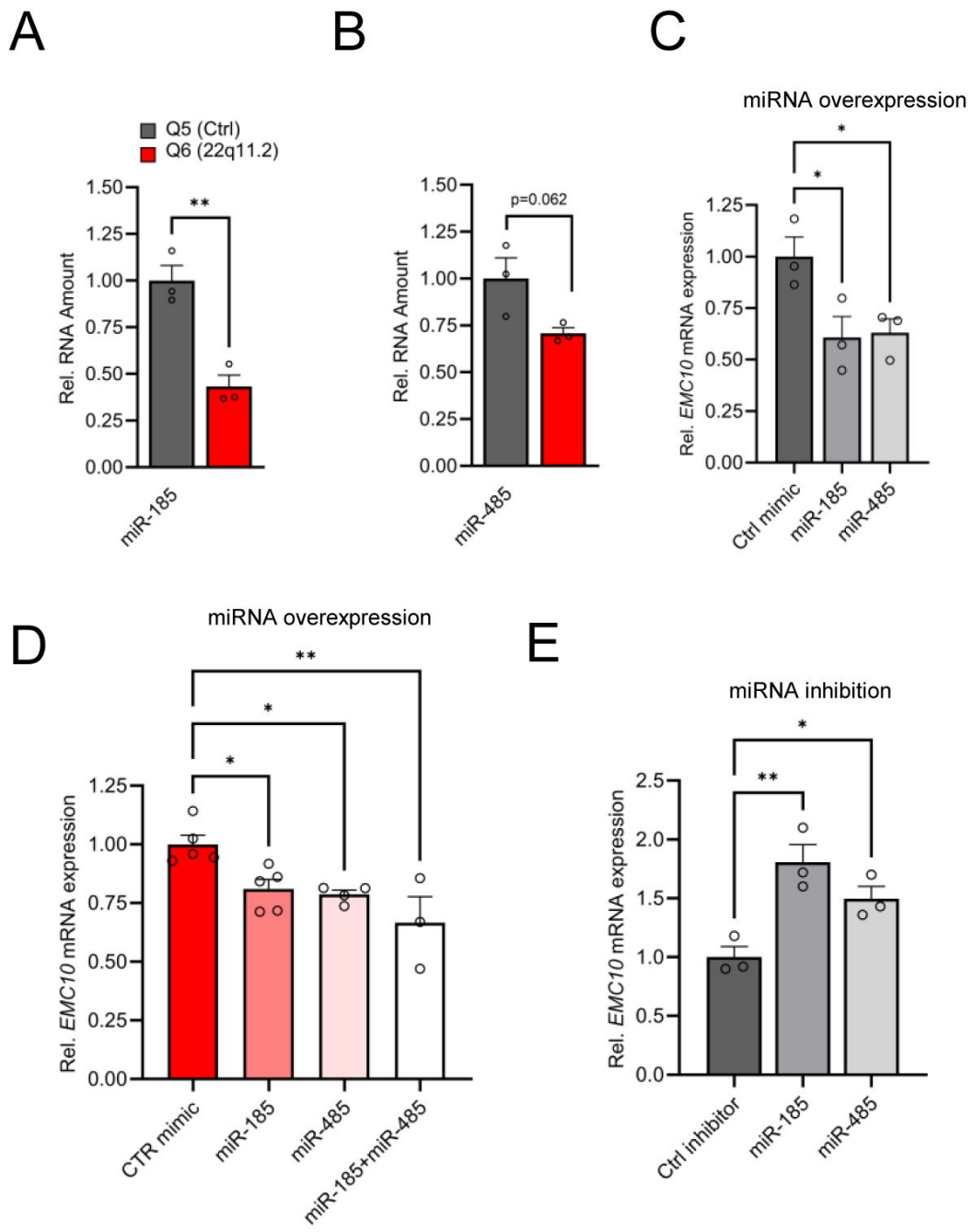

Fig. 2.

Altered miRNA expression in hiPSC-derived cortical neurons from 22q11.2 deletion carriers.

(A) Precursor miRNA expression level of miR-185 (P= 0.0038), predicted to target *EMC10*, are downregulated in Q6 (22q11.2) cortical neurons as assayed by qRT-PCR (Q5: n=3, Q6: n=3). **(B)** Precursor miRNA expression level of miR-485 (P= 0.0622), predicted to target *EMC10*, are downregulated in Q6 (22q11.2) cortical neurons as assayed by qRT-PCR (Q5: n=3, Q6: n=3). **(C-E)** miR-185 and miR-485 modulate *EMC10* in human iPSC-derived cortical neurons. **(C)** qRT-PCR quantification shows reduced expression levels of *EMC10* mRNA in Q5 (Ctrl) line derived cortical neurons at day 10 of differentiation transfected with miR-185 [one-way ANOVA, F (2, 6) = 6.079, P=0.0361; post hoc Bonferroni, P=0.0366] or miR-485 [post hoc Bonferroni, P=0.0464] mimics at day 8 of differentiation. Expression levels in miR-185 or miR-485 mimic-treated neurons were normalized to expression levels under scramble mimic controls treatment (n= 3, each treatment). **(D)** qRT-PCR quantification shows reduced expression levels of *EMC10* mRNA in Q6 line-derived cortical neurons transfected with miR-185 [one-way ANOVA, F (3, 13) = 7.167, P=0.0044; post hoc Tukey, P=0.0345] or miR-485 [post hoc Tukey, P=0.0251] or a combination of both miRNA mimics [post hoc Tukey, P=0.0020]. Expression levels in miR-185, miR-485 or the combination of both mimic-treated neurons were normalized to expression levels under scramble mimic controls treatment. Ctrl mimic n=5, miR-185 mimic n=5, miR-485 mimic n=4 and miR185+miR485 mimics n=3. **(E)** qRT-PCR quantification shows increased expression levels of *EMC10* mRNA in Q5 line derived cortical neurons transfected with miRNA inhibitors miR-185 [one-way ANOVA, F (2, 6) = 11.94, P=0.0081; post hoc Bonferroni, P=0.0057]or miR-485 [post hoc Bonferroni, P=0.0491] at day 8 of differentiation. Expression levels in miR-185 or miR-485 inhibitor-treated neurons were normalized to expression levels under scramble miRNA inhibitor controls treatment (n=3, each treatment). Data are presented as mean ±SEM, unpaired two-tailed t-test or one-way ANOVA as indicated, *P<0.05, **P<0.01.

To investigate the relevance of *EMC10* de-repression in the development and function of patient neurons, we generated derivatives of the Q6 patient hiPSC line carrying either heterozygous (Q6/EMC10^{HET}) or homozygous (Q6/EMC10^{HOM}) *EMC10* LoF mutations using standard CRISPR/Cas9 editing approaches (**Fig. S6A**). Mutations were confirmed by sequencing (**Fig. S6A**, lower panel) and karyotyping confirmed normal chromosome complement (**Fig. S6B**). We confirmed reduced expression levels of 22q11.2 gene *RANBP1* by western blot in both derivative hiPSC lines (**Fig. S6C**) whereas stem-cell marker *NANOG* and *OCT4* were equally expressed in all lines assayed by qRT-PCR (**Fig. S6D, E**). EMC10 mRNA and protein levels were reduced by ~50% in the Q6/EMC10^{HET} hiPSC line and abolished in the Q6/EMC10^{HOM} line (**Fig. S6F, G**). It is noteworthy that we did not observe an upregulation of *EMC10* mRNA levels in the Q6 hiPSC lines (**Fig. S6F**), a finding likely attributed to the general low expression level of miR-185 and miR-485 in hiPSCs (38). Indeed both miRNAs are developmentally regulated and show increased expression levels during neuronal development (*https://ethz-ins.org/igNeuronsTimeCourse/*) (37). Additional characterization of hiPSC-derived NGN2-iNs (**Fig. 3A**), conclusively demonstrated a reduction (Q6/EMC10^{HET}) or elimination (Q6/EMC10^{HOM}) of *EMC10* mRNA (**Fig. 3B**). Expression assays of a panel of cell type-specific markers did not reveal significant differences between NGN2-iNs from the Q6 patient line and both derivative lines, indicating that gene editing has no adverse effect on neuronal differentiation (**Fig. S6H**).

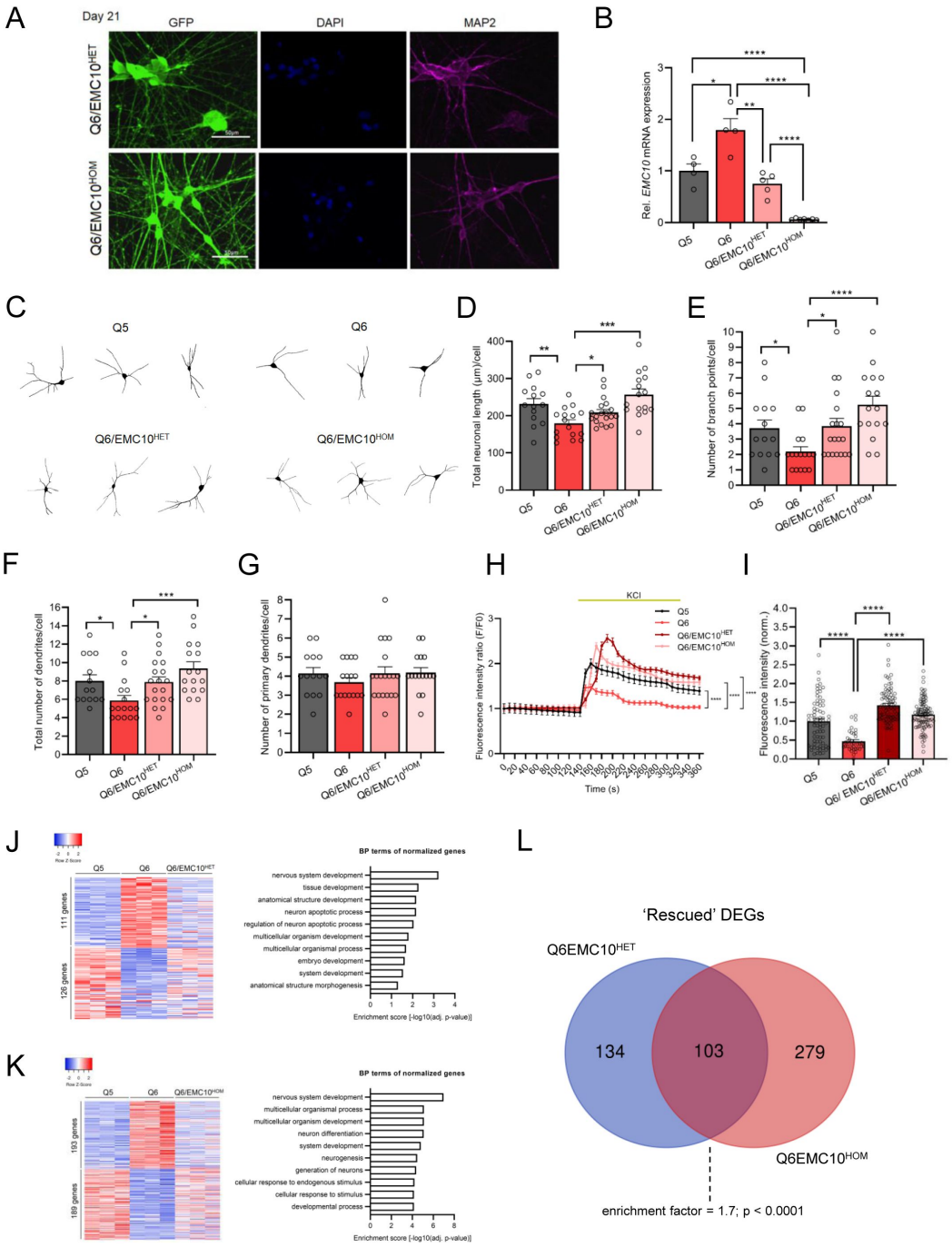

Fig. 3.

Reduction of *EMC10 levels* restores defects in neurite outgrowth and calcium signaling in neurons from 22q11.2 deletion carriers.

(A) Representative images of NGN2-iNs at DIV21 from Q6/EMC10^{HET} and Q6/EMC10^{HOM} hiPSC lines identified via EGFP fluorescence and immunostained for neuronal dendrite marker MAP2 and the nuclear marker DAPI. Scale bars=50 µm. **(B)** qRT-PCR assay of *EMC10* mRNA expression level in NGN2-iNs at DIV21. *EMC10* expression is normalized to near WT levels level in Q6/EMC10^{HET} line (P=0.166) and abolished in Q6/EMC10^{HOM} line (P<0.0001). Q5 (Ctrl) n=4, Q6 (22q11.2/SCZ) n=4, Q6/EMC10^{HET} n=5 and Q6/EMC10^{HOM} n=7. **(C-G)** Neuronal morphology analysis in Q5, Q6 (22q11.2), Q6/EMC10^{HET} and Q6/EMC10^{HOM} neurons. **(C)** Representative images of traced neurons. **(D)** Total

neuronal length is reduced in Q6 line (P=0.0044) and restored in Q6/ EMC10^{HET} (P=0.0253) and Q6/EMC10^{HOM} line (P=0.0001). **(E)** Reduction in number of branch points/cell in Q6 (P=0.0195) is restored in the Q6/EMC10^{HET} (P=0.0134) and Q6/EMC10^{HOM} lines (P<0.0001). **(F)** Reduction in the total number of dendrites/cells in Q6 (P=0.0202) is reversed in the Q6/EMC10^{HET} (P=0.0166) and Q6/EMC10^{HOM} lines (P=0.0005) **(G)** The number of primary dendrites per cell is unchanged. Q5 (Ctrl) n=14, Q6 (22q11.2) n=16, Q6/EMC10^{HET} n=19 and Q6/EMC10^{HOM} n=16 neuronal cells. **(H-I)** Defects in cytoplasmic calcium signaling in Q6 (22q11.2) neurons are reversed in Q6/EMC10^{HET} and Q6/EMC10^{HOM} lines. **(H)** Changes in Fluo4-AM fluorescence signal intensity in response to 75mM KCl in Q5 (Ctrl), Q6 (22q11.2). Q6/EMC10^{HET} and Q6/EMC10^{HOM} hiPSC-derived neurons at DIV38. Q5 vs. Q6 (KS D=0.5405, P<0.0001), Q6 vs. Q6 EMC10^{HET} (KS D=0.5556, P<0.0001) and Q6 vs. Q6 EMC10^{HOM} (KS D=0.5676, P<0.0001). **(I)** Quantification of KCl-induced Fluo4 intensity peak amplitude (ΔF) demonstrates a reduction in Q6 line (P<0.0001) that is reversed in Q6/EMC10^{HET} (P<0.0001) and Q6/EMC10^{HOM} lines (P<0.0001). Q5 (Ctrl) n=70, Q6 (22q11.2/SCZ) n=37, Q6/EMC10^{HET} n=82, Q6/EMC10^{HOM} n=97 neuronal cells. **(J)** Heatmap (left) showing the expression of differentially regulated 237 genes in Q5 (Ctrl) and Q6 (22q11.2) that are normalized in the Q6/EMC10^{HET} NGN2-iNs at DIV21 (n=3 per genotype). Gene Ontology (GO) biological process (BP) terms (right) associated with the up- and down-regulated genes normalized in the Q6/EMC10^{HET} NGN2-iNs. **(K)** Heatmap (left) showing the expression of differentially regulated 382 genes in Q5 (Ctrl) and Q6 (22q11.2) that are normalized in the Q6/EMC10^{HOM} NGN2-iNs at DIV21 (n=3 per genotype). Gene Ontology (GO) biological process (BP) terms (right) associated with the up- and down-regulated genes normalized in the Q6/EMC10^{HOM} NGN2-iNs. **(L)** Intersection of rescued up- and down-regulated DEGs in the Q6/ EMC10^{HET} and Q6/EMC10^{HOM} lines: Venn diagram highlighting the 103 rescued DEGs (enrichment factor = 1.7; p < 0.0001, based on a hypergeometric test). Data are presented as mean ±SEM, unpaired two-tailed t-test or Kolmogorov–Smirnov test as indicated, *P<0.05, **P<0.01, ***P<0.001, ****P<0.0001.

Df(16)A$^{+/-}$ mice show impaired formation of dendrites in deep layer cortical neurons, which are faithfully recapitulated in primary neuronal cultures and are partially reversed by reduction of *Emc10* levels (7). We asked whether impaired dendritic formation is also observed in human neuronal cultures from patients with 22q11.2 deletions and whether reduction of *EMC10* levels could prevent such morphological alterations during neuronal maturation. We employed monolayer neuronal cultures of NGN2-iNs. Neuronal cells were fixed at DIV21 of differentiation, immuno-stained, traced and key indices of dendritic architecture were quantified (see Materials and Methods). Our analysis confirmed a reduced dendritic complexity in mutant neurons as reflected in total neuronal length, the number of branch points and the total number of dendrites per cell (**Fig. 3C-F**). The number of primary dendrites per cell were unchanged (**Fig. 3G**) in accordance with previous findings from the murine 22q11.2 deletion model where only subtle changes were detected in the number of primary neurons (7). Importantly, we found that reduction or elimination of *EMC10 expression* restored to WT levels neuronal length and branchpoints. Importantly, we found that reducing or eliminating EMC10 expression restored neuronal length and branch points to WT levels. Notably, the number of branch points in Q6/EMC10^{HOM} neurons exceeded those in WT neurons (**Fig. 3E**) likely suggesting that reduced (or abolished) *Emc10* expression can alter normal neurite growth, resulting in excessive responses, potentially triggered upon gene restoration by the mutant system's adaptation to dysfunction, leading to altered receptor sensitivity or signaling dynamics. This highlights the critical importance of precise *Emc10* expression for maintaining proper neuronal development and function.

Our previous evaluation of Ca^{2+} homeostasis perturbations caused by 22q11.2 deletions using Ca^{2+} imaging on primary neurons from *Df(16)A*$^{+/-}$ mice revealed a significantly lower amplitude of Ca^{2+} elevation following KCl evoked depolarization (9). This impairment was replicated in human cortical neurons from patients with 22q11.2 deletions (39) and shown to be partially restored by exogenous expression of *DGCR8*, indicating a potential role of miRNA dysregulation. Using the green-fluorescent calcium indicator Fluo-4 and time-lapse microscopy we confirmed a decrease in the amplitude of Ca^{2+} rise following KCl evoked depolarization, in patient (Q6) derived NGN2-iNs at DIV37/38 compared to the healthy twin (Q5) (**Fig. S7A, B**). We asked whether reduction of EMC10 levels could reverse such alterations. Notably, the observed defect in Ca^{2+} signaling were

reversed in both Q6/EMC10^{HET} and Q6/EMC10^{HOM} NGN2-iNs as demonstrated by the increased amplitude of Ca^{2+} rise following depolarization (**Fig. 3H, I**). Interestingly, the amplitudes of Ca^{2+} rise in Q6/EMC10^{HET} and Q6/EMC10^{HOM} were slightly elevated compared to the WT control group, consistent with the effects on neurite outgrowth (**Fig. 3H**). The observation that reduction of *EMC10* levels fully restores the Ca^{2+} signaling deficits observed in patient neurons suggests that miRNA-dependent elevation of *EMC10* may interfere with one or more sources of intracellular Ca^{2+} and a wide range of calcium-dependent processes.

Differentially expressed genes are often organized into functional groups or pathways based on their known biological roles. We used transcriptional profiling as an indirect measure of cellular pathways affected by the reduction of EMC10 levels by identifying genes differentially expressed between the parental Q6/Q5 lines whose expression differences are abolished or nearly abolished ("rescued") in either Q6/EMC10^{HET} or Q6/EMC10^{HOM} NGN2-iNs (**Fig. 3J, K**). In the Q6/EMC10^{HET} line, 237 DEGs (6%) were rescued (111 downregulated and 126 upregulated), while in the Q6/EMC10^{HOM} line, 382 DEGs (11%) were rescued (193 downregulated and 189 upregulated) (Supplementary Table 6). In both cases, functional annotation analysis indicated highest enrichment scores for terms related to nervous system development as well as an enrichment in GO terms relevant to neuronal generation and differentiation. Intersection of "rescued" genes in Q6/EMC10^{HET} and Q6/EMC10^{HOM} NGN2-iNs identified 103 shared DEGs (**Fig. 3L** and Supplementary Table 7). To assess the significance of the overlap between the rescued DEGs in Q6/EMC10^{HET} and Q6/EMC10^{HOM} NGN2-iNs, we performed a hypergeometric test, which calculates the probability of observing the degree of overlap between two gene groups under the null hypothesis that the overlap occurs by chance. Our analysis revealed a significant overlap (enrichment factor = 1.7; $p < 0.0001$), indicating that the overlap is much greater than expected by chance. These 103 shared DEGs likely play a key role in pathways influenced by EMC10 levels, particularly those involved in nervous system development, as suggested by our functional annotation analysis. To further investigate the functional relationships among these shared DEGs, we conducted a protein-protein interaction (PPI) network analysis. This analysis highlighted a functional cluster including 30 of these genes, such as the SCZ-linked genes *PCDHA2* (40), *RBFOX1* (41) and *RGS4* (42, 43) (**Fig. S8A**), involved in nervous system development (**Fig. S8B**). It should be noted that the beneficial effect of elimination of EMC10 expression is consistent with previous findings that lack of EMC10 does not compromise EMC assembly (44) and implying an auxiliary or modulatory role of EMC10 in the EMC function.

Taken together, our analysis of neurons from 22q11.2 deletion carriers indicate that elevation of *EMC10* expression disrupts their development and maturation in a way similar to observations in murine neurons, and support normalization of *EMC10* expression as a disease-modifying intervention. While our previous work has shown that constitutive genetic reduction of *Emc10* levels rescues key cognitive and behavioral alterations in the *Df(16)A*$^{+/-}$ mice, translating these observations into therapeutic interventions requires demonstration that it is the sustained elevation of *EMC10* throughout the adult life that interferes with the underlying neural processes rather than an irreversible impact on brain maturation during early development. Toward this end, we first investigated whether restoration of *Emc10* levels in the brain of adult (2– 4-month-old) *Df(16)A*$^{+/-}$ mice is effective at reversing cognitive alterations (5, 19). Specifically, we examined the effects of *Emc10* reduction in adult brain on social memory (SM), a cognitive domain robustly and reproducibly affected in adult *Df(16)A*$^{+/-}$mice (6, 19, 45). Notably, SM deficits are also present in juvenile *Df(16)A*$^{+/-}$ mice as early as postnatal day 22 (**Fig. S9A, B**), underscoring the severity of this phenotype, which emerges during early adulthood. In humans, SM, a key component of social cognition, involves encoding, storing, and retrieving information about social experiences, such as recognizing familiar individuals and recalling past interactions and emotions. Social cognition, the broader ability to perceive, interpret, and respond to social cues, is essential for forming relationships and understanding others' behavior. Disruptions in SM can impair social cognition, contributing to the functional deficits commonly observed in schizophrenia (46). Deficits in social cognition are present in individuals with 22q11.2 deletions

(47) and use of rodent tasks that evaluate SM can serve as a useful proxy of the human condition. Impaired SM in *Df(16)A*$^{+/-}$mice is fully restored by constitutive genetic reduction of *Emc10* levels (19).

To manipulate the expression of the *Emc10* gene in adult *Df(16)A*$^{+/-}$ mice we used a *Emc10* conditional 'knockout-first' design by conducting a Flp- and Cre-dependent genetic switch strategy (**Fig. S10A**). Parental *Emc10*$^{+/-\ tm1a}$ mice were crossed to a germline Flp mouse line that activates global Flp function and leads to the deletion of the frt-flanked sequence(s) in the offspring. The *Emc10*^{tm1c} offspring from this cross carry a *loxP* flanked WT *Emc10* allele and are essentially WT. To achieve temporal control of *Emc10* expression we used an inducible UBC-Cre/ERT2 mouse line that activates global Cre function upon tamoxifen (TAM) treatment. This approach enables postnatal normalization of *Emc10* expression at its endogenous locus preserving *Emc10* expression within its physiological levels. We used UBC-Cre/ERT2 mice in crosses to generate compound *Emc10*$^{tm1c+/-}$; UBC-cre/ERT2; *Df(16)A*$^{+/-}$mice. These mice have two WT *Emc10* copies upregulated, as expected in the *Df(16)A* background, until TAM-induced Cre expression deletes the tagged *Emc10* allele. We used oral gavage to deliver TAM and implement Cre-mediated *Emc10* deletion during adulthood (postnatal day 56-70). Corn oil treatment served as a control. Behavioral analysis was performed on the following four groups: *Emc10*$^{tm1c+/-}$; UBC-cre/ERT2; *Df(16)A*$^{+/+}$ mice treated with TAM (WT + TAM), *Emc10*$^{tm1c+/-}$; UBC-cre/ERT2; *Df(16)A*$^{+/-}$mice treated with TAM (*Df(16)A*$^{+/-}$+ TAM), *Emc10*$^{tm1c+/-}$; UBC-cre/ERT2; *Df(16)A*$^{+/+}$ mice treated with corn oil vehicle (WT + oil), and *Emc10*$^{tm1c+/-}$; UBC-cre/ERT2; *Df(16)A*$^{+/-}$ mice treated with corn oil vehicle (*Df(16)A*$^{+/-}$ + oil). Investigation of the efficiency of Cre-mediated deletion in brain lysate preparations from prefrontal cortex (PFC) (**Fig. S10B, C**), hippocampus (HPC) (**Fig. S10D, E**) and cerebellum (CB) (**Fig. S10F**) confirmed that upon TAM treatment, *Emc10* mRNA and protein levels were restored to near WT levels in the adult brain of *Df(16)A*$^{+/-}$ mice. As expected, *Df(16)A*$^{+/-}$ + oil mice showed impaired SM performance compared to WT + oil control littermates, which was fully rescued upon TAM treatment. Specifically, upon reintroduction of a familiar juvenile mouse *Df(16)A*$^{+/-}$+ TAM mice showed a strong reduction in social interaction, indicative of intact SM, comparable to TAM-treated WT littermates and significantly different from *Df(16)A*$^{+/-}$ mice treated with corn oil (**Fig. S10G**). The intact SM of the *Df(16)A*$^{+/-}$ + TAM mice was further evident in analysis of difference score (**Fig. S10H**) compared to the corn oil-treated *Df(16)A*$^{+/-}$ mice. Interaction times during the first trial of the SM assay, which measures general social interest, were unaffected by TAM treatment. In contrast to SM, *Df(16)A*$^{+/-}$mice hyperactivity in the open field was not affected upon TAM treatment consistent with our previous results from constitutive genetic reduction of *Emc10* levels (**Fig. S10I**). Notably, TAM treatment did not alter the time spent in the center area of the open field, indicating an absence of changes in anxiety-related behavior. These findings demonstrate that restoring Emc10 levels in adult *Df(16)A*$^{+/-}$mice can significantly improve cognitive deficits, underscoring a broad therapeutic window and establishing Emc10 as a promising target for postnatal interventions.

We explored the translation potential of this finding by employing transient injection of single stranded ASOs targeting the mouse gene as dictated by their demonstrated efficacy as a therapeutic modality in preclinical models (48–53) and clinical studies of neurodevelopmental disorders (NDDs) or neurodegenerative disorders (54–56). Over 300 chimeric 2'-O-methoxyethyl (2'MOE)/DNA gapmer ASOs were generated and screened for *Emc10* mRNA reduction in 4T1 cells via electroporation (**Fig. S11A**). Lead ASOs were then confirmed in a dose-response assay (**Fig. S11B**), including the lead ASO (1081815, herein referred to as Emc10^{ASO1}), which targets intron 2 of mouse *Emc10* (**Fig. 4A**). Emc10^{ASO1} was selected for subsequent studies, as it was effective in lowering *Emc10* expression both in vitro and in vivo. Specifically, following transient intracerebral ventricular (ICV) injection in the posterior ventricle of 8 weeks old WT mice, Emc10^{ASO1} effectively suppressed the levels of *Emc10* mRNA (**Fig. S11C**) and protein (**Fig. S11D**) in both left and right HPC compared to WT mice treated with a control ASO (Ctrl^{ASO1}) without complementarity in the mouse. Analysis of *Gfap* and *Aif1* expression did not reveal any changes (**Fig. S11E, F**) suggesting lack of astroglial and microglial

activation upon Emc10^{ASO1} injection. Emc10^{ASO1} injected mice showed normal gait and no signs of behavioral toxicity. IHC analysis using an antibody that selectively recognizes the phosphorothioate backbone verified a robust diffusion primarily in HPC and to a lesser degree in surrounding brain areas. Colocalization with the neuronal marker NeuN and glial fibrillary acidic protein (GFAP) confirmed accumulation in hippocampal neurons as well as GFAP-expressing astrocytes (**Fig. 4B**). Analysis of *Df(16)A*$^{+/-}$mice treated by intraventricular injection at 8 weeks of age showed that Emc10^{ASO1} effectively lowered hippocampal *Emc10* mRNA to nearly WT levels 3 weeks post-injection resulting in normalization of *Emc10* expression (**Fig. 4C**, left panel). By contrast, consistent with the pattern of ASO distribution, we did not observe a significant reduction of *Emc10* expression levels in the PFC of *Df(16)* $^{+/-}$ mice treated with Emc10^{ASO1} (**Fig. 4C**, right panel). In addition to targeted assays, we performed bulk RNA-sequencing analysis of Ctrl^{ASO1} and Emc10^{ASO1}-treated *Df(16)A*$^{+/-}$ mice and WT littermates to evaluate the effect of Emc10^{ASO1} treatment on the hippocampal transcriptome profile. In the Ctrl^{ASO1} treated group (**Fig. 4D**, left panel), we observe the tripartite differential gene expression signature characteristic of *Df(16)A*$^{+/-}$mice: upregulation of *Emc10* and non-coding RNAs (pri-forms of miRNAs and long non-coding RNAs (**Fig. 4D**, left panel and inset, Log2Fold Change = 0.5) as well as the expected downregulation of genes included within the *Df(16)A* deficiency. In the Emc10^{ASO1} treated group (**Fig. 4D**, right panel and inset), *Emc10* is no longer upregulated in *Df(16)A*$^{+/-}$ mice while non-coding RNAs remain upregulated, and genes included in the deficiency are robustly downregulated. Apart from *Emc10*, seven other genes (*Mir9-3hg*, *Plxnd1*, *Cd68*, *Mir22hg*, *Gm28439*, *Adgre1*, and *Tnn*) are significantly upregulated in *Df(16)A*$^{+/-}$ mice in the Ctrl^{ASO1} but not in the Emc10^{ASO1}-treated group (**Supplementary Table S8**). We used the Bowtie mapping tool (57) to align short sequencing reads on both genomic and transcript sequence to assess whether these expression changes represent potential off-target effects of the Emc10^{ASO1} in the mouse transcriptome. Emc10^{ASO1} exclusively aligned with full complementarity to an intronic region in the *Emc10* gene (**Fig. 4A**) providing additional support for high target specificity. The observed changes might represent downstream effects of *Emc10* level reduction or reflect expression variability due to low expression levels of the upregulated genes.

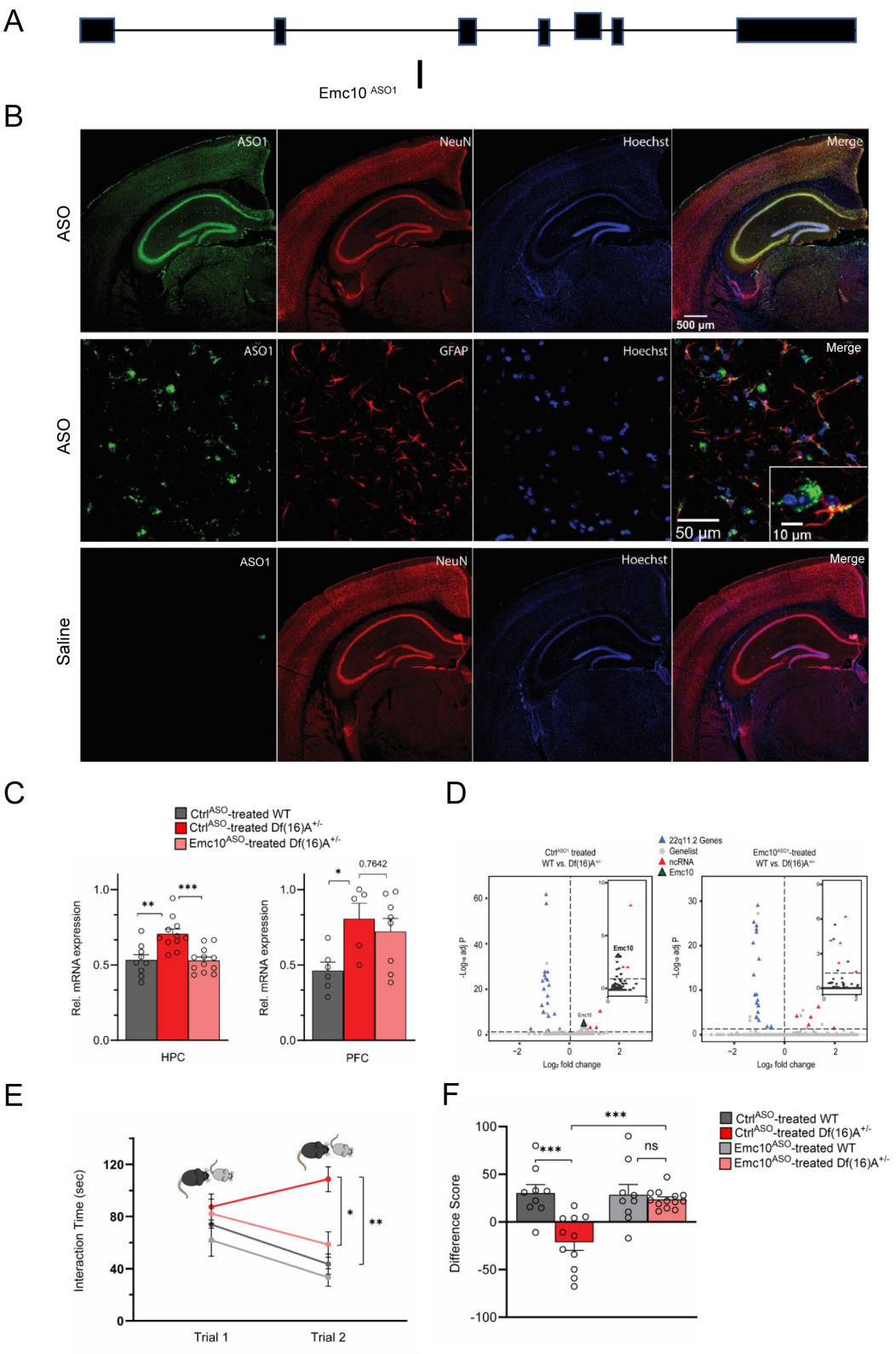
A
Emc10 ASO1
B
ASO
ASO1
NeuN
Hoechst
Merge
500 µm
ASO
ASO1
GFAP
Hoechst
Merge
50 µm
10 µm
Saline
ASO1
NeuN
Hoechst
Merge
C
CtrlASO-treated WT
CtrlASO-treated Df(16)A+/-
Emc10ASO-treated Df(16)A+/-
Rel. mRNA expression
HPC
PFC
0.7642
D
22q11.2 Genes
Genelist
ncRNA
Emc10
Emc10
E
Interaction Time (sec)
Trial 1
Trial 2
F
Difference Score
ns
CtrlASO-treated WT
CtrlASO-treated Df(16)A+/-
Emc10ASO-treated WT
Emc10ASO-treated Df(16)A+/-

Fig. 4.

ASO-mediated suppression of murine *Emc10 in vivo*.

(A) Mouse *Emc10* gene map plot (ENSMUST00000118808) showing the *Emc10*^{ASO1} target site. **(B)** Mouse brains collected three weeks post ICV injection were stained with an ASO antibody (green), counterstained with neuronal marker NeuN (red) and nuclear stain Hoechst (blue). A robust and uniform ASO diffusion (top panel) is observed in the HPC. No signal is detected in saline injected mice (bottom panel). Overlap with NeuN (yellow, top-right panel) confirms presence in neuronal cells. Accumulation in glial cells, specifically GFAP labeled astrocytes is also observed (middle-right panel and inset; ASO in green, GFAP in red, and Hoechst in blue). Images are taken with 4x, 20x and 40x objectives. **(C)** qRT-PCR analysis shows Emc10^{ASO} meditated normalization of *Emc10* mRNA levels in the HPC of *Df(16)A*$^{+/-}$ mice (left panel). Significant upregulation of *Emc10* mRNA expression levels is seen in Ctrl^{ASO} treated-*Df(16)A*$^{+/-}$ compared to WT mice [one-way ANOVA, F (2, 29) = 11.65, P<0.001; post hoc Tukey, P= 0.001]. Following ASO treatment, *Emc10* expression is normalized to WT levels in Emc10^{ASO} treated-*Df(16)A*$^{+/-}$ compared to Ctrl^{ASO} treated-*Df(16)A*$^{+/-}$ mice (post hoc Tukey, P= <0.001). Ctrl^{ASO}-treated WT mice: n=9 (5 males, 4 females), Ctrl^{ASO}-treated *Df(16)A*$^{+/-}$ mice: n=11 (5 males, 6 females), and Emc10^{ASO}-treated *Df(16)A*$^{+/-}$ mice: n=12 (7 males, 5 females). qRT-PCR analysis shows a significant up-regulation of *Emc10* mRNA expression levels in the PFC of Ctrl^{ASO} treated-*Df(16)A*$^{+/-}$ (right panel) compared to WT mice [one-way ANOVA, F (2, 16) = 4.253, P=0.0330; post hoc Tukey, P= 0.0385]. ASO injection does not normalize *Emc10* expression levels in PFC of *Df(16)A*$^{+/-}$ mice injected with Emc10^{ASO} (post hoc Tukey vs Ctrl^{ASO} treated *Df(16)A*$^{+/-}$ mice, P= 0.7642). Ctrl^{ASO} treated-WT male mice: n=6, Ctrl^{ASO} treated-*Df(16)A*$^{+/-}$ male mice: n=5, and Emc10^{ASO} treated-*Df(16)A*$^{+/-}$ male mice: n=8. **(D)** Volcano plots showing up-regulation of *Emc10* expression in the Ctrl^{ASO} treated-*Df(16)A*$^{+/-}$ compared to the Ctrl^{ASO}-treated WT mice (left panel and inset) but not in the Emc10^{ASO} treated-*Df(16)A*$^{+/-}$ compared to the Emc10^{ASO}-treated WT mice (right panel and inset). The expected down-regulation of genes included in the *Df(16)A*$^{+/-}$ deletion (blue) and upregulation of non-coding RNAs (ncRNAs, red) is also evident in both panels. Downregulated genes from the 22q11.2 locus (*Dgcr8*, *Ranbp1* and *Tango2*) as well as the upregulated ncRNA (miRNA-containing) gene *Mirg*, are highlighted. Ctrl^{ASO} treated-*Df(16)A*$^{+/-}$males: n=5, Emc10^{ASO} treated-*Df(16)A*$^{+/-}$ males: n= 4, Ctrl^{ASO} treated WT males: n=4, and Emc10^{ASO} treated-WT males: n=4. **(E-F)** ASO mediated behavioral rescue of SM deficit in *Df(16)A*$^{+/-}$ mice. **(E)** Ctrl^{ASO}-treated *Df(16)A*$^{+/-}$ mice show a robust SM deficit compared to Ctrl^{ASO}-treated WT mice as indicated by the significant difference in trial 2 interaction time upon reintroduction of a familiar juvenile mouse [three-way ANOVA for Trial X Genotype X Treatment Interaction matching by trial: F (1, 38) = 9.393 P=0.0040; post hoc Tukey, P= 0.0012]. A reduction in trial 2 interaction time indicates rescue of the SM deficit in Emc10^{ASO}-treated *Df(16)A*$^{+/-}$ compared to Ctrl^{ASO}-treated *Df(16)A*$^{+/-}$ mice (post hoc Tukey, P= 0.0114). **(F)** A negative difference score (trial 1-trial 2) confirms the SM deficit in Ctrl^{ASO}-treated adult *Df(16)A*$^{+/-}$ mice compared to WT littermates [two-way ANOVA for Genotype X Treatment interaction: F (1, 38) =9.369, P=0.0040; post hoc Tukey, P= 0.0002]. Increase in the difference score of *Df(16)A*$^{+/-}$ mice in the Emc10^{ASO}-vs Ctrl^{ASO}-treated group demonstrates SM rescue (post hoc Tukey, P= 0.0004). [Ctrl^{ASO}-treated WT mice: n=9 (5 males, 4 females), Ctrl^{ASO}-treated *Df(16)A*$^{+/}$ mice: n=11 (5 males, 6 females), Emc10^{ASO} treated WT mice: n=9 (5 males, 4 females), and Emc10^{ASO}-treated *Df(16)A*$^{+/}$ mice: n=13 (7 males, 6 females)]. Data are presented as mean ± SEM, *P < 0.05; **P < 0.01; ***P < 0.001.

Eight-week-old *Df(16)A*$^{+/-}$ mice and WT littermates were treated by ICV injection of Emc10^{ASO1} and Ctrl^{ASO1} and tested 3 weeks later in SM assays. *Df(16)A*$^{+/-}$ mice treated with Ctrl^{ASO1} showed the expected deficits in SM as reflected in the sustained high interaction time with the reintroduced familiar juvenile mouse. By contrast, *Df(16)A*$^{+/-}$ mice injected with Emc10^{ASO1} had significantly improved memory performance to levels indistinguishable from Emc10^{ASO1}-treated WT littermates, consistent with improvement of function arising from adult restoration of *Emc10* levels (**Fig. 4E, F**). Interaction times during the first trial of the SM assay, which measures general social interest, were unaffected by ASO treatment. Rescue was observed in both sexes and no significant differences were seen in treatment across sexes. In control experiments, we did not observe any effects of genotype or treatment upon reintroduction of a novel juvenile mouse in trial 2 (**Fig. S12A, B**), strongly indicating that SM deficits are not driven by a simple task fatigue. To evaluate the consistency and reproducibility of the ASO-mediated SM rescue we generated additional ASOs targeting different regions within the Emc10 transcript and screened them for *Emc10* mRNA reduction *in vivo* (**Fig. S13A-C**). One of these ASOs (1466182, herein referred to as

Emc10^{ASO2}), which targets intron 1 of mouse *Emc10* (**Fig. 5A**) was selected as the lead ASO candidate for the replication analysis based on its efficacy in reducing *Emc10* levels, distribution pattern, as well as the lack of any signs of astroglial/microglial activation or behavioral toxicity (see Materials and Methods). IHC analysis showed robust ASO distribution in both the hippocampus (HPC, **Fig. S14A**, first and second panel) and prefrontal cortex (PFC, **Fig. S14A**, third and fourth panel), as well as diffusion into both neuronal and non-neuronal cells. This was indicated by colocalization with the neuronal marker NeuN and the glial marker GFAP (**Fig. S14A**, bottom panel). Higher-magnification (40x) analysis revealed extensive overlap between the ASO signal and NeuN staining, demonstrating that the vast majority (>97%) of neurons exhibited ASO uptake. qRT-PCR analysis of *Df(16)A*$^{+/-}$mice treated by intraventricular injection at 8 weeks of age showed that Emc10^{ASO2} effectively lowered *Emc10* mRNA to nearly WT levels 3 weeks post-injection resulting in normalization of *Emc10* expression in the HPC (**Fig. 5B**), PFC (**Fig. 5C**) and somatosensory cortex (SSC) (**Fig. 5D**). To study the effects of Emc10^{ASO2}-mediated *Emc10* reduction on SM performance, 8-week-old *Df(16)A*$^{+/-}$ male mice and WT littermates were treated by ICV injection of Emc10^{ASO2} and Ctrl^{ASO2} and tested 3 weeks later. *Df(16)A*$^{+/-}$ mice injected with Emc10^{ASO2} had significantly improved SM performance to levels indistinguishable from Emc10^{ASO2}-treated WT littermates (**Fig. 5E, F**).

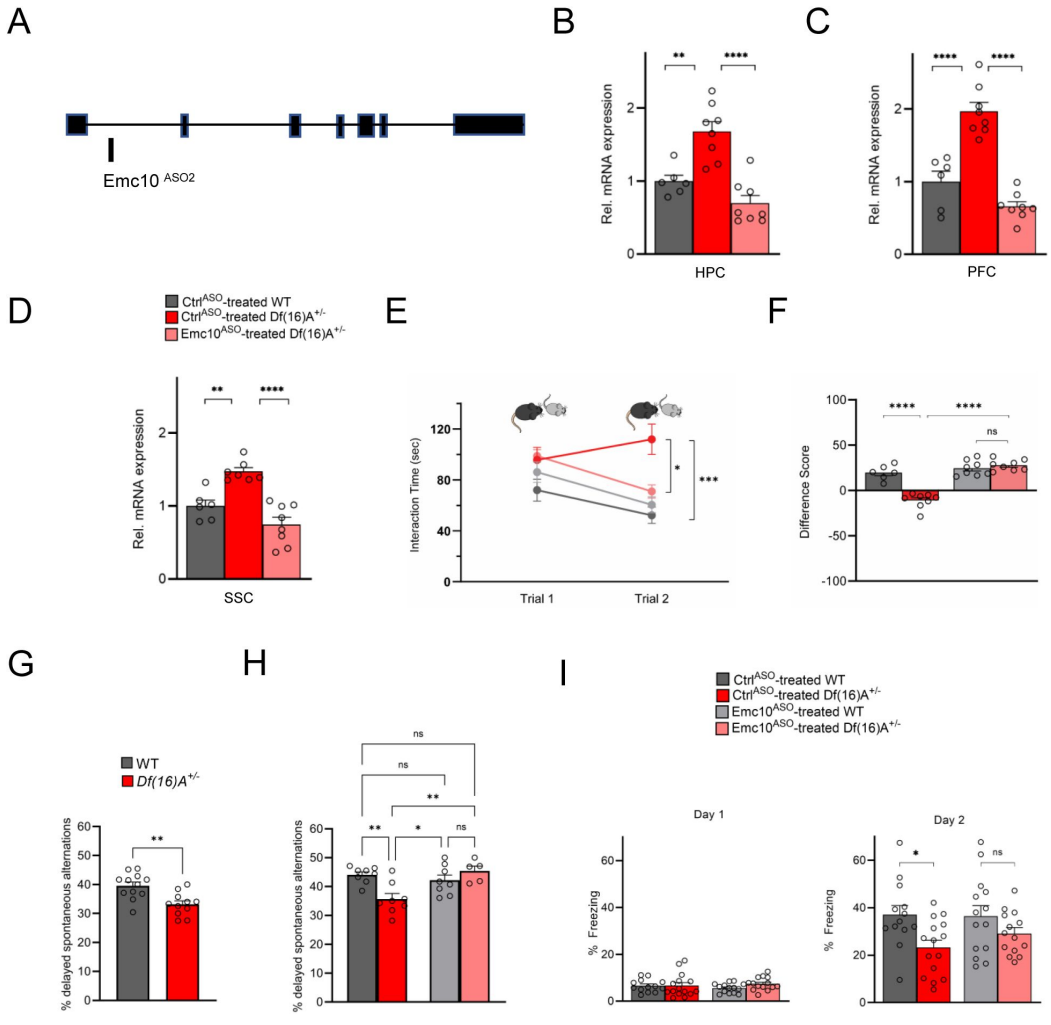

Figure 5

Restoration of cognitive function in *Df(16)A*$^{+/-}$ mice using an independent *Emc10* ASO.

(A) Mouse *Emc10* gene map plot (ENSMUST00000118808) showing the Emc10^{ASO2} target site. **(B)** qRT-PCR analysis shows significant upregulation of *Emc10* mRNA expression levels in the HPC of Ctrl^{ASO} treated-*Df(16)A*$^{+/-}$ compared to WT mice [one-way ANOVA, F (2, 19) = 20.92, P<0.0001; post hoc Tukey, P= 0.0018]. Following ASO treatment, *Emc10* expression is normalized to WT levels in Emc10^{ASO} treated-*Df(16)A*$^{+/-}$ compared to Ctrl^{ASO} treated-*Df(16)A*$^{+/-}$ mice (post hoc Tukey, P= <0.0001). **(C)** qRT-PCR analysis shows a significant up-regulation of *Emc10* mRNA expression levels in the PFC of Ctrl^{ASO} treated-*Df(16)A*$^{+/-}$ compared to WT mice [one-way ANOVA, F (2, 19) = 40.75, P= <0.0001; post hoc Tukey, P=<0.0001]. Following ASO treatment, *Emc10* expression is normalized to WT levels in the Emc10^{ASO} treated-*Df(16)A*$^{+/-}$ compared to Ctrl^{ASO} treated-*Df(16)A*$^{+/-}$ mice (post hoc Tukey, P=<0.0001). Ctrl^{ASO}-treated WT male mice: n=6, Ctrl^{ASO}-treated *Df(16)A*$^{+/}$ male mice: n=8, and Emc10^{ASO}-treated *Df(16)A*$^{+/}$ mice: n=8. **(D)** qRT-PCR analysis shows a significant up-regulation of *Emc10* mRNA expression levels in Somatosensory Cortex (SSC) of Ctrl^{ASO} treated-*Df(16)A*$^{+/-}$ compared to WT mice [one-way ANOVA, F (2, 18) = 21.53, P=<0.0001; post hoc Tukey, P= <0.0026]. Following ASO treatment, *Emc10* expression is normalized to WT levels in Emc10^{ASO} treated-*Df(16)A*$^{+/-}$ compared to Ctrl^{ASO} treated-*Df(16)A*$^{+/-}$ mice (post hoc Tukey, P=<0.0001). Ctrl^{ASO}-treated WT mice: n=6, Ctrl^{ASO}-treated *Df(16)A*$^{+/}$ mice: n=7, and Emc10^{ASO}-treated *Df(16)A*$^{+/}$ mice: n=8. **(E)** Ctrl^{ASO}-treated *Df(16)A*$^{+/-}$ mice show a robust SM deficit compared to Ctrl^{ASO}-treated WT mice as indicated by the significant difference in trial 2 interaction time upon reintroduction of a familiar juvenile mouse [three-way ANOVA for Trial X Genotype X Treatment Interaction matching by trial: F (1, 26) = 35.74 P<0.0001; post hoc Tukey, P= 0.0004]. A reduction in trial 2 interaction time indicates rescue of the SM deficit in Emc10^{ASO}-treated *Df(16)A*$^{+/-}$ compared to Ctrl^{ASO}-treated *Df(16)A*$^{+/-}$ mice (post hoc Tukey, P= 0.0255). [Ctrl^{ASO}-treated WT male mice: n=6, Ctrl^{ASO}-treated *Df(16)A*$^{+/}$ mice: n=8, Emc10^{ASO} treated WT mice: n=8, and Emc10^{ASO}-treated *Df(16)A*$^{+/}$ mice: n=8. **(F)** A negative difference score (trial 1-trial 2) confirms the SM deficit in Ctrl^{ASO}-treated adult *Df(16)A*$^{+/-}$ mice compared to WT littermates [two-way ANOVA for Genotype X Treatment interaction F (1, 26) = 35.74, P<0.0001; post hoc Tukey, P<0.0001. Increase in the difference score of *Df(16)A*$^{+/-}$ mice in the Emc10^{ASO}-vs Ctrl^{ASO}-treated group demonstrates SM rescue (post hoc Tukey, P<0.0001). **(G)** Y-maze task displayed memory impairments in adult *Df(16)A*$^{+/-}$ mice. Impaired short-term spatial memory in *Df(16)A*$^{+/-}$ mice shown by the reduced amount of delayed alternations (%) after a delay of 1h (P=0.0015). WT mice: n=12, *Df(16)A*$^{+/}$ mice: n=11. **(H)** Deficits in short-term spatial memory in the Y-maze task in Ctrl^{ASO}-treated adult *Df(16)A*$^{+/-}$ mice can be rescued in Emc10^{ASO}-treated *Df(16)A*$^{+/-}$ mice (one-way ANOVA, F(3, 25) = 6.727, P=0.0018, post hoc Tukey, P=0.0042) after 3-weeks of ASO-injection. Ctrl^{ASO}-treated WT mice: n=8, Emc10^{ASO} treated WT mice: n=8, Ctrl^{ASO}-treated *Df(16)A*$^{+/}$ mice: n=8 and Emc10^{ASO}-treated *Df(16)A*$^{+/}$ mice: n=5. **(I)** In a contextual fear memory assay, minimal freezing is observed on day 1 (left) with no significant changes across groups [two-way ANOVA for Genotype X Treatment interaction: F (1, 52) = 1.003, P=0.3211]. In the Ctrl^{ASO}-treated group, *Df(16)A*$^{+/-}$ mice show the expected contextual fear memory deficit compared to WT mice (right panel) [one-way ANOVA, F (3, 52) = 3.524 P=0.0212; post hoc Tukey, 0.0384]. Emc10^{ASO} treatment was not sufficient to fully rescue the learning deficit in *Df(16)A*$^{+/-}$ mice compared to Ctrl^{ASO}-treated WT levels (post hoc Tukey, P= 0.1045). However, there is increased freezing in *Df(16)A*$^{+/-}$ mice injected with Emc10^{ASO}-versus Ctrl^{ASO}-treated group, which results in a non-significant difference in freezing between Emc10^{ASO}-treated *Df(16)A*$^{+/-}$ and WT mice (two-way ANOVA for genotype x treatment F (1, 52) = 0.8524, P=0.3601; post hoc Tukey, P= 0.4676) indicating a partial rescue of the contextual fear memory deficit. Ctrl^{ASO}-treated WT: n=13 (9 males, 4 females), Emc10^{ASO} treated WT mice: n=14 (10 males, 4 females), Ctrl^{ASO}-treated *Df(16)A*$^{+/}$ mice: n=15 (11 males, 4 females and Emc10^{ASO}-treated *Df(16)A*$^{+/}$ mice: n=14 (10 males, 4 females). Unpaired students t-test, one-two- or three-way ANOVA as indicated. Data are presented as mean ± SEM, *P < 0.05, **P < 0.01, ***P < 0.01, ****P<0.0001.

In addition to SM deficits, mouse models of the 22q11.2 deletion show a spectrum of cognitive impairments in episodic and spatial memory as reflected, for example, in impaired performance in an Y-maze-based delayed alternations task that probes short-term spatial memory (58) and contextual fear conditioning a form of associative learning test used for studying episodic learning and spatial memory (5). We investigated the impact of ASO-mediated Emc10 reduction in the adult brain on both of these cognitive tasks. First, we confirmed that adult male *Df(16)A*$^{+/-}$ mice exhibit impaired short-term spatial memory during novelty exploration in a two-trial delayed alternation Y-maze task (**Fig. 5G**) as previously described for another mouse model of the

22q11.2 deletion (60). The total number of arm entries remained unchanged, indicating no alternations in locomotor activity (**Fig. S14B**). To determine whether reducing Emc10 expression in the brain via ASO treatment could rescue short-term spatial memory deficits, we tested a new cohort of *Df(16)A*$^{+/-}$mice and WT littermates 3-weeks following ASO administration (**Fig. 5H**). ASO-treated *Df(16)A*$^{+/-}$ mice exhibited a significant improvement in delayed alternations compared to *Df(16)A*$^{+/-}$ mice treated with control ASO (**Fig. 5H**). Furthermore, no significant differences in total number of arm entries were observed between the groups (**Fig. S14C**). We confirmed the reduction of *Emc10* levels in the ASO-treated animals through qRT-PCR assays of the HPC, PFC and SSC brain regions (**Fig. S14D-F**). In the contextual fear conditioning task, while ASO treatment was not sufficient to fully rescue the learning deficit in *Df(16)A*$^{+/-}$ mice to WT levels (**Fig. 5I**, right panel), there was a modest improvement in fear memory of ASO-treated *Df(16)A*$^{+/-}$ mice, since these mice did not differ significantly from the ASO-treated WT littermates. Interestingly, we have previously shown that genetic reduction of *Emc10* levels in *Df(16)A*$^{+/-}$ mice resulted in only partial restoration of deficits in contextual fear memory (19). Thus our finding faithfully recapitulates results from our previous constitutive genetic rescue assays (19) and likely indicates a more limited role of *Emc10* upregulation in the 22q11.2-linked fear memory deficits rather than requirement for additional treatment time or for earlier onset of *Emc10* normalization.

The application of ASOs as a novel therapeutic strategy has seen a significant rise in recent years, in part due to their versatility in durably modifying RNA transcripts. Therefore, we investigated the longevity of ASO-mediated repression of *Emc10* as an indicator of future therapeutic relevance for the treatment of 22q11.2DS. To this end, we conducted the SM and Y-maze assays on a new cohort of *Df(16)A*$^{+/-}$ mice at 3-4 weeks and 8-9 weeks post injection with Emc10^{ASO2} (**Fig. 6A**). We observed behavioral rescue in Emc10^{ASO2}-treated *Df(16)A*$^{+/-}$ mice in the SM assay at three weeks (**Fig. 6B**, left panel) and in the Y-maze assay at four weeks post ASO-administration (**Fig. 6C**, left panel) in accordance to our previous findings (**Fig. 5F, H**). Remarkably, we replicated these results at 8-9 weeks post injection, demonstrating sustained behavioral rescue of SM (**Fig. 6B**, right panel) and spatial memory deficits (**Fig. 6C**, right panel). Importantly, locomotor activity remained unchanged in the Y-maze assays at both, four weeks (**Fig. S14G**) and nine weeks (**Fig. S14H**) post injection. Finally, we confirmed the downregulation of *Emc10* in ASO-treated animals via qRT-PCR assays of the HPC, PFC, and SSC brain regions at ten weeks post-treatment (**Fig. 6D-F**). These results suggest that normalizing *Emc10* expression in the brain can ameliorate social and spatial memory deficits in adult *Df(16)A*$^{+/-}$ mice in a time period of at least two months.

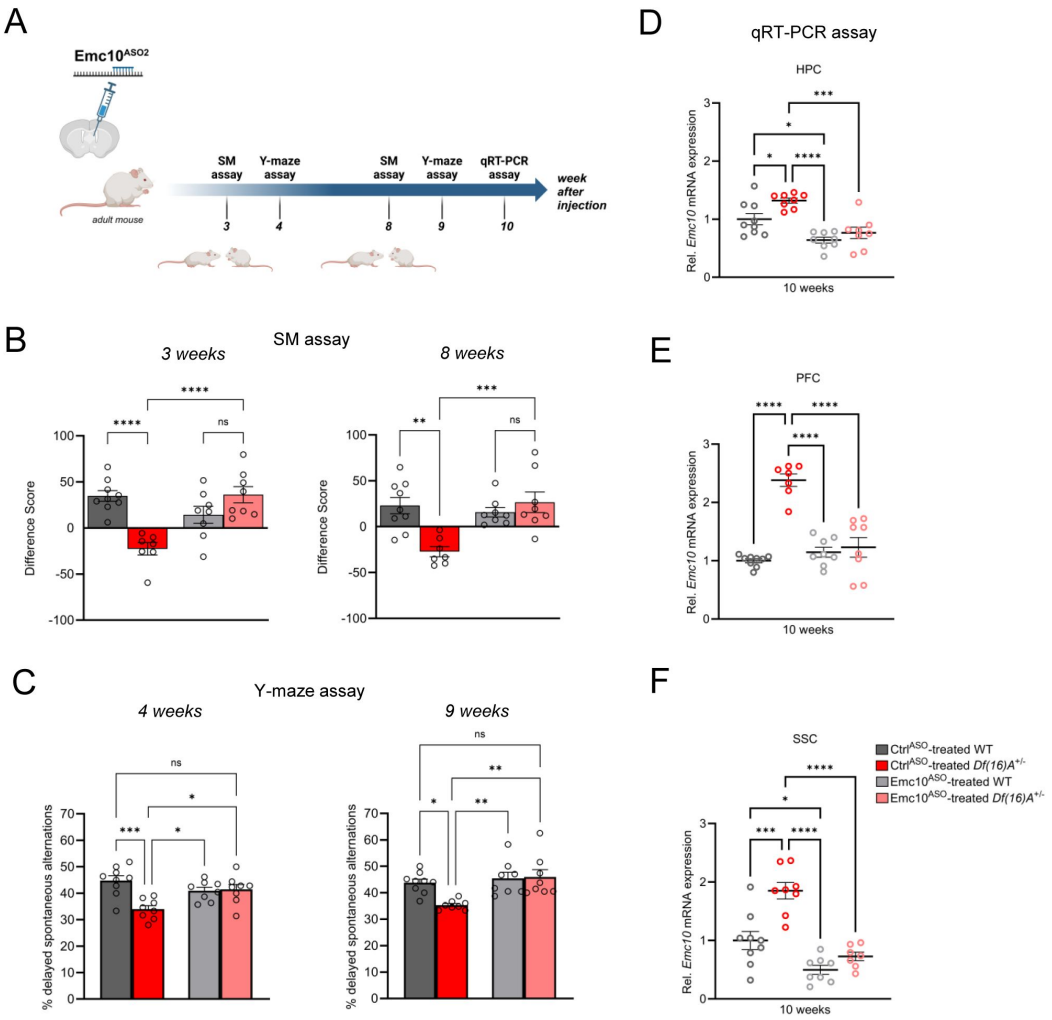

Figure 6

Sustained rescue of cognitive deficits in *Df(16)A*$^{+/-}$ mice following ASO administration.

(A) Experimental timeline of Emc10^{ASO2}-treated adult *Df(16)A*$^{+/-}$ mice to determine long-term rescue effect of Emc10 de-repression. This panel was created with *BioRender.com*. **(B-C)** Sustained ASO effect on behavioral rescue of Emc10^{ASO}-treated *Df(16)A*$^{+/-}$ mice in HPC- and PFC-dependent tasks. **(B)** Rescue of SM deficit in *Df(16)A*$^{+/-}$ mice after 3- and 8-weeks of ASO injection. After 3-weeks of ASO treatment (left panel), a negative difference score (trial 1-trial 2) confirms the SM deficit in Ctrl^{ASO}-treated adult *Df(16)A*$^{+/-}$ mice compared to WT littermates [two-way ANOVA for Genotype X Treatment interaction F (1, 28) = 26.20, P<0.0001; post hoc Tukey, P<0.0001]. Increase in the difference score of *Df(16)A*$^{+/-}$ mice in the Emc10^{ASO}-vs Ctrl^{ASO}-treated group demonstrates SM rescue (post hoc Tukey, P<0.0001). After 8-weeks of ASO treatment (right panel), a negative difference score (trial 1-trial 2) confirms the SM deficit in Ctrl^{ASO}-treated adult *Df(16)A*$^{+/-}$ mice compared to WT littermates [two-way ANOVA for Genotype X Treatment interaction F (1, 28) = 13.36, P=0.0010; post hoc Tukey, P=0.0012. Increase in the difference score of *Df(16)A*$^{+/-}$ mice in the Emc10^{ASO}- vs Ctrl^{ASO}-treated group demonstrates prolonged SM rescue (post hoc Tukey, P=0.0007). Ctrl^{ASO}-treated WT mice: n=9, Ctrl^{ASO}-treated *Df(16)A*$^{+/}$ mice: n=7, Emc10^{ASO}-treated WT mice: n=8 and Emc10^{ASO}-treated *Df(16)A*$^{+/}$ mice: n=8. **(C)** Y-maze task displayed rescue of memory impairments in adult *Df(16)A*$^{+/-}$ male mice 4- and 9-weeks after Emc10^{ASO} injection. Deficits in short-term spatial memory shown by the reduced number of delayed alternations (%) in Ctrl^{ASO}-treated adult *Df(16)A*$^{+/-}$ mice can be rescued in Emc10^{ASO}-treated *Df(16)A*$^{+/-}$ mice after 4-weeks of ASO injection (left panel) [one-way ANOVA, F(3, 29) = 7.585, P=0.0007, post hoc Tukey, P=0.0193]. Deficits in short-term spatial memory in Ctrl^{ASO}-treated adult *Df(16)A*$^{+/-}$ mice can be rescued in

Emc10^{ASO}-treated *Df(16)A*$^{+/-}$ mice after 4-weeks of ASO injection (left panel) [one-way ANOVA, F(3, 29) = 7.585, P=0.0007, post hoc Tukey, P=0.0193]. Deficits in short-term spatial memory in Ctrl^{ASO}-treated adult *Df(16)A*$^{+/-}$ mice can be rescued in Emc10^{ASO}-treated *Df(16)A*$^{+/-}$ mice also after 9-weeks of ASO injection (right panel) [one-way ANOVA, F(3, 29) = 6.547, P=0.0016, post hoc Tukey, P=0.0029]. Ctrl^{ASO}-treated WT mice: n=9, Ctrl^{ASO}-treated *Df(16)A*$^{+/}$ mice: n=8, Emc10^{ASO}-treated WT mice: n=8 and Emc10^{ASO}-treated *Df(16)A*$^{+/}$ mice: n=8. **(D-F)** Sustained Emc10 de-repression after two months of Emc10^{ASO} injection. ASO-mediated inhibition of *Emc10* in different brain regions of *Df(16)A*$^{+/-}$ mice after 10-weeks of injection. **(D)** qRT-PCR analysis shows significant upregulation of *Emc10* mRNA expression levels in the HPC of Ctrl^{ASO} treated-*Df(16)A*$^{+/-}$ compared to WT mice [one-way ANOVA, F (3, 29) = 13.97, P<0.0001; post hoc Tukey, P=0.0331]. Following ASO treatment, *Emc10* expression is normalized to WT levels in Emc10^{ASO} treated-*Df(16)A*$^{+/-}$ compared to Ctrl^{ASO} treated-*Df(16)A*$^{+/-}$ mice (post hoc Tukey, P= <0.0002). Ctrl^{ASO}-treated WT mice: n=9, Ctrl^{ASO}-treated *Df(16)A*$^{+/}$ mice: n=8, Emc10^{ASO}-treated WT mice: n=8 and Emc10^{ASO}-treated *Df(16)A*$^{+/}$ mice: n=8. **(E)** qRT-PCR analysis shows a significant up-regulation of *Emc10* mRNA expression levels in the PFC of Ctrl^{ASO} treated-*Df(16)A*$^{+/-}$ compared to WT mice [one-way ANOVA, F (3, 28) = 32.47, P<0.0001; post hoc Tukey, P<0.0001]. Following ASO treatment, *Emc10* expression is normalized to WT levels in the Emc10^{ASO} treated-*Df(16)A*$^{+/-}$ compared to Ctrl^{ASO} treated-*Df(16)A*$^{+/-}$ mice (post hoc Tukey, P<0.0001). Ctrl^{ASO}-treated WT mice: n=9, Ctrl^{ASO}-treated *Df(16)A*$^{+/}$ mice: n=7, Emc10^{ASO}-treated WT mice: n=8 and Emc10^{ASO}-treated *Df(16)A*$^{+/}$ mice: n=8. **(F)** qRT-PCR analysis shows a significant up-regulation of *Emc10* mRNA expression levels in Somatosensory Cortex (SSC) of Ctrl^{ASO} treated-*Df(16)A*$^{+/-}$ compared to WT mice [one-way ANOVA, F (3, 28) =23.18, P<0.0001; post hoc Tukey, P=0.0001]. Following ASO treatment, *Emc10* expression is normalized to WT levels in Emc10^{ASO} treated-*Df(16)A*$^{+/-}$ compared to Ctrl^{ASO} treated-*Df(16)A*$^{+/-}$ mice (post hoc Tukey, P<0.0001). Ctrl^{ASO}-treated WT mice: n=9, Ctrl^{ASO}-treated *Df(16)A*$^{+/}$ mice: n=8, Emc10^{ASO}-treated WT mice: n=8 and Emc10^{ASO}-treated *Df(16)A*$^{+/}$ male mice: n=7. One- or two-way ANOVA as indicated. Data are presented as mean ± SEM, *P < 0.05, **P < 0.01, ***P < 0.01, ****P<0.0001.

Discussion

Despite an understanding of the molecular mechanisms of 22q11.2DS, especially ones related to abnormal expression and processing of miRNAs (5, 7, 19, 39, 59), we still do not have a promising therapeutic avenue for the cognitive and neuropsychiatric symptoms associated with the 22q11.2 deletion. By leveraging our recent understanding of the molecular, cellular and behavioral consequences of 22q11.2-linked miRNA dysregulation, the present study represents an advancement towards developing a potential therapeutic strategy in two ways:

First, we show that 22q11.2 deletion results in abnormal processing of miRNAs in human neurons and in turn drives upregulation of *EMC10* levels as previously described in mouse models (5). Effective reduction to near WT levels or even complete depletion of *EMC10* leads to restoration of key alterations in morphological and functional neuronal maturation emerging due to 22q11.2 deletions. The miRNA regulatory mechanism underlying *EMC10* upregulation and the restoration of cellular deficits are very similar to the ones we previously described in *Df(16)A*$^{+/-}$ mice, highlighting the robustness of this molecular alteration as well as the translational value of using animal models to probe the link between *Emc10* upregulation and 22q11.2-linked behavioral dysfunction.

Second, we show that normalization of *Emc10* levels in adult *Df(16)A*$^{+/-}$ mouse brain, by ASO-mediated targeted knockdown, is effective in rescuing SM deficits (which emerge during postnatal development and are present as early as postnatal day 22) as well as short-term spatial memory deficits. Significantly, these improvements in cognition were sustained for over two months post-ASO administration. These findings strongly suggest that at least for a subset of 22q11.2-associated cognitive deficits it is the sustained miRNA dysregulation and elevation of *Emc10* throughout the adult life that interferes with the underlying neural processes rather than an irreversible impact on brain maturation during early development and demonstrate the therapeutic potential for treating a wide range of cognitive symptoms associated with 22q11.2DS.

In vivo delivery of ASOs offers a potential venue for emerging treatments of genetically driven and postnatally reversible symptoms of neurodevelopmental disorders (NDDs) focusing in reduction of culprit gene expression via sequence-specific knockdown of mRNA transcripts (60). A common challenge in efforts to employ gene-knockdown therapies for dosage-sensitive genes such as *EMC10* is restricting target gene expression within optimal levels to avoid potential toxicity due to target hyper-knockdown or complete elimination (61–64). A large number of relatively rare LoF variants or potentially damaging missense variants have been identified in the human *EMC10* gene among likely healthy individuals in gnomAD (63, 65) which is depleted of individuals known to be affected by severe NDDs. Taken together with our previous analysis of constitutive heterozygous Emc10 knockout mice (19) that showed no evidence of motor deficits or anxiety-like behavior, these observations strongly suggest that partial reductions in Emc10 levels of approximately 50% are well tolerated at the organismal level and do not result in behavioral abnormalities. The highest dose for both Emc10-specific ASOs used in mutant *Df(16)A*$^{+/-}$mice was limited to ~300 µg and reduced *Emc10* mRNA to either normal or below normal (30-50% of WT) expression while attaining full behavioral rescue. While higher dose may be required to ameliorate other behavioral deficits (61, 63), it should be noted that an acute injection of 700µg Emc10^{ASO} in WT mice that resulted in ~50% reduction of Emc10 levels (**Fig. S13**) did not cause secondary cellular and behavioral toxicity. Thus, available evidence indicates that therapeutically effective ASO-mediated normalization of *EMC10* levels can be up- or down-titrated within a well-tolerated range. However, further work is needed to establish a comprehensive safety profile, including the evaluation of non-cognitive phenotypes, to fully validate the therapeutic potential of Emc10-targeting approaches. Additionally, the long-term effects of Emc10 reduction beyond two months post-injection require further investigation to determine the full extent of its therapeutic benefits. Future studies will also explore whether ASO-mediated normalization of adult Emc10 levels can restore additional 22q11.2 behavioral and cognitive alterations and whether earlier postnatal ASO treatment could prevent the onset of behavioral deficits or mitigate those resistant to adult interventions.

In addition to reduction of *Emc10* expression our findings have implications for therapeutic interventions aiming to manipulate its downstream targets. In that respect, it is attractive to speculate that different *EMC10* upregulation-linked phenotypes and their developmental requirements may be driven by dysregulation of distinct, individually or in combinations, downstream EMC targets. Such targets are typically multi-transmembrane domain (TMD) proteins (17, 18, 66) that contain low-hydrophobicity TMDs which are hard to insert into ER membrane and thus require the aid of EMC as a membrane insertase (11, 12, 17). Identification of neurotransmitter receptors, channels, and transporters whose biogenesis, trafficking and membrane insertion are affected by EMC10 upregulation could help establish a link between such targets and 22q11.2-related behavioral dysfunction and guide efforts to develop treatments for specific 22q11.2 deletion symptoms.

Overall, by highlighting the manipulation of EMC10 expression and activity, as well as its downstream targets, as a promising alternative or augmentation to currently available treatments, and emphasizing a broad temporal window for therapeutic and preventive intervention in 22q11.2 deletion-associated cognitive and behavioral symptoms, our results lay the foundation for developing mechanism-based therapeutic strategies. These strategies aim to leverage insights from both human and animal models to improve clinical outcomes in precision medicine for neuropsychiatric disorders. Furthermore, our findings may have broader implications for understanding the role of miRNA dysregulation and ER-mediated membrane protein translocation in other neurodevelopmental and neuropsychiatric disorders with overlapping genetic or phenotypic features.

Materials and Methods

Mice

We used *Emc10* conditional knockout (see below) and *Df(16)A*$^{+/-}$ mice (5) in C57BL/6J background. *Df(16)A*$^{+/-}$ male mice were crossed to C57BL/6J female mice to obtain either *Df(16)A*$^{+/-}$ or WT littermates. For further details, see Supplemental Materials and Methods.

Generation of *Emc10* conditional knockout compound mouse lines

To manipulate the expression of the *Emc10* gene in *Df(16)A*$^{+/-}$mice we used a *Emc10* conditional 'knockout-first' mouse design by conducting Cre- and Flip-dependent genetic switch strategies as described earlier (67). This approach enables postnatal manipulation of *Emc10* expression at its endogenous locus keeping Emc10 expression within its physiological levels. *Emc10*$^{tm1a+/}$ mice (2310044h10rik-Tm1a, MRC Harwell Institute, Oxfordshire, UK) were crossed to a germline Flp mouse line (B6.129S4-Gt(ROSA)26Sortm1(FLP1)Dym/RainJ_JAX:009086) that activates global *Flp* function and leads to the deletion of the frt-flanked sequence(s) in the offspring. The *Emc10*^{tm1c} offspring from these cross carries a *loxP* flanked WT *Emc10* allele. We used UBC-Cre/ERT2 mice (B6.Cg-Ndor1 Tg(UBC-cre/ERT2)1Ejb /2J_JAX:008085) in crosses to generate compound *Emc10*$^{tm1c+/-}$; UBC-cre/ERT2; *Df(16)A*$^{+/-}$mice.

Cell line differentiation

The cell line donors used in this study are listed in Supplementary Table S1. Human iPSC lines were maintained in mTeSR Plus medium on Matrigel coated tissue culture plate and neuronal induction of hiPSC lines into cortical neurons were conducted by using either a combination of small molecule inhibitors or NGN2 overexpression approaches. For further details, see Supplemental Material and Methods.

Genome editing of Q6(22q11.2) hiPCS line

We generated derivatives of the Q6 (22q11.2) hiPSC line carrying either heterozygous (Q6/EMC10^{HET}) or homozygous (Q6/EMC10^{HOM}) *EMC10* LoF mutations using standard CRISPR/Cas9 genome editing approaches. For further details, see Supplemental Materials and Methods.

ASOs

Mouse *Emc10*-targeting ASOs used in these studies were 20 bases in length, chimeric 2'-O-(2-methoxyethyl) (MOE)/DNA) oligonucleotides with phosphodiester and phosphorothioate linkages. The central gap of 10 deoxynucleotides is flanked on its 5' and 3' sides by five MOE modified nucleotides. Oligonucleotides were synthesized at Ionis Pharmaceuticals (Carlsbad, CA, USA) as described previously (68, 69). ASOs were solubilized in 0.9% sterile saline or PBS.

Stereotactic Intracerebroventricular (ICV) Injections of ASOs

ASOs were delivered to 8 weeks old mice via ICV injections using a Hamilton syringe (Hamilton Company, Reno, NV, USA) connected to a motorized Stoelting Quintessential Stereotaxic Injector QSI/53311 (Stoelting Co., Wood Dale, IL, USA). For further details, see Supplemental Materials and Methods.

Analysis of dendritic complexity

iNs were prepared on coverslips, fixed at DIV21 and immunostained for TBR1 and MAP2 to identify dendritic branches. For further details, see Supplemental Materials and Methods.

Calcium imaging

Calcium imaging was performed as previously described (70) with a few modifications. For further details, see Supplemental Materials and Methods.

Bulk RNAseq and bioinformatic analysis of mouse hippocampal samples

Total RNA was isolated from 4 WT $Ctrl^{ASO1}$, 4 WT $Emc10^{ASO1}$, 5 Df16 $Ctrl^{ASO1}$ and 4 Df16 $Emc10^{ASO1}$ treated male hippocampi. Stranded polyA+ enriched RNA sequencing libraries were prepared at the Columbia Genome Center (Columbia University, New York, USA) to generate 40 million paired-end reads on Illumina Novaseq 6000 instrument using STRYPOLYA library prep kit. For further details, see Supplemental Material and Methods.

Bulk RNAseq and small RNA/miRNAseq of hiPSC-derived cortical neurons

Total RNA was extracted from hiPSC-derived cortical neurons using the miRVana miRNA isolation kit (#AM1560, Ambion, Thermo Fisher Scientific, Waltham, MA, USA) before bulk RNAseq (paired-ended sequencing; llumina NovaSeq 6000) or miRNAseq (single-end sequencing; Illumina Hiseq 2500) were performed. For further details, see Supplemental Material and Methods.

Behavioral assays

Mice were 11-17 weeks old at the time of behavioral testing except of the social memory assay in juveniles which was performed in 3 week old animals. Behavior was assayed 3-9 weeks following surgical delivery of ASOs or 1 week following TAM/corn oil treatment. The following behavioral assays were performed in this study: Open field assay, social memory assay, contextual fear conditioning and Y-maze delayed alternation task. For further details, see Supplemental Material and Methods. The experimenter was blind to mouse genotype and treatments while performing behavioral assays and data analysis. Animals were given at least one-week intervals between behavioral tests.

Statistical Analysis

Data were analyzed using GraphPad Prism (Graphpad Software, Inc., San Diego, CA, USA). Data were evaluated as indicated, using either unpaired two-tailed t-test, Kolmogorov–Smirnov test, one-way, two-way or three-way analysis of variance (ANOVA) tests followed by post hoc Tukey's multiple comparison test for comparisons across all groups. Data are presented as mean ±SEM. P values for each comparison are described in the figure legends.

Supplementary information

Supplementary Figures

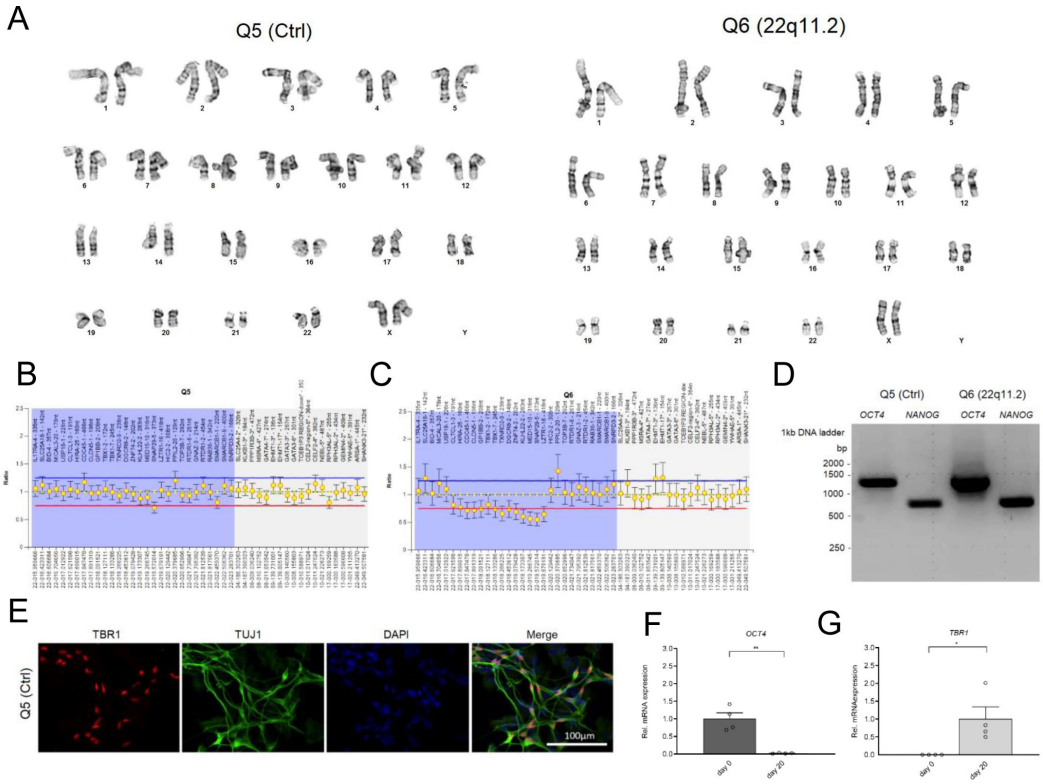

Fig. S1.

Validation and characterization of hiPSCs and hiPSC-derived neurons.

(A) Characterization of Q5 (Ctrl) and Q6 (22q11.2) hiPS cells demonstrate normal karyotype distribution in both lines. **(B-D)** Characterization of the Q5 and Q6 hiPSC lines. Multiplex Ligation-dependent Probe Amplification (MLPA) assay of gene copies within and around 22q11.2 locus for Q5 (Ctrl) **(B)** and Q6 (22q11.2) **(C)** line shows that copy number of genes in the 22q11.2 locus (highlighted in light blue) are reduced by half in the Q6 (22q11.2) hiPSC line. **(D)** qRT-PCR assays of embryonic stem cell marker *OCT4/POU5F1* and *NANOG* shows that they are highly expressed in both hiPSC lines (Q5 Ctrl and Q6 22q11.2). **(E)** TBR1 and TUJ1 expression of cortical neurons by immunocytochemistry at day 20 of differentiation indicates the efficiency of hiPSC differentiation into cortical neurons. TBR1 (red), TUJ1 (green) and DAPI (blue). Scale bar: 100 µm. **(F-G)** Time-course qRT-PCR analysis at day 0 and day 20 of differentiation of human pluripotency marker **(F)** *OCT4/POU5F1* (P= 0.0012) and **(G)** *TBR1* (P= 0.0273), a preplate, subplate and cortical Layer VI neuron marker in Q5 (Ctrl) line. Day 0: n=4, Day 20 n=4. Data are presented as mean ± SEM, unpaired two-tailed t-test, *P<0.05, **P<0.01.

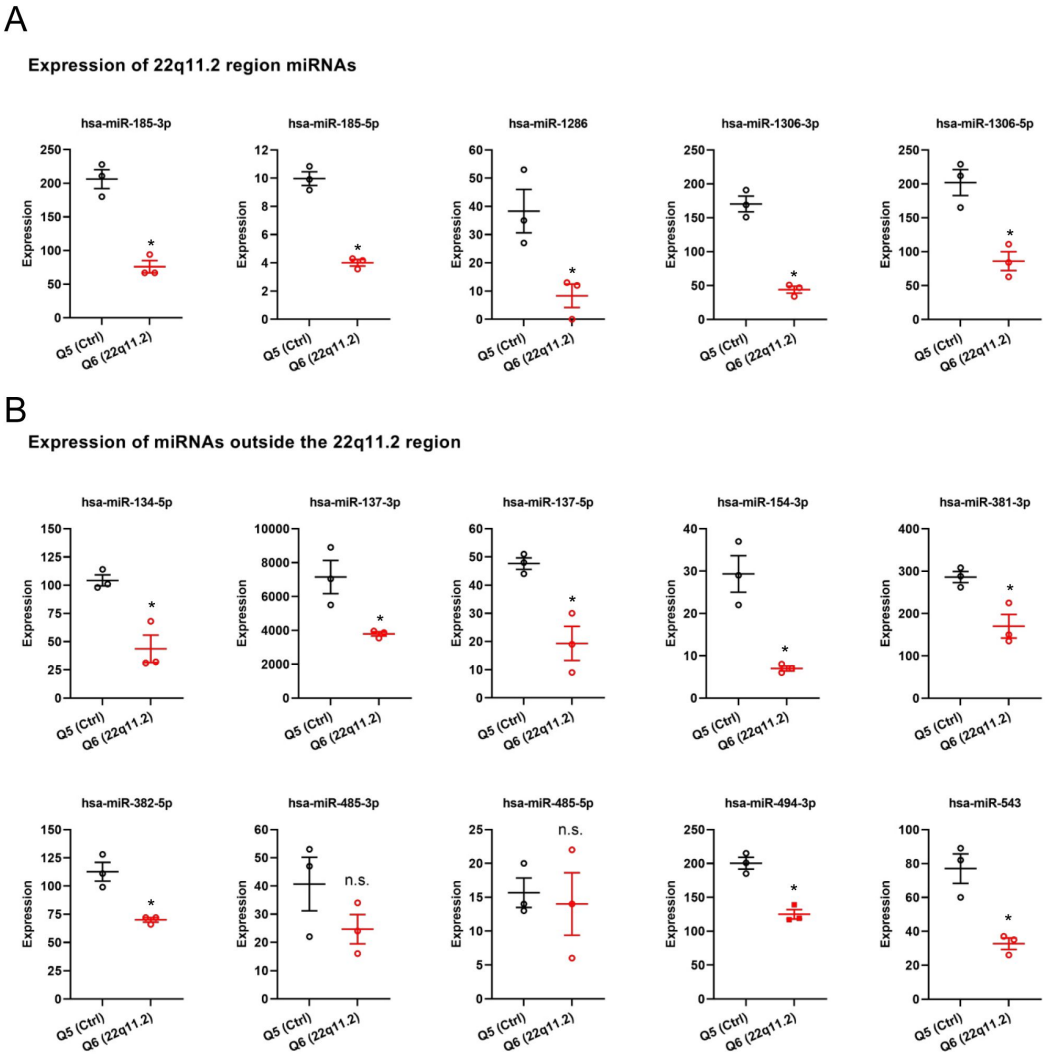

Fig. S2

Expression profile of selected miRNAs in Q5 (Ctrl) and Q6 (22q11.2) cortical neurons at day 8 of differentiation.

(A) 22q11.2 region residing miRNAs and **(B)** selected miRNAs residing outside the 22q11.2 region (Q5 n=3, Q6 n=3). Data are presented as mean ± SEM; *P < 0.05, Students t-test.

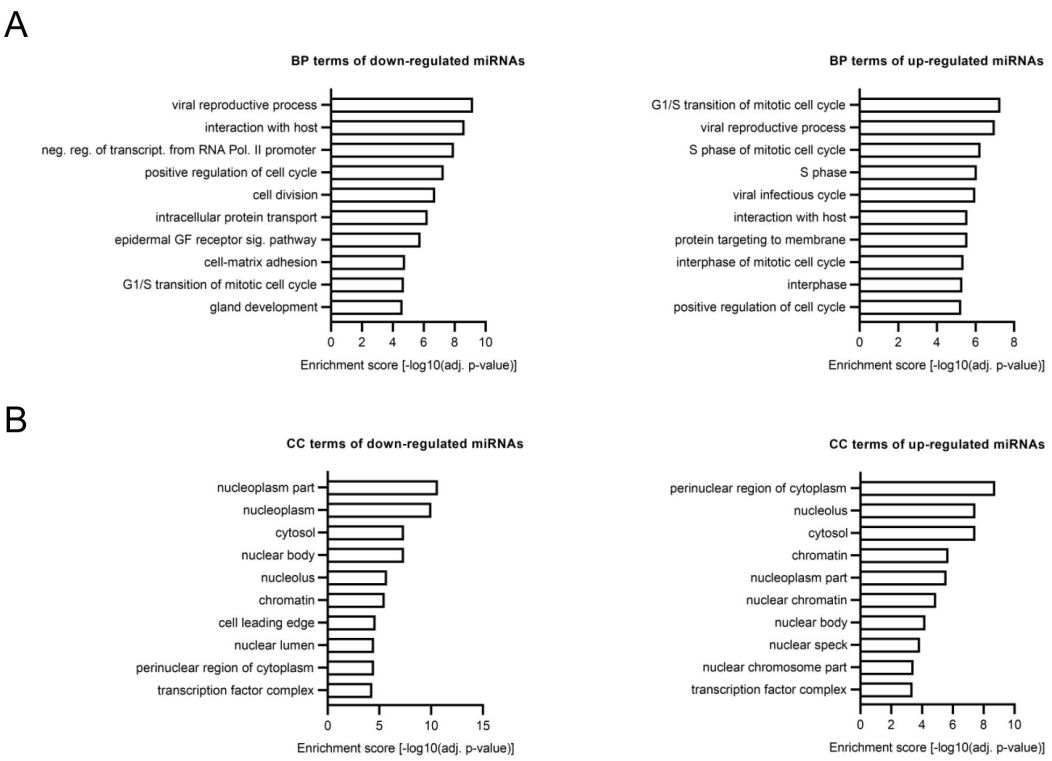

Fig. S3

GO-term analysis of altered miRNA expression in hiPSC-derived cortical neurons with 22q11.2 deletion.

(A-B) Gene Ontology (GO) term enrichment analysis of up- and down-regulated DEmiRs highlighted cell cycle and cell division relevant terms. **(A)** Biological Process. **(B)** Cellular Component.

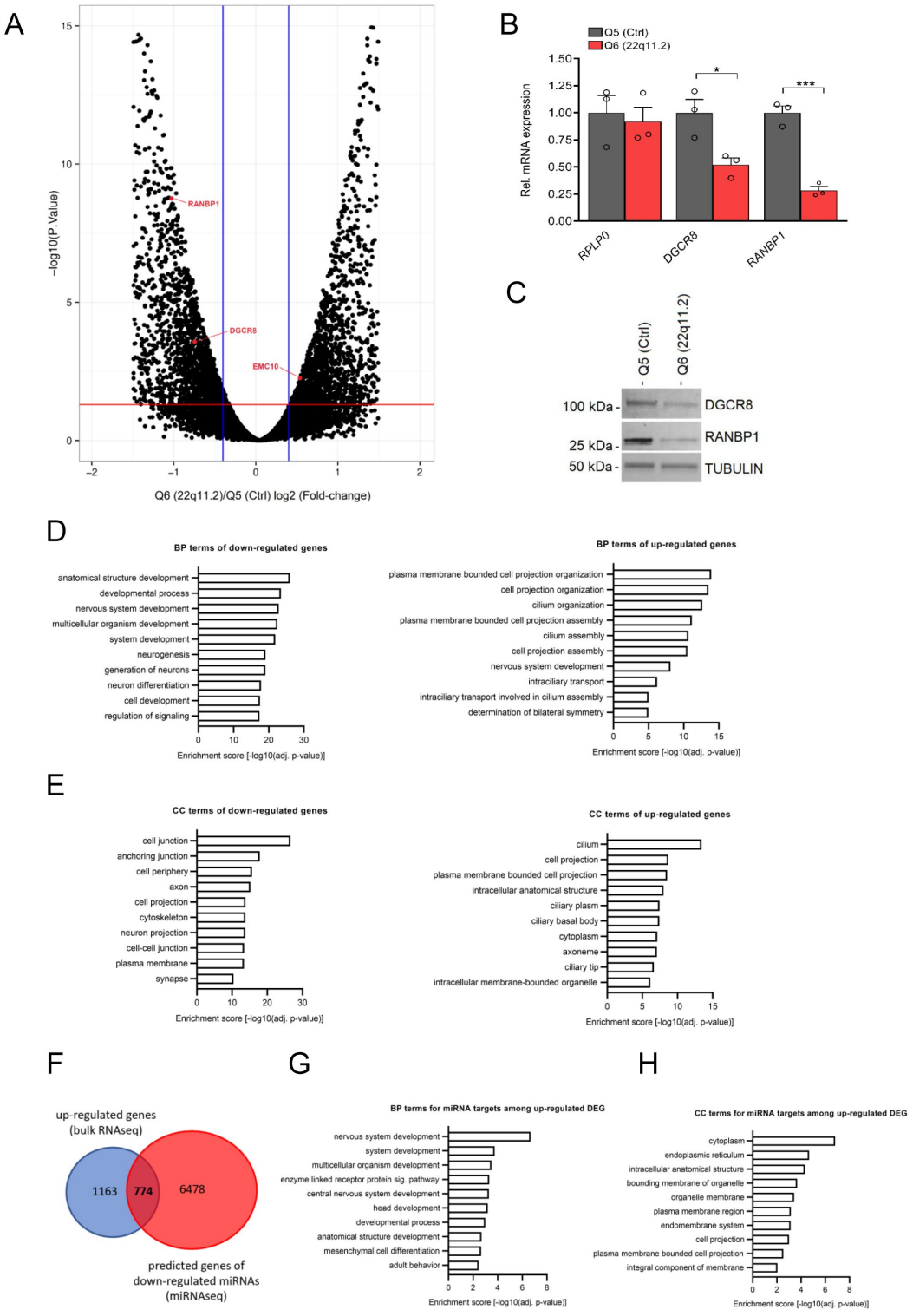
A
−log10(P.Value)
RANBP1
DGCR8
EMC10
Q6 (22q11.2)/Q5 (Ctrl) log2 (Fold-change)
B
Q5 (Ctrl)
Q6 (22q11.2)
Rel. mRNA expression
RPLP0
DGCR8
RANBP1
C
Q5 (Ctrl)
Q6 (22q11.2)
100 kDa
25 kDa
50 kDa
DGCR8
RANBP1
TUBULIN
D
BP terms of down-regulated genes
anatomical structure development
developmental process
nervous system development
multicellular organism development
system development
neurogenesis
generation of neurons
neuron differentiation
cell development
regulation of signaling
Enrichment score [-log10(adj. p-value)]
BP terms of up-regulated genes
plasma membrane bounded cell projection organization
cell projection organization
cilium organization
plasma membrane bounded cell projection assembly
cilium assembly
cell projection assembly
nervous system development
intraciliary transport
intraciliary transport involved in cilium assembly
determination of bilateral symmetry
Enrichment score [-log10(adj. p-value)]
E
CC terms of down-regulated genes
cell junction
anchoring junction
cell periphery
axon
cell projection
cytoskeleton
neuron projection
cell-cell junction
plasma membrane
synapse
Enrichment score [-log10(adj. p-value)]
CC terms of up-regulated genes
cilium
cell projection
plasma membrane bounded cell projection
intracellular anatomical structure
ciliary plasm
ciliary basal body
cytoplasm
axoneme
ciliary tip
intracellular membrane-bounded organelle
Enrichment score [-log10(adj. p-value)]
F
up-regulated genes
(bulk RNAseq)
1163
774
6478
predicted genes of
down-regulated miRNAs
(miRNAseq)
G
BP terms for miRNA targets among up-regulated DEG
nervous system development
system development
multicellular organism development
enzyme linked receptor protein sig. pathway
central nervous system development
head development
developmental process
anatomical structure development
mesenchymal cell differentiation
adult behavior
Enrichment score [-log10(adj. p-value)]
H
CC terms for miRNA targets among up-regulated DEG
cytoplasm
endoplasmic reticulum
intracellular anatomical structure
bounding membrane of organelle
organelle membrane
plasma membrane region
endomembrane system
cell projection
plasma membrane bounded cell projection
integral component of membrane
Enrichment score [-log10(adj. p-value)]

Fig. S4

Altered gene expression in hiPSC-derived cortical neurons from 22q11.2 deletion carriers.

(A) Volcano plot showing differential gene expression in cortical neurons at day 8 of differentiation. Significantly differentially expressed genes (FDR<5%) are shown above red line; Q5 (Ctrl) n=3, Q6 (22q11.2) n=3. 1937/2094 genes were significantly up- and downregulated in Q6 (22q11.2) hiPSC-derived cortical neurons, respectively. 22q11.2 deletion region residing genes *RANBP1* and *DGCR8* as well as *EMC10* are highlighted. **(B)** qRT-PCR analysis confirming reduction of *DGCR8* (P= 0.0261) and *RANBP1* (P= 0.0.0006) mRNAs but not for the housekeeping control *RPLP0* (P= 0.7155) gene at day 8 of differentiation in Q6 (22q11.2) compared to Q5(Ctrl) lines derived cortical neurons (Q5: n=3, Q6: n=3). **(C)** Western blot analysis showing reduced amount of DGCR8 and RANBP1 protein in Q6 (22q11.2) line derived cortical neurons at day 8 of differentiation. Tubulin was probed as a loading control. **(D-E)** Gene Ontology (GO) term enrichment analysis of up- and down-regulated DEGs reveals several neuronal related components. **(D)** Biological Process. **(E)** Cellular Component. **(F)** Intersection of predicted miRNA targets and gene expression analysis. Venn diagram highlighting up-regulated DEGs (from bulk RNAseq) that are predicted targets of down-regulated miRNAs (774). **(G-H)** Gene Ontology (GO) term enrichment analysis of predicted targets reveals several neuronal related components for the up-regulated genes. **(G)** Biological Process. **(H)** Cellular Component.

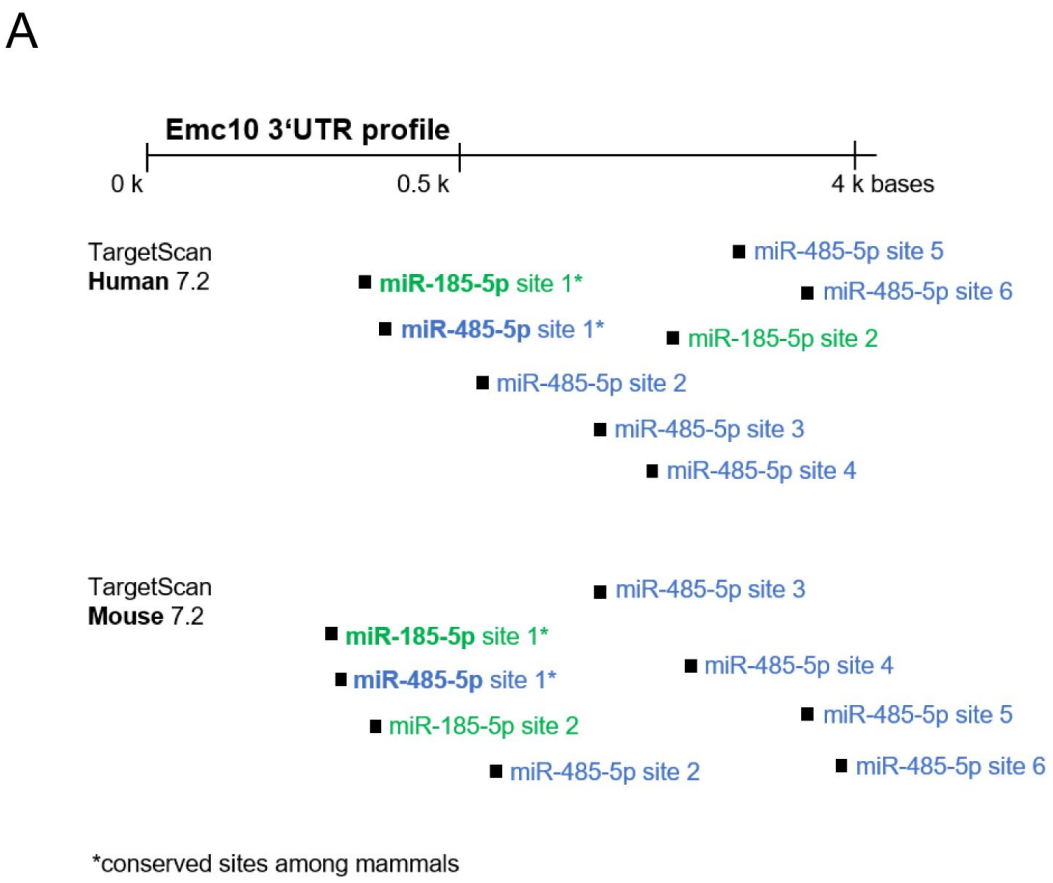

Fig. S5

Predicted miRNA targets.

(A) Schematic of human and mouse *Emc10* 3'UTR showing miR-185 (green) and miR-485 (blue) binding sites predicted by TargetScan. Conserved target sites in mammals are marked with an asterisk. Specific binding site positions in *Emc10* 3'UTR are indicated in brackets. Human *EMC10* 3'UTR: miR-185-5p site 1* (467–474), site 2 (2807–

2813), miR-485-5p site 1* (473–479), site 2 (585–591), site 3 (1530–1536), site 4 (1996–2002), site 5 (3516–3522), site 6 (4158–4164). Mouse *Emc10* 3'UTR: miR-185-5p site 1* (400–407), site 2 (454–460), miR-485-5p site 1* (406–412), site 2 (513–519), site 3 (796–802), site 4 (2842–2848), site 5 (4013–4020), site 6 (4576–4582).

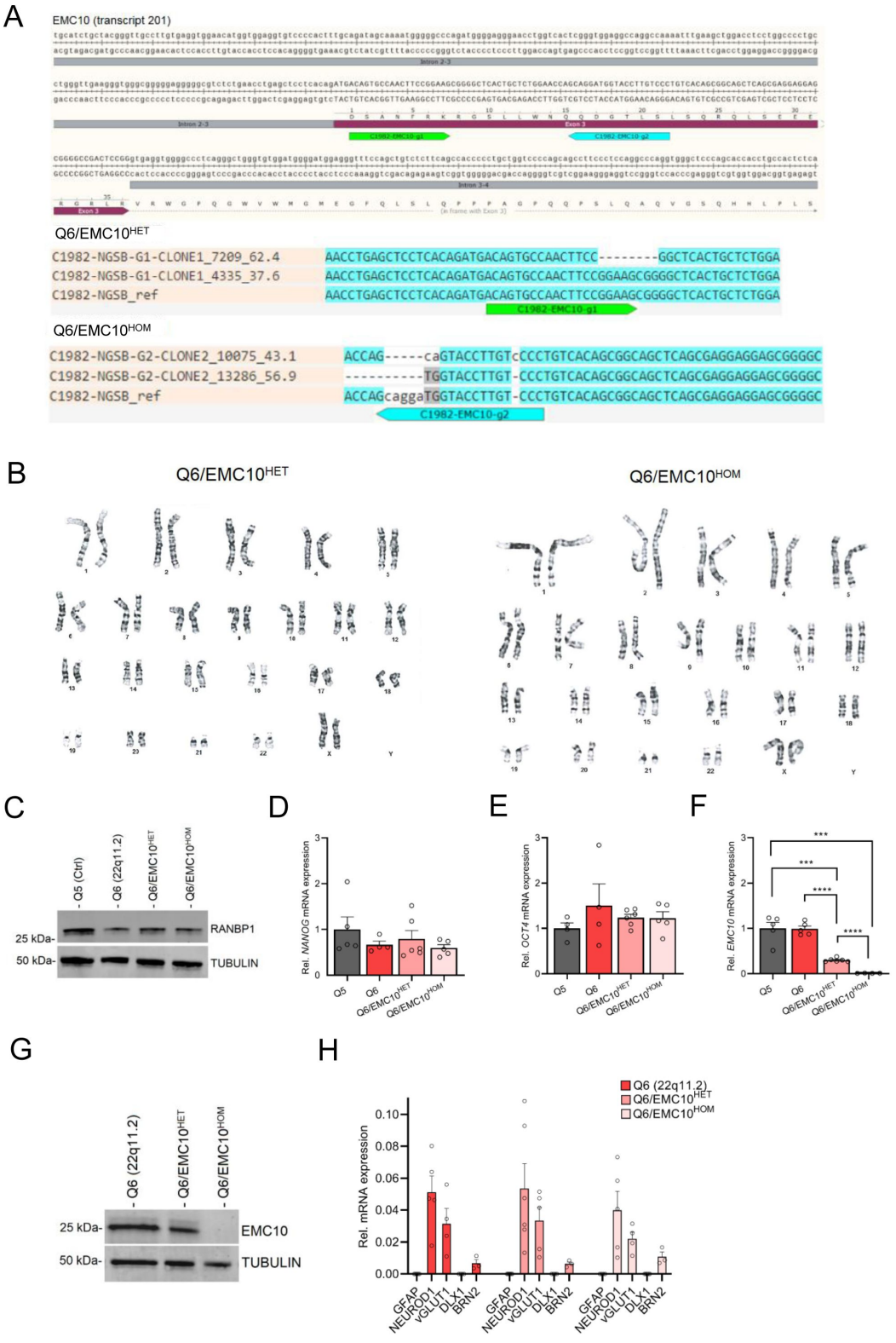

Fig. S6

Characterization of hiPSC lines carrying an *EMC10* LoF mutation.

(A) CRISPR/Cas9 genome editing in Q6 (22q11.2) hiPSCs to obtain *EMC10* LoF mutation lines. Two 20bp guided RNAs (gRNAs) were designed to specifically target the *EMC10* exon 3 region (transcript 201, ENNST00000334976.11), to generate a frameshift mutation as indicated by the green (EMC10-g1) and blue (EMC10-g2) arrow in the gRNA profiles at *EMC10* locus (**Fig. S6A**, upper panel). Upper panel (**Fig. S6A**): gRNA design and profile at the targeted *EMC10* locus that leads to frameshift mutations. Lower panel (**Fig. S6A**): Genotyping of positive clones for Q6/EMC10^{HET} and Q6/EMC10^{HOM} lines confirms frameshift mutation. **(B)** Characterization of Q6/EMC10^{HET} and Q6/EMC10^{HOM} hiPS cells demonstrate normal karyotype distribution **(C-G)** Western Blot assay and qRT-PCR assays in hiPSC lines. **(C)** Western blot analysis confirmed reduction of RANBP1 protein levels in Q6, Q6/EMC10^{HET} and Q6/EMC10^{HOM} lines. Embryonic stem cell marker **(D)** *NANOG* and **(E)** *OCT4/POU5F1* are highly expressed in all four hiPSC lines assayed. **(F)** qRT-PCR assay in hiPSC lines. *EMC10* expression is reduced or abolished in Q6/EMC10^{HET} line (P=0.0002) and Q6/EMC10^{HOM} line (P=0.0003), respectively, when compared to Q5 (Ctrl) line. Note that *EMC10* is not upregulated in Q6 hiPSCs. Q5 (Ctrl) n=5, Q6 (22q11.2) n=5, Q6/EMC10^{HET} n=6 and Q6/EMC10^{HOM} n=4. **(G)** Western blot analysis showing reduction (Q6/EMC10^{HET}) or elimination (Q6/EMC10^{HOM}) of EMC10 protein levels in the *EMC10* LoF mutant hiPSC lines. Tubulin was probed as a loading control**. (H)** qRT-PCR assay of neuronal differentiation (*NEUROD1*), excitatory (*vGLUT1*) and cortical projection (*BRN2*) markers demonstrating similar mRNA expression pattern in Q6 (22q11.2) and derivative Q6/EMC10^{HET} and Q6/EMC10^{HET} NGN2-iNs at DIV21 whereas the glia marker *GFAP* and the inhibitory marker *DLX1* were not detected. Q6 (22q11.2) n=3-5, Q6/EMC10^{HET} n=3-6, Q6/EMC10^{HOM} n=3-5. Data are presented as mean ± SEM, unpaired two-tailed t-test, *P<0.05, **P<0.01, ***P<0.001, ****P<0.0001.

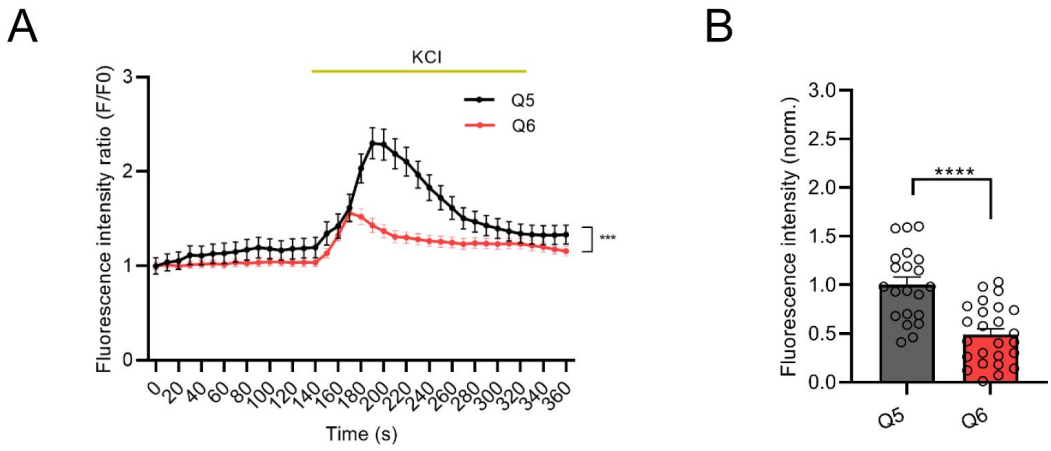

Fig. S7

Defects in cytoplasmic calcium signaling in Q6 (22q11.2) neurons.

(A) Changes in Fluo4-AM fluorescence signal intensity in response to 75mM KCl in Q5 (Ctrl) and Q6 (22q11.2) hiPSC-derived neurons at DIV37 (KS D=0.4865, P=0.003). (B) Quantification of KCl-induced Fluo4 intensity peak amplitude (ΔF) shows a reduction in Q6 line (P<0.0001). Q5 (Ctrl) n=21, Q6 (22q11.2) n=24 neuronal cells. Data are presented as mean ±SEM, unpaired two-tailed t-test or Kolmogorov–Smirnov test as indicated, *P<0.05, **P<0.01, ***P<0.001, ****P<0.0001.

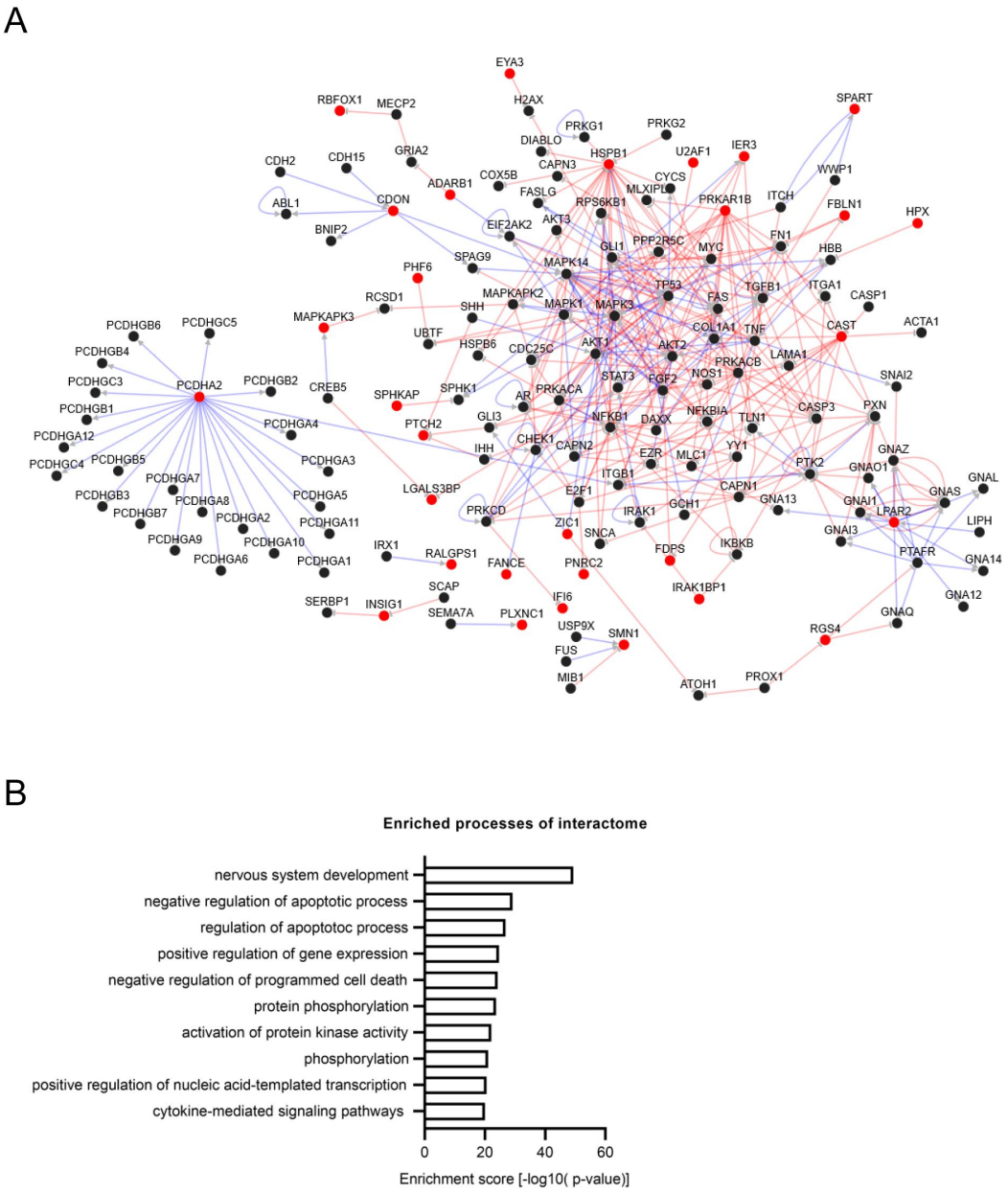

Fig. S8

PPI network analysis of the 103 shared DEGs normalized in both Q6/EMC10^{HET} and Q6/EMC10^{HOM} NGN2-iNs.

(**A**) Constructed directional PPI network out of the 30 matched candidates shown in red (PPI network; number of nodes: 150, number of edges: 365, average degree: 4.867, cluster of coefficient: 0.065). (**B**) GO term biological process: Enrichment analysis of matched proteins network.

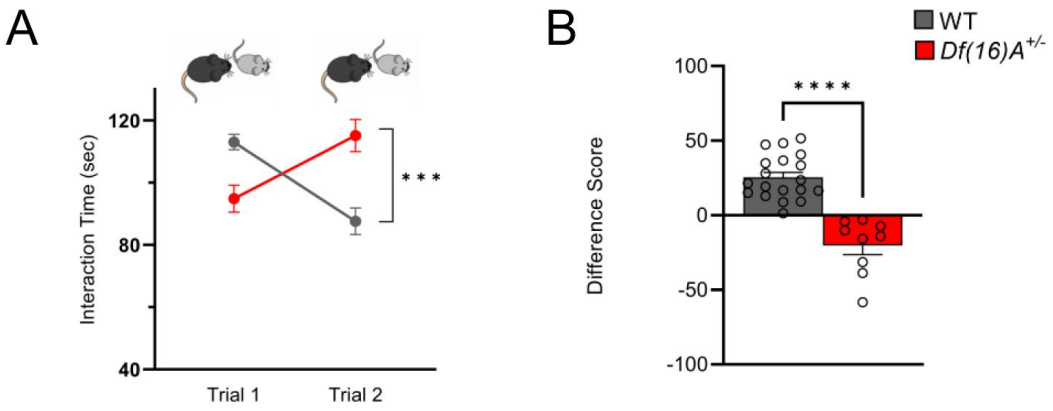

Fig. S9

Social Memory is impaired in juvenile *Df(16)A*$^{+/-}$ mice.

(A) Three-week-old juvenile *Df(16)A*$^{+/-}$ mice show a robust SM deficit compared to WT mice as indicated by the significant difference in trial 2 interaction time upon reintroduction of a familiar juvenile mouse [two-way ANOVA for Trial X Genotype Interaction matching by trial: F (1, 52) = 28.76 P<0.0001; post hoc Tukey, P= 0.0002]. **(B)** A negative difference score (trial 1-trial 2) confirms the SM deficit in juvenile *Df(16)A*$^{+/-}$ mice compared to WT littermates [unpaired two-tailed t-test]. WT mice pairs: n=19 (8 males, 11 females), *Df(16)A*$^{+/-}$ mice pairs: n=9 (7 males, 2 females). Data are presented as mean ± SEM, ***P < 0.001; ****P<0.0001.

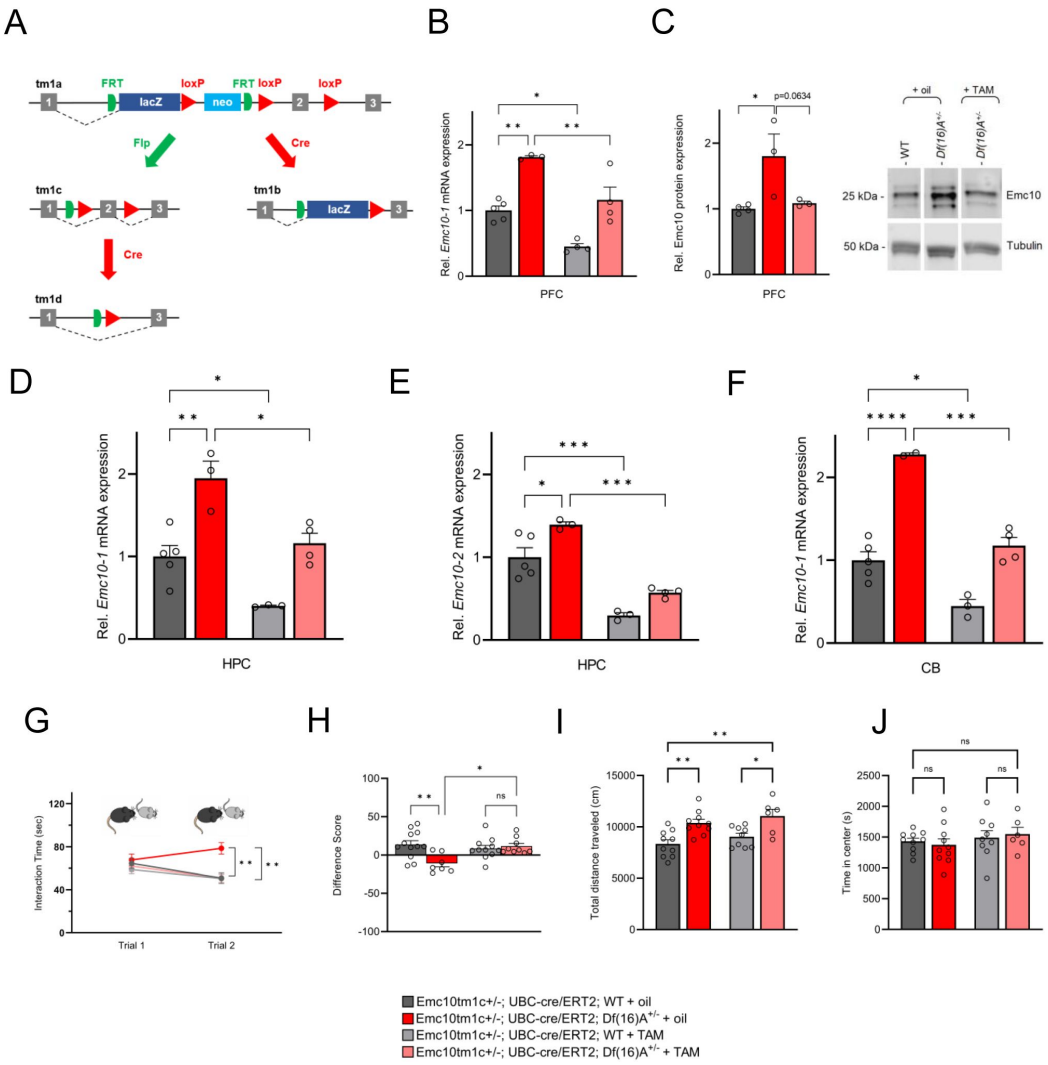

Fig. S10.

Genetic restoration of Emc10 levels in adulthood rescues SM performance in *Df(16)A*$^{+/-}$mice.

(A) *Emc10* 'knockout-first' conditional allele. The 'knockout-first' allele (tm1a) contains an IRES:lacZ trapping cassette and a floxed promoter-driven neo cassette inserted into the intron of Emc10 gene, disrupting gene function. Flp converts the 'knockout-first' allele to a conditional allele (tm1c), restoring gene activity. Cre deletes the promoter-driven selection cassette and floxed exon of the tm1a allele to generate a lacZ-tagged allele (tm1b) or deletes the floxed exon of the tm1c allele to generate a frameshift mutation (tm1d), triggering NMD of the deleted transcript. **(B)** *E*xpression levels of *Emc10-1 mRNA* transcript in PFC of *Emc10*$^{tm1c+/-}$*; UBC-cre/ERT2; Df*(16)*A*$^{+/+}$ and *Emc10*$^{tm1c+/-}$*; UBC-cre/ERT2; Df*(16)*A*$^{+/-}$ mice [referred to as WT and *Df(16)A*$^{+/-}$] following adult TAM treatment. qRT-PCR analysis shows TAM-mediated normalization of *Emc10-1* mRNA levels in the PFC of *Df(16)*$^{+/-}$ mice. Significant upregulation of *Emc10-1* mRNA expression level seen in corn oil-treated *Df(16)A*$^{+/-}$ compared to corn oil-treated WT mice [one-way ANOVA, F(3, 12)=22.58, P<0.0001; post hoc Tukey, P=0.0013]. Following TAM treatment, *Emc10-1* expression is normalized to near WT levels in TAM-treated *Df(16)A*$^{+/-}$ compared to corn oil-treated *Df(16)A*$^{+/-}$ mice (post hoc Tukey, P=0.0098). *Emc10-1* reduction is also observed in TAM-treated WT compared to corn oil-treated WT mice (post hoc Tukey, P=0.0131). Corn oil-treated WT mice: n=5, corn oil-treated *Df(16)A*$^{+/-}$ mice: n=3, TAM-treated WT mice: n=4, and TAM-treated *Df(16)A*$^{+/-}$ mice: n=4. **(C)** Emc10 protein levels in PFC of WT and *Df(16)A*$^{+/-}$ mice following adult TAM treatment. Left panel: Emc10 protein levels are significantly elevated in corn oil-treated *Df(16)A*$^{+-}$ compared to corn

oil-treated WT mice [one-way ANOVA, F(3, 12)=22.58, P<0.0001; post hoc Tukey, P=0.0013]. Following TAM treatment, *Emc10-1* expression is normalized to near WT levels in TAM-treated *Df(16)A*$^{+/-}$ compared to corn oil-treated *Df(16)A*$^{+/-}$ mice (post hoc Tukey, P=0.0098). *Emc10-1* reduction is also observed in TAM-treated WT compared to corn oil-treated WT mice (post hoc Tukey, P=0.0131). Corn oil-treated WT mice: n=5, corn oil-treated *Df(16)A*$^{+/-}$ mice: n=3, TAM-treated WT mice: n=4, and TAM-treated *Df(16)A*$^{+/-}$ mice: n=4. **(C)** Emc10 protein levels in PFC of WT and *Df(16)A*$^{+/-}$ mice following adult TAM treatment. Left panel: Emc10 protein levels are significantly elevated in corn oil-treated *Df(16)A*$^{+-}$ compared to corn oil-treated WT mice [one-way ANOVA, F(2, 7)=6.216, P=0.0281, post hoc Tukey, P=0.0300]. Emc10 protein level is reduced in TAM-treated *Df(16)A*$^{+/-}$ compared to corn oil-treated *Df(16)A*$^{+/-}$ mice (post hoc Tukey, P=0.0634). Corn oil-treated WT mice: n=4, corn oil-treated *Df(16)A*$^{+/-}$ mice: n=3, TAM-treated *Df(16)A*$^{+/-}$ mice: n=3. Right panel: Representative Western Blot. Tubulin was used as loading control. **(D-E)***Emc10* mRNA expression levels of both *Emc10* isoforms: *Emc10-1***(D)** and *Emc10-2***(E)**, with or without a TMD respectively (7), as assayed by qRT-PCRs in the HPC of the *Emc10*$^{tm1c+/-}$*; UBC-cre/ERT2; Df*(16)*A*$^{+/+}$ and *Emc10*$^{tm1c+/-}$*; UBC-cre/ERT2; Df*(16)*A*$^{+/-}$ mice [referred to as WT and *Df(16)A*$^{+/-}$] following adult TAM treatment. **(D)** qRT-PCR analysis shows TAM-mediated restoration of *Emc10-1* mRNA levels in the HPC of *Df(16)A*$^{+/-}$ mice. Significant upregulation of *Emc10-1* mRNA expression level seen in corn oil-treated *Df(16)A*$^{+/-}$ compared to corn oil-treated WT mice [one-way ANOVA, F(3, 11)=16.77, P<0.001; post hoc Tukey, P=0.0027]. Following TAM treatment, *Emc10-1* expression is restored to near WT levels in *Df(16)A*$^{+/-}$ compared to corn oil-treated *Df(16)A*$^{+/-}$ mice (post hoc Tukey, P=0.0132). *Emc10-1* reduction is also observed in TAM-treated WT compared to corn oil-treated WT mice (post hoc Tukey, P=0.0485). **(E)** qRT-PCR analysis shows TAM-mediated restoration of *Emc10-2* mRNA levels in the HPC of *Df(16)A*$^{+/-}$ mice. Significant upregulation of *Emc10-2* mRNA expression level seen in corn oil-treated *Df(16)A*$^{+/-}$ compared to corn oil-treated WT mice [one-way ANOVA, F(3, 11)=28.28, P<0.0001; post hoc Tukey, P=0.0284]. Following TAM treatment, *Emc10-2* expression is restored to near WT levels in *Df(16)A*$^{+/-}$ compared to corn oil-treated *Df(16)A*$^{+/-}$ mice (post hoc Tukey, P=0.0002). *Emc10-2* reduction is also observed in TAM-treated WT compared to corn oil-treated WT mice (post hoc Tukey, P=0.0005). Corn oil-treated WT mice: n=5, corn oil-treated *Df(16)A*$^{+/-}$ mice: n=3, TAM-treated WT mice: n=3, and TAM-treated *Df(16)A*$^{+/-}$ mice: n=4. **(F)** Expression levels of *Emc10-1 mRNA* transcript in cerebellum (CB) of WT and *Df(16)A*$^{+/-}$ mice following adult TAM treatment. qRT-PCR analysis shows TAM mediated normalization of *Emc10-1* mRNA levels in the PFC of *Df(16)A*$^{+/-}$ mice. Significant upregulation of *Emc10-1* mRNA expression level seen in corn oil-treated *Df(16)A*$^{+/-}$ compared to corn oil-treated WT mice [one-way ANOVA, F(3, 10)=37.43, P<0.0001; post hoc Tukey, P<0.0001]. Following TAM treatment, *Emc10-1* expression is normalized to WT levels in TAM-treated *Df(16)A*$^{+/-}$ compared to corn oil-treated *Df(16)A*$^{+/-}$ mice (post hoc Tukey, P=0.0003). *Emc10-1* downregulation is also observed in TAM-treated WT compared to corn-oil-treated WT mice (post hoc Tukey, P=0.0122). Corn oil-treated WT mice: n=5, corn oil-treated *Df(16)A*$^{+/-}$ mice: n=2, TAM-treated WT mice: n=3, and TAM-treated *Df(16)A*$^{+/-}$ mice: n=4. **(G)** Corn oil-treated *Df(16)A*$^{+/-}$ mice show a robust SM deficit compared to corn oil-treated WT mice as indicated by the significant difference in trial 2 interaction time upon reintroduction of a familiar juvenile mouse [three-way ANOVA for Trial X Genotype X Treatment Interaction matching by trial: F (1, 35) = 8.823 P=0.0053; post hoc Tukey, P= 0.0047]. A reduction in trial 2 interaction time indicates rescue of the SM deficit in TAM-treated *Df(16)A*$^{+/-}$ compared to corn oil-treated *Df(16)A*$^{+/-}$ mice (post hoc Tukey, P= 0.0082). **(H)** A negative difference score (trial 1-trial 2) confirms the SM deficit in corn oil-treated adult *Df(16)A*$^{+/-}$ mice compared to WT littermates [two-way ANOVA for Genotype X Treatment interaction: F (1, 35) =8.823, P=0.0053; post hoc Tukey, P= 0.0048]. Increase in the difference score of *Df(16)A*$^{+/-}$ mice in TAM- vs corn oil-treated group demonstrates rescue of SM performance (post hoc Tukey, P= 0.0181). Corn oil-treated WT mice: n=12 (7 males, 5 females), corn oil-treated *Df(16)A*$^{+/-}$ mice: n=7 (3 males, 4 females), TAM-treated WT mice: n=11 (6 males, 5 females), and TAM-treated *Df(16)A*$^{+/-}$ mice: n=9 (4 males, 5 females). **(I)** Tamoxifen (TAM) mediated Emc10 down-regulation does not rescue hyperactivity in *Df(16)A*$^{+/-}$ mice in the open field (OF) assay as demonstrated in the total distance traveled. In a 1-h exposure to a novel OF arena *Df(16)A*$^{+/-}$+ TAM mice compared with WT + TAM mice remain as hyperactive [one-way ANOVA, F(3, 31)= 8.052, P=0.0004; post hoc Tukey, P= 0.0222] as *Df(16)A*$^{+/-}$ + oil mice compared with WT + oil mice [one-way ANOVA, F(3, 31)= 8.052, P=0.0004; post hoc Tukey, P= 0.0047]. **(J)** The time spent in the center of the open field did not differ significantly between animal groups, suggesting an absence of an anxiety-related phenotype. Corn-oil treated WT mice: n= 10 (8 males, 2 females), TAM-treated WT mice: n= 9 (4 males, 5 females), corn-oil treated *Df(16)A*$^{+/-}$mice: n= 10 (6 males, 4 females), TAM-treated *Df(16)A*$^{+/-}$mice: n= 6 (3 males, 3 females). Data are presented as mean ± SEM, *P<0.05, **P<0.01, ***P<0.001, ****P<0.0001.

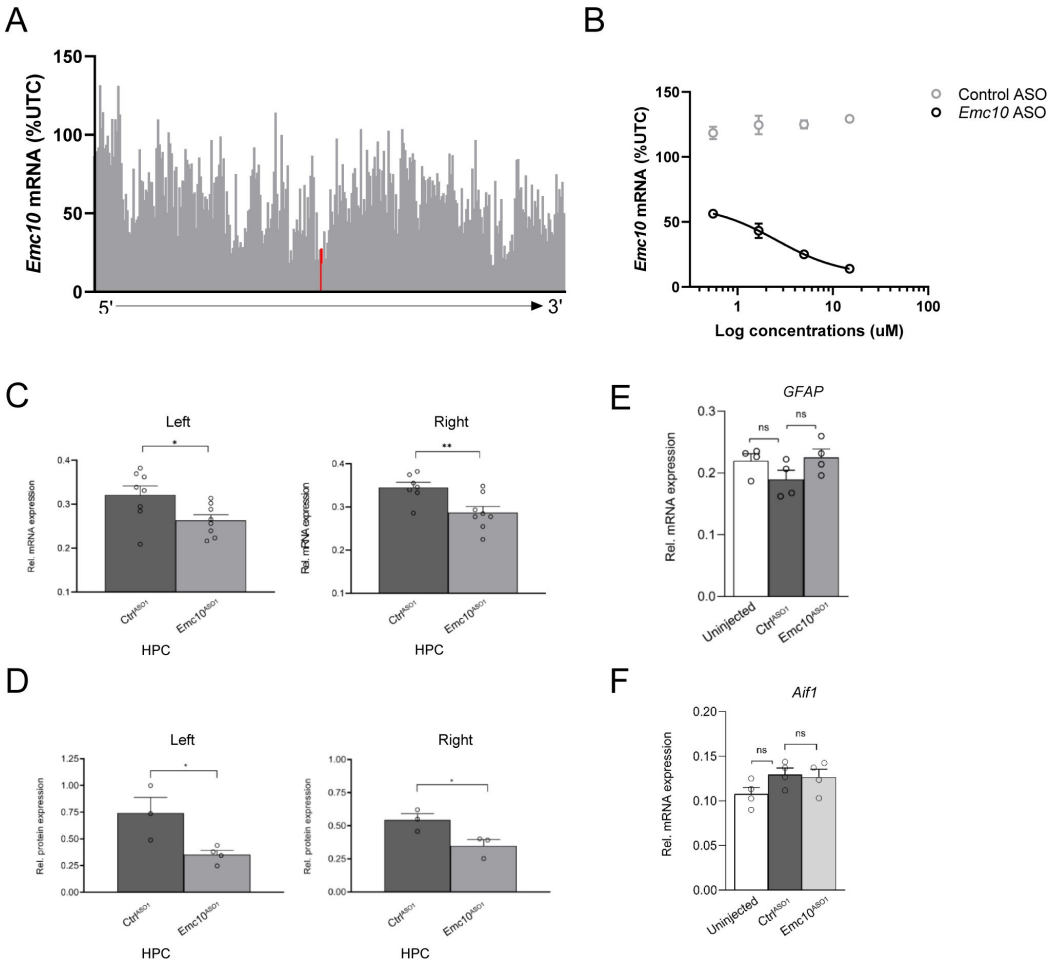

Fig. S11

In vitro and in vivo screening of designed ASOs.

(A) *Emc10* mRNA levels in 4T1 cells following 7μM treatment with *Emc10* ASOs, data normalized to untransfected controls (UTC), and lead *Emc10*^{ASO1} noted in red. **(B)** Dose dependent reductions in *Emc10* mRNA levels in 4T1 cells following treatment with lead *Emc10*^{ASO1}, but not with a negative control^{ASO1}. Data expressed at % UTC. **(C)** qRT-PCR analysis shows bilateral reduction of *Emc10* mRNA expression levels in *Emc10*^{ASO1} compared to the Ctrl^{ASO1} treated WT mice in the left (unpaired two-tailed t-test, P= 0.0285; Ctrl^{ASO1} treated-WT male mice: n=8, *Emc10*^{ASO1} treated-WT male mice: n=8) and the right HPC (unpaired two tailed t-test, P= 0.0087; Ctrl^{ASO1} treated-WT mice: n=7, and *Emc10*^{ASO1} treated-WT mice: n=8). **(D)** Western blot analysis shows bilateral reduction of Emc10 protein expression in the left (P= 0.0321; unpaired two-tailed t-test; Ctrl^{ASO1} treated-WT male mice: n=3, *Emc10*^{ASO1} treated-WT male mice: n=4) and right HPC (P= 0.0448; unpaired two-tailed t-test; Ctrl^{ASO1} treated-WT male mice: n=3, *Emc10*^{ASO1} treated-WT male mice: n=3). **(E)** mRNA expression analysis of astroglial (*Gfap*, left panel; P= 0.177; one-way ANOVA) and microglial (*Aif1*, right panel; P= 0.1527; one-way ANOVA) activation revealed no significant differences across groups. Untreated male mice; n=4, Ctrl^{ASO1} treated-WT male mice: n=4, *Emc10*^{ASO1} treated-WT male mice: n=4.

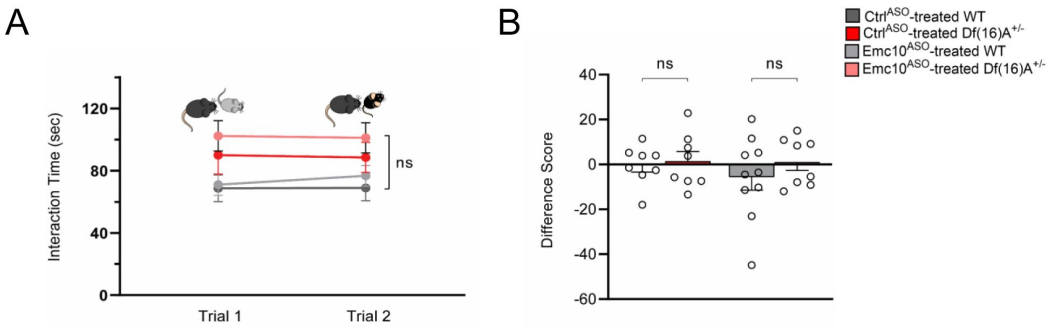

Fig. S12

Social memory interaction task with novel stimulus mice.

(A-B) Control experiment for direct interaction test using two different novel mice in trials 1 and 2. **(A)** No significant difference in SM trials is observed across groups upon reintroduction of a novel juvenile mouse indicating SM rescue is not due to task fatigue [three-way ANOVA for Trial X Genotype X Treatment matching by trial; F (1, 30) = 0.3001, P=0.5878]. **(B)** No significant changes across groups in SM difference score upon reintroduction of a novel juvenile mouse [two-way ANOVA for Genotype X Treatment interaction; F(1, 30)=0.3001 P=0.5878]. Ctrl^{ASO}-treated WT: n=8 (4 males, 4 females), Emc10^{ASO} treated WT: n= 10 (4 males, 6 females), n=8 Ctrl^{ASO}-treated *Df(16)A*$^{+/}$ (3 males, 5 females) and Emc10^{ASO}-treated *Df(16)A*$^{+/}$: n=8 (4 males, 4 females). Data are presented as mean ± SEM, *P < 0.05; ***P < 0.001.

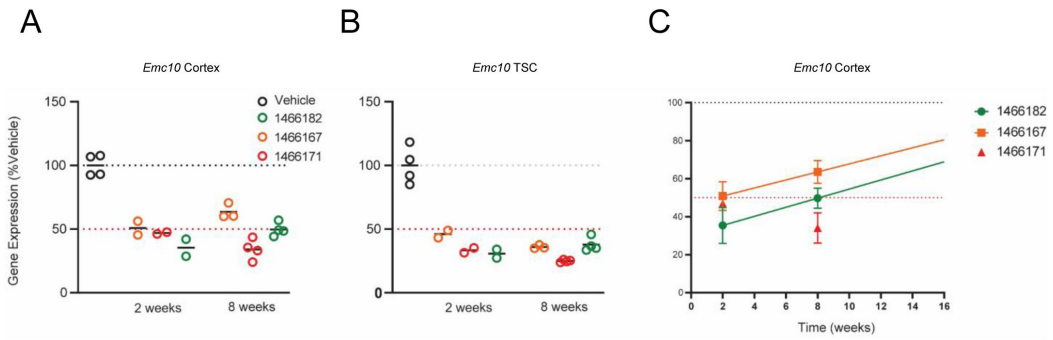

Fig. S13

In vivo post-injection screening of designed ASOs.

(A-C) *In vivo* efficacy of selected ASOs in suppressing the levels of *Emc10* mRNA in the cortex of WT mice at 2- and 8-weeks post injection. Three ASOs were selected from an initial screen for the analysis shown here, based on their pharmacological efficacy. 700 ug of ASOs were injected into the right lateral ventricle of C57Bl/6 mice. Depicted is their efficacy in suppressing the levels of *Emc10* mRNA in the **(A)** retrosplenial cortex (cortex) and **(B)** thoracic spinal cord (TSC) at both 2- and 8-wks following a single bolus dose. **(C)** Calculation of the approximate time to normal expression (~T100%) from the 2- and 8-week *Emc10* expression data. ~T100% for Emc10 #1466182 ASO is 26 weeks but this remains to be empirically determined.

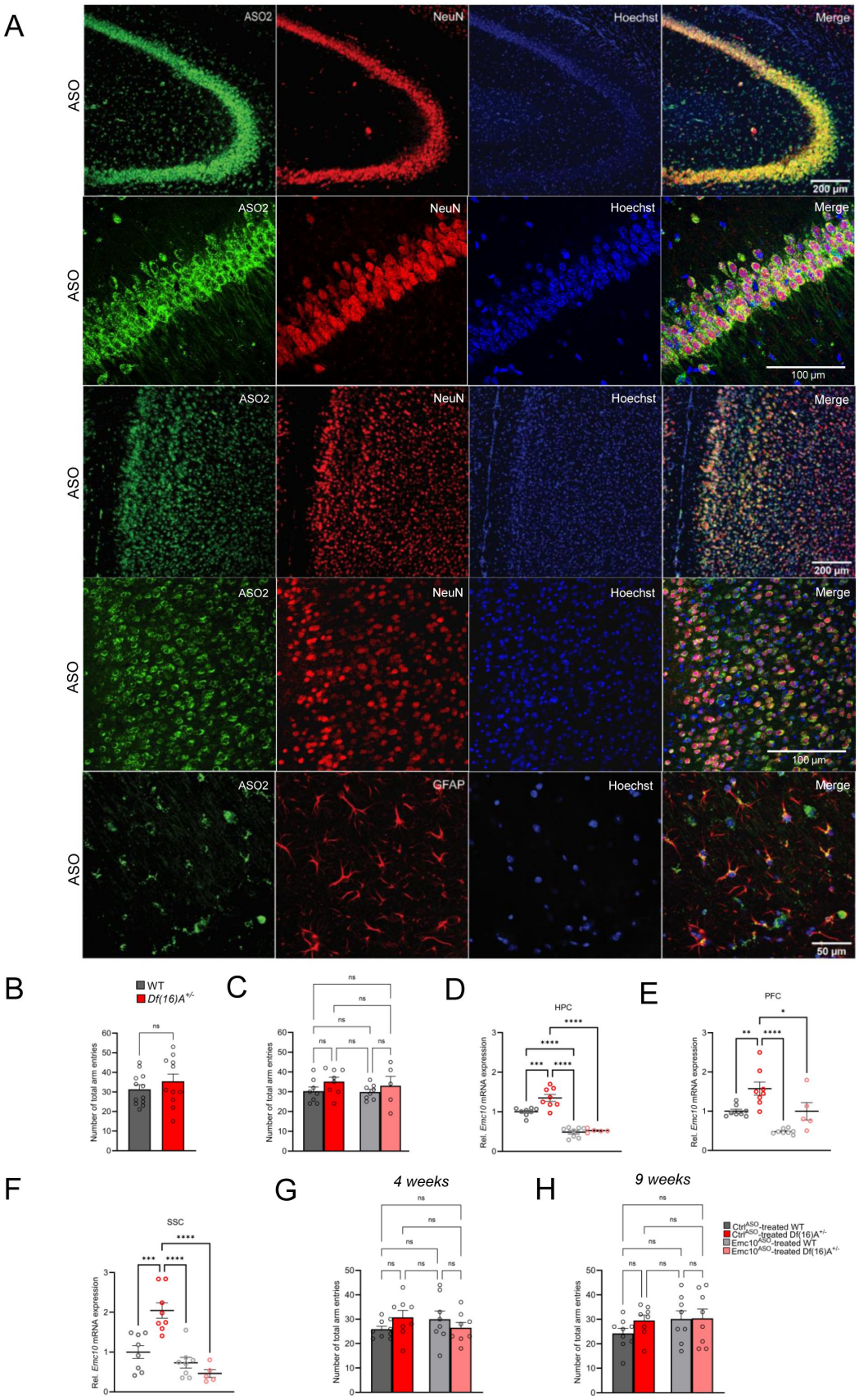
A
ASO
ASO2
NeuN
GFAP
Hoechst
Merge
200 µm
100 µm
50 µm
B
WT
Df(16)A+/-
Number of total arm entries
C
D
HPC
Rel. Emc10 mRNA expression
E
PFC
F
SSC
G
4 weeks
H
9 weeks
Ctrl^ASO-treated WT
Ctrl^ASO-treated Df(16)A+/-
Emc10^ASO-treated WT
Emc10^ASO-treated Df(16)A+/-

Fig. S14

Emc10^{ASO2} reduces Emc10 expression in adult *Df(16)A*$^{+/-}$ mice.

(A) Mouse brains collected three weeks post ICV injection were stained with an ASO antibody (green) and counterstained with neuronal marker NeuN (red) and nuclear stain Hoechst (blue). A robust and uniform ASO2 diffusion is observed in the HPC (first and second panel) and PFC (third and fourth panel). Overlap with NeuN confirms its presence in neuronal cells. The ASO signal extensively colocalizes with NeuN, demonstrating robust ASO uptake in neurons. High magnification images (panel 2 and 4) showing an almost complete overlap (97%) between ASO and NeuN signals. Accumulation in glial cells in PFC, specifically GFAP labeled astrocytes is also observed (bottom panel). Images are taken with 10x and 20x, 40x objectives. **(B-C)** Y-maze task in adult male mice. **(B)** Locomotor activity is unchanged between WT and *Df(16)A*$^{+/}$ mice (P=0.8844) reflected by the number of total arm entries in the Y-maze task. WT mice: n=12, *Df(16)A*$^{+/}$ mice: n=11. **(C)** No significant changes in the number of total arm entries between the groups after 3-weeks of ASO-injection, indicating normal locomotor activity in this task. Ctrl^{ASO}-treated male WT mice: n=8, Emc10^{ASO} treated male WT mice: n=8, Ctrl^{ASO}-treated male *Df(16)A*$^{+/}$ mice: n=8 and Emc10^{ASO}-treated male *Df(16)A*$^{+/}$ mice: n=5). **(D-F)** ASO-mediated inhibition of *Emc10* in different brain regions of *Df(16)A*$^{+/-}$ mice used in the Y-maze assay after 3-weeks of injection. **(D)** qRT-PCR analysis shows significant upregulation of *Emc10* mRNA expression levels in the HPC of Ctrl^{ASO} treated-*Df(16)A*$^{+/-}$ compared to WT mice [one-way ANOVA, F (3, 25)=50.42, P<0.0001; post hoc Tukey, P= 0.0009]. Following ASO treatment, *Emc10* expression is normalized to WT levels in Emc10^{ASO} treated-*Df(16)A*$^{+/-}$ compared to Ctrl^{ASO} treated-*Df(16)A*$^{+/-}$ mice (post hoc Tukey, P= <0.0001). **(E)** qRT-PCR analysis shows a significant up-regulation of *Emc10* mRNA expression levels in the PFC of Ctrl^{ASO} treated-*Df(16)A*$^{+/-}$ compared to WT mice [one-way ANOVA, F (3, 25)=14.45, P=<0.0001; post hoc Tukey, P=0.0097]. Following ASO treatment, *Emc10* expression is normalized to WT levels in the Emc10^{ASO} treated-*Df(16)A*$^{+/-}$ compared to Ctrl^{ASO} treated-*Df(16)A*$^{+/-}$ mice (post hoc Tukey, P=0.0258). **(F)** qRT-PCR analysis shows a significant up-regulation of *Emc10* mRNA expression levels in Somatosensory Cortex (SSC) of Ctrl^{ASO} treated-*Df(16)A*$^{+/-}$ compared to WT mice [one-way ANOVA, F (3, 25) =17.91, P=<0.0001; post hoc Tukey, P<0.0004]. Following ASO treatment, *Emc10* expression is normalized to WT levels in Emc10^{ASO} treated-*Df(16)A*$^{+/-}$compared to Ctrl^{ASO} treated-*Df(16)A*$^{+/-}$ mice (post hoc Tukey, P=<0.0001). Ctrl^{ASO}-treated WT male mice: n=8, Ctrl^{ASO}-treated *Df(16)A*$^{+/}$ male mice: n=8, Emc10^{ASO}-treated WT male mice: n=5 and Emc10^{ASO}-treated *Df(16)A*$^{+/}$ male mice: n=5. **(G-H)** Y-maze task in adult male mice: No significant changes were observed in the total number of arm entries between groups, indicating normal locomotor activity in this task at both 4 weeks **(G)** and 9 weeks **(H)** following ASO injection. Ctrl^{ASO}-treated WT: n=9, Emc10^{ASO} treated WT mice: n=8, Ctrl^{ASO}-treated *Df(16)A*$^{+/}$ mice: n=8 and Emc10^{ASO}-treated *Df(16)A*$^{+/}$ mice: n=8. Unpaired students t-test or one-way ANOVA as indicated. Data are presented as mean ± SEM, *P < 0.05, **P < 0.01, ***P < 0.01, ****P<0.0001.

Supplementary Tables

Columbia ID	Rutgers University ID	Gender	Diagnosis
QR20 (1)	MH0159020	male	none
QR27 (1)	MH0159027	male	schizoaffective disorder/22q11.2DS
Q1 (2*)	-	male	schizophrenia/22q11.2DS
Q2 (2*)	-	male	none
Q5 (2**)	-	female	none
Q6 (2**)	-	female	schizophrenia/22q11.2DS

1 hiPSC lines were obtained from the Stem Cell Repository of National Institute of Mental Health

2 hiPSC lines were generated by the Columbia Stem Cell Core Facility

*sibling pair

**sibling pair, same age

Table S1

Clinical and demographic characteristics of 22q11.2DS/SCZ patients and healthy controls.

Table S2: Differentially expressed microRNAs in cortical neurons (DIV8) from 22q11.2DS/SCZ (Q6) and control line (Q5) derived using small-molecule inhibitors of SMAD and WNT signaling pathways.

Table S3: DEGs in cortical neurons (DIV8) from 22q11.2DS/SCZ (Q6) and control line (Q5) derived using small-molecule inhibitors of SMAD and WNT signaling pathways.

Table S4: List of targets of downregulated miRNAs identified from the intersection of predicted targets of downregulated miRNAs and up-regulated DEGs in hiPSC-derived cortical neurons at DIV8.

EMC10	hsa-miR-185-5p	predicted occupancy	hsa-miR-1306-5p	predicted occupancy	hsa-miR-1286	predicted occupancy
conserved site	**8mer***	**0.2091**	-	-	-	-
poorly conserved site	7mer-A1**	0.2091	7mer-m8**	0.0082	7mer-A1***	0.0189
	-	-	-	-	7mer-A1***	0.0189
	-	-	-	-	7mer-A1***	0.0189

*conserved miRNA binding sites among mammals
**poorly conserved miRNA binding sites among human, chimp and rhesus
***poorly conserved miRNA binding sites among human and chimp

Table S5

Predicted targets of miR-185-5p, miR-1286 and miR-1306-5p in EMC10 3'UTR.

Table S6: DEGs in NGN2-iNs (DIV21) from 22q11.2DS/SCZ (Q6) and control line (Q5) that were normalized ('rescued') in Q6 EM10 HET and Q6 EMC10 HOM lines.

Table S7: List of 103 DEGs normalized in both Q6 EMC10 HET and EMC10 HOM lines, used for PPI konnect2prot network analysis.

Gene	Chromosome	Description
Emc10	7	ER Membrane protein Complex subunit 10
Mir9-3hg	7	Mir9-3 host gene
Plxnd1	6	Plexin D1
Cd68	11	CD68 antigen
Gm28439	1	Predicted gene 28439
Mir22hg	11	Mir22 host gene (non-protein coding)
Adgre4	17	Adhesion G protein-coupled receptor E4
Tnn	1	Tenascin N

Table S8

List of genes upregulated in Ctrl^{ASO1} treated-*Df(16)A*$^{+/-}$ mice compared to Ctrl^{ASO1} treated-WT mice but not in the Emc10^{ASO1} treated-*Df(16)A*$^{+/-}$ compared to Emc10^{-ASO1} treated-WT mice.

Target	Forward Primer	Reverse Primer
U6 snRNA	CTCGCTTCGGCAGCACA	AACGCTTCACGAATTTGCGT
pre-miR-134	TGTGACTGGTTGACCAGAGGG	GGTGACTAGGTGGCCCACAG
pre-miR-137	GGTGACGGGTATTCTTGGGT	CGACTACGCGTATTCTTAAGCAAT
pre-miR-185	GCGAGGGATTGGAGAGAAAG	GAGGGAAGGACCAGAGGAAA
pre-miR-212	CACCTTGGCTCTAGACTGCTT	GCCGTGACTGGAGACTGTTA
pre-miR-377	TTGAGCAGAGGTTGCCCT	CAAACAAAAGTTGCCTTTGTGT
pre-miR-485	GAGAGGCTGGCCGTGATG	GACACTAGAAGAGAGGAGAG
NANOG	TTTGTGGGCCTGAAGAAAACT	AGGGCTGTCCTGAATAAGCAG
OCT4	ACAACAATGAGAACCTTCAGGAG	GCCGGTTACAGAACCACACT

Table S9

List of primer sequences used for qRT-PCRs.

Supplemental Materials and Methods

Mice

Mice of both sexes and genotypes (mutant and WT littermates) were used for behavioral testing. Separate cohorts of mice were used for Social Memory and Fear Conditioning assays. In general, mice were group housed under a 12-h light/12-h dark cycle with controlled room temperature and humidity. Food and water were provided *ad libitum*. All behavioral experiments were performed on adult male and female mice during the light cycle. All animal procedures were carried out in accordance with and approved by the Columbia University Institutional Animal Care and Use Committee.

Cell line donors

Q6 and Q5 lines

The Q6 line donor is a 20-year-old female patient with a history of developmental delay and an overall Full-Scale IQ in the low 80s. She was clinically diagnosed with 22q11.2DS by FISH testing. Her psychotic symptoms, including disorganized behavior and command auditory hallucinations, started when she was 17 years old. During the first break episode, due to the severity of her psychotic symptoms, the patient was hospitalized and was diagnosed with schizophrenia. The patient also developed depressive symptoms, including frequent suicidal ideation. One year after her schizophrenia diagnosis, in addition to her severe psychotic symptoms, the patient was also diagnosed to be in a catatonic state. The patient has remained severely psychotic since the onset of these symptoms at age 17 and has been on multiple antipsychotics without experiencing any clinically meaningful benefit. Regarding her treatment history includes various first-line antipsychotics (including olanzapine, stelazine, aripiprazole, haloperidol, risperidone and clozapine); several antidepressants (sertraline and fluoxetine); a mood stabilizer (lithium) and benzodiazepines (e.g., lorazepam). None of these medications reportedly led to any clinically significant improvement in either the psychotic or the depressive symptoms. The patient has also undergone 2 rounds of electroconvulsive treatment (ECT), but with only short-lived improvement. The Q5 line donor is the probands dizygotic twin sister who does not carry a 22q11.2 deletion and her psychiatric evaluation ruled out any history of psychiatric symptoms (Supplementary Table S1). Sibling are of Caucasian Western European descent.

Q1 and Q2 lines

The Q1 and Q2 line were previously described (as DEL3 and WT3) (71). The Q1 line donor is a 32-year-old male patient with a history of developmental and speech delay. He was clinically diagnosed with 22q11.2DS by FISH testing at age 4. His psychotic symptoms, started when he was 12 years old. The patient was hospitalized once at age 10 before he was formally diagnosed with schizophrenia. During that time, he also experienced one seizure. The patient also developed mood lability and has OCD-like symptoms although does not meet full criteria for DSM-IV/V OCD. Regarding his treatment history, it includes various first-line antipsychotics as well as metyrosine (started when he was 15). The Q2 line donor is the proband's brother, who does not carry a 22q11.2 deletion and his psychiatric evaluation ruled out any history of psychiatric symptoms (Supplementary Table S1). Siblings are of Caucasian Western European descent.

QR20 and QR27 lines

QR20 (MH0159020) and QR27 (MH0159027) lines were obtained from the NIMH Repository and Genomics Resource (*http://www.nimhstemcells.org/*) (72). The donor of the QR27 line, 31-year-old male was diagnosed with schizoaffective disorder and 22q11.2DS (72) while the donor of the QR20 line (58 year old male) was free from any psychiatric symptoms (Supplementary Table S1). Both are of Caucasian descent.

hiPSC generation and characterization

Q5 and Q6 hiPSC lines were generated at the Columbia Stem Cell Core via non-integrating Sendai virus-based reprogramming (73) of monocytes from a donor with 22q11.2DS and SCZ and a healthy sibling control. The Q1 and Q2 lines were generated at the Columbia Stem Cell Core and characterized as described earlier (71). QR20 and QR27 lines were obtained from the NIMH Repository and Genomics Resource (*http://www.nimhstemcells.org/*) (72). Karyotyping was performed on twenty G-banded metaphase cells at 450–500 band resolution as previously described (74) to ensure the absence of chromosomal abnormalities in all patient and control derived cell lines (**Fig. S1A**, **Fig. S6B**). We confirmed the genotypes of Q6 patient- and Q5 control-derived hiPSCs using a Multiplex Ligation-dependent Probe Amplification (MLPA) assay to detect copy number changes (**Fig. S1B, C**). To confirm stemness of hiPSC lines, we performed qRT-PCR for markers *NANOG* and *OCT4/POU5F1* (**Fig. S1D**).

Genome editing of Q6(22q11.2) hiPCS line

The genomic gRNA target sequences were EMC10-g1: ACAGTGCCAACTTCCGGAAG (PAM suffix: CGG) and EMC10-g2: GGGACAAGGTACCATCCTGC (PAM suffix: TGG). Mutations in *EMC10* were confirmed by NGS and no off-target candidates were predicted in both lines using COSMID tool (*https://crispr.bme.gatech.edu*) (75). Karyotyping confirmed normal chromosome complement in both modified lines (**Fig. S6B**). qRT-PCR and WB assays were performed in both lines for the hiPSC markers *NANOG* and *OCT4/POU5F1* to confirm stemness as well as the RNABP1 gene located within 22q11.2 locus to confirm the deletion (**Fig. S6C-E**). qRT-PCR and western blot assays were performed to confirm reduction or elimination of EMC10 levels in the *EMC10* LoF mutant lines (**Fig. S6F-G**).

Culture and neuronal induction of hiPSC lines

hiPSC lines were maintained in mTeSR Plus medium (catalog#05825, Stemcell Technologies, Vancouver, Canada) on Matrigel (catalog#354277, Corning, Corning, NY, USA) coated tissue culture plate. Cells were fed on any other day and passaged weekly using RelesR (catalog#05872, Stemcell Technologies, Vancouver, Canada) dissociation reagent in accordance to their manual. Disassociated cells were pre-plated as reported earlier(20) at a density of 200,000 cells/cm^2 supplemented with 10 µM Y-27632 (catalog# 1254, Tocris Bioscience, Bristol, United Kingdom) on Matrigel-coated plates and differentiation started when confluent. Differentiation of hiPSC was performed as indicated below: *(i)* hiPSC differentiation into cortical neurons, via a combination of small molecule inhibitors, was performed as described with few modifications (20). This protocol has been shown to robustly generate cortical neurons while actively suppressing glial differentiation, as evidenced by the lack of upregulation of glial markers such as GFAP, AQP4, or OLIG2. In brief, inhibitors used in LSB+X/P/S/D induction included LDN193189 (250 nM; catalog#04-0074, Stemgent, REPROCELL USA Inc., Beltsville, MD, USA), SB431542 (10 µM; catalog#1614, Tocris Bioscience, Bristol, United Kingdom), XAV939 (5 µM; catalog#3748, Tocris Bioscience, Bristol, United Kingdom), PD0325901 (1 µM; catalog#4192, Tocris Bioscience, Bristol, United Kingdom), SU5402 (5 µM; catalog#1645-05, BioVision Inc., Milpitas, CA, USA), DAPT (10 µM; catalog#2634, Tocris Bioscience, Bristol, United Kingdom). Until day 4 of differentiation, TeSR E6 medium (catalog#05946, Stemcell Technologies, Vancouver, Canada) was added in 1/3 increments every other day. Then, neurobasal (NB) plus medium supplemented with N2 (catalog#17502-048,

Gibco, Life Technologies, Grand Island, NY, USA) and B27 plus supplement (catalog#A35828-01, Gibco, Life Technologies, Grand Island, NY, USA) was added in 1/3 increments every other day from day 4, until reaching 100% neurobasal plus/B27 plus L-glutamine (catalog#35050-061, Gibco, Life Technologies, Grand Island, NY, USA) containing medium supplemented with BDNF (20 ng/ml; catalog#248-BDB, R&D Systems, Minneapolis, MN, USA), cAMP (0.5 mM; catalog#A92902, Sigma-Aldrich, St. Louis, MO, USA) and ascorbic acid (0.2 mM; Sigma-Aldrich, St. Louis, MO, USA) (BCA) at day 8 as described (20). For long-term culture, cells were passaged on day 8 of differentiation by Accutase (catalog#AT-104, Innovative Cell Technologies Inc., San Diego, CA, USA) dissociation for 6 min at 37 °C. Cells were replated at 200,000 cells/cm^2 onto Matrigel coated culture dishes. NB plus/B27 plus and BCA medium were used for passaging and long-term culture. Culture medium was changed every 3–4 days. *(ii)* hiPSC differentiation into neurons via NGN2 overexpression was performed as described previously with few modifications (31–33). In brief, differentiation of hiPSC into neurons (iNs) was conducted by using the lentiviral infection of NGN2 and the reverse tetracycline transactivator rtTa into hiPSCs, followed by selection on puromycin. The lentiviral particles were commercially produced by VectorBuilder (Chicago, IL, USA) using the established and published plasmids pLenti-FUW-M2rtTA (FUW-M2rtTA deposited by Rudolf Jaenisch, Addgene plasmid #20342; *http://n2t.net/addgene:20342*; RRID:Addgene_20342, (76)), pLenti-TetO-hNGN2-eGFP-puro (pLV-TetO-hNGN2-eGFP-Puro deposited by Kristen Brennand, Addgene, plasmid#79823; *http://n2t.net/addgene:79823*; RRID:Addgene_79823, (33)) and for calcium imaging, the pLenti-TetO-hNGN2-puro (pLV-TetO-hNGN2-Neo deposited by Kristen Brennand, Addgene plasmid # 99378; *http://n2t.net/addgene:99378*; RRID:Addgene_99378,(77)). Around 200k cells per well (24-well format) were plated on Matrigel coated wells/coverslips in mTeSR plus media supplemented with 10 µM Y-27632. On day 0, lentiviruses were added in fresh basic media, containing always DMEM/F12 (catalog#11330032, Thermo Fisher Scientific, Waltham, MA, USA), human BDNF (10 ng/ml), human NT-3 (10 ng/ml, catalog#450-03, PeproTech, East Windsor, NJ, USA), mouse laminin (0.1 µg/ml, catalog#354232, Corning, NY, USA), N2 supplement, B27 plus supplement, non-essential amino acids (NEAA, catalog#SH30238.01, Cytiva, Marlborough, MA, USA) supplement and doxycycline (1 mg/ml, catalog#D9891-1G, Sigma-Aldrich, St. Louis, MO, USA) to induce TetO gene. On day 1, the culture medium was completely replaced with fresh basic media and a 48-hour puromycin selection (1 mg/l, catalog#P8833-10MG, Sigma-Aldrich, St. Louis, MO, USA) period was started. On day 3, for calcium imaging and morphology analysis, ca. 25% mouse glia cells (prepared as previously reported in (33)) were added to the basic media plus Ara-C (2µM, catalog#C1768-100M, Sigma-Aldrich, St. Louis, MO, USA) and 10% mouse astrocyte conditioned media (catalog#M1811-57, ScienCell, Carlsbad, CA, USA) to promote neuronal health and maturation. On day 5, total medium was changed with basic media plus Ara-C and 10% mouse astrocyte conditioned media. On day 7, total media was removed and replaced with BrainPhys Neuronal media with SM1 supplement (catalog#05792, STEMCELL Technologies, Vancouver, Canada) containing always human BDNF (10 ng/ml), human NT-3 (10 ng/ml), mouse laminin (0.1 µg/ml), N2 supplement, doxycycline (1 mg/ml) and 10% mouse astrocyte conditioned media. From day 9 on, half of the media were removed and replaced with supplemented BrainPhys media every other day. 2.5% FBS (catalog#16141079, Thermo Fisher Scientific, Waltham, MA, USA) was added to the culture medium on day 11 to those cells which were co-cultured with astrocytes to support astrocyte viability. iN cells were assayed for experiments as indicated.

Cell culture transfection

Transfection of cortical neurons at day 8 of differentiation were performed with the transfection reagent Lipofectamine 2000 (#11668-030, Life Technologies, Carlsbad, CA, USA) as described earlier (26)). Cells were transfected for 48 hours with 25 pmol per well (24-well format) of miRNA mimic Pre-miR miRNA precursors (Ambion, Thermo Fisher Scientific, Waltham, MA, USA) as indicated: pre-miR Negative Control #1 (catalog#17110), hsa-miR-185-5p (catalog#17100, PM12486) and hsa-miR-485-5p (catalog#17100, PM10837) or with 50 pmol per well (24-well format) of miRNA miRVana inhibitors (Ambion, Thermo Fisher Scientific, Waltham, MA, USA) as indicated: miRNA inhibitor Neg. Ctrl #1 (catalog#4464076), hsa-miR-185-5p inhibitor (catalog#4464084, MH12485), hsa-miR-485-5p inhibitor (catalog#4464084, MH10837).

TAM preparation and feeding

We used oral gavage for TAM delivery during postnatal day 56-70. A TAM feeding protocol were used as previously described (67). In brief, TAM (catalog#T5648, Sigma-Aldrich, St. Louis, MO, USA) was dissolved in corn oil (catalog#C8267, Sigma-Aldrich, St. Louis, MO, USA) at 20mg/ml by vortexing. To avoid toxicity, the following dosages were used for adult animals (8-10 weeks): mice at 17–21 g body weight were fed 5 mg/day; mice at 22–25g body weight were fed 6mg/day; mice at 26–29g body weight were fed 7mg/day; mice at 30–35g body weight were fed 8mg/day. Adult animals were fed for 5 consecutive days followed by 2 days of rest. Animals were then fed for 5 more consecutive days followed by one week of rest before RNA/protein or SM assays were performed. Corn oil was used as vehicle control treatment.

ASOs

Mouse *Emc10*-targeting ASOs used in these studies were 20 bases in length, chimeric 2'-O-(2-methoxyethyl) (MOE)/DNA) oligonucleotides with phosphodiester and phosphorothioate linkages. The central gap of 10 deoxynucleotides is flanked on its 5' and 3' sides by five MOE modified nucleotides. Oligonucleotides were synthesized at Ionis Pharmaceuticals (Carlsbad, CA, USA) as described previously (68, 69). ASOs were solubilized in 0.9% sterile saline or PBS.

In vitro screening of ASOs

4T1 cells were trypsinized, counted and diluted to 200,000 cells per ml in room temperature growth medium before adding 100 µL of the cell suspension to the wells of a 2 mm electroporation plate (Harvard Apparatus, Holliston, MA, USA) which contained 11 µL of 10X ASO in water. Cells were pulsed once at 130V for 6 mS with the ECM 830 instrument (Harvard Apparatus). After electroporation, the cells were transferred to a Corning Primeria 96 well culture plate (catalog #353872, Corning, NY, USA) containing 50 µL of growth medium. The cells were then incubated at 37° C and 5% CO2. After 24 hours, the cells were washed 1 x with PBS before lysing for RNA isolation and analysis. For each treatment condition duplicate wells were tested. ASO1081815 (TTGTTCCTACAGATCTAGGG, referred to in the manuscript as $Emc10^{ASO1}$) was used in behavioral and immunocytochemical assays.

In vivo screening of ASOs

Candidate *Emc10*-targeting ASOs (700ug) were stereotactically injected into the right lateral ventricle of C57Bl/6 mice (0.3 mm anterior, 1.0 mm dextrolateral, 3.0 mm ventral from bregma). Reduction of *Emc10* mRNA in the retrosplenial cortex and thoracic spinal cord was evaluate by qRT-PCR at 2 weeks following a single bolus dose. Three ASOs were selected from the screen based on their pharmacological efficacy: 1466167, 1466171 and 1466182. Animals were injected with these ASOs in the right lateral ventricle as described above (n= 4) and euthanized 8 weeks post injection. Animals were evaluated with an observational functional battery test at 3 hours after dosing and then every two weeks until euthanasia. The retrosplenial cortex and thoracic spinal cord were harvested for qRT-PCR analysis of *Emc10*, *Aif1* (microglia marker), *Cd68* (phagocytic microglia marker) and *Gfap* (reactive astrocyte marker) mRNA. Brain and spinal cord were also harvested and fixed in formalin solution for histological evaluation. Tissues were stained for H&E and IBA1 (microglia marker), CD68 (phagocytic microglia marker) GFAP (reactive astrocyte marker) and Calbindin (Purkinje Cell marker). Bolus injections of all three candidate ASOs resulted in similar reductions of the *Emc10* mRNA at both 2 and 8 weeks. Of the three candidate ASOs, ASO1466182 (GCCATATCTTTATTAATTAC, referred to in the manuscript as $Emc10^{ASO2}$) showed no signs of in life toxicity and the tolerability marker gene expression was similar between ASO- and vehicle-treated animals in the tissues evaluated. There was no positive IBA1 IHC staining in the CNS of any of the treated animals. Therefore, it was ranked as the best candidate for further behavioral analysis in mutant mice.

Stereotactic Intracerebroventricular (ICV) Injections of ASOs

The syringe was attached to a glass pipette with a long-tapered end made using a Sutter pipette puller model P-87. Anesthesia was delivered using Kent Scientific VetFlo Traditional Vaporizer VetFlo-1205S (Kent Scientific Corporation, Torrington, CT, USA). Mice were initially put in the isoflurane chamber using 3% isoflurane mixture for 5 minutes, which was lowered to 2-2.5% when fixed to the stereotactic station. We used KOPF Small Animal Stereotaxic Instruments (Model 940). Carprofen (5 mg/kg, Zoetis Inc., Kalamazoo, MI, USA), and Bupivacaine (2 mg/kg, Hospira, Inc., Lake Forest, Il, USA) were delivered subcutaneously before the incision was made. Additionally, Dexamethasone (2 mg/kg, Bimeda-MTC Animal Healt Inc., Cambridge, ON, Canada) was delivered intramuscularly. The surgical site was shaved and sterilized with betadine and 70% ethanol three times. A small midline incision was made and a hole was drilled in the skull. Stereotactic bregma coordinates used for the right ventricle were - 0.5 mm posterior, −1.1 lateral, and −2.8 mm dorsoventral. Mice were injected with 4 ul of either the $Ctrl^{ASO1/ASO2}$ or $Emc10^{ASO1/ASO2}$ ($Emc10^{ASO1}$: 292 ug, $Emc10^{ASO2}$: 280 ug) at a rate of 0.5ul/minute. The needle was left in the injection site for 10 minutes to allow diffusion and avoid back flow of the ASO upon retraction of the glass pipette. Mice were maintained at a temperature of 37°C for the duration of the surgery using a water regulated heating pad (T/Pump TP 700, Stryker Corporation, Kalamazoo, MI, USA). Mice were placed on heating pads for in cage recovery and Carprofen was administered subcutaneously for three days post-surgery. Mice were then subjected to behavioral experiments/immunohistochemistry three weeks post-surgery. qRT-PCR assays were performed one week post behavioral assays.

Quantitative Real Time PCR (qRT-PCR)

Total RNA was extracted from HPC, PFC and Somatosensory Cortex (SSC) using the RNeasy Mini Kit (catalog#1038703, Qiagen, Hilden, Germany) or using the miRVana miRNA isolation kit (#AM1560, Ambion, Thermo Fisher Scientific, Waltham, MA, USA) for RNA extraction of hiPSC and derived neurons samples in accordance to their manuals. cDNA was synthesized using High-Capacity RNA-to-cDNA Kit from Applied Biosystems (cat#4387406, Thermo Fisher Scientific Baltics, Vilnius, Lithuania). qRT-PCR was performed using the Bio-Rad CFX-384 qPCR instrument (Bio-Rad, Hercules, CA, USA) using TaqMan Universal Master Mix II, with UNG (catalog#4440038, Thermo Fisher Scientific Baltics, Vilnius, Lithuania). Mouse *Gapdh* Endogenous Control (cat# 4352339E, Life Technologies, Warrington, United Kingdom) served as housekeeping gene and TaqMan Mm01197551_m1 (catalog#4351372) probe for mouse *Emc10* as well as Mm01208065_m1 for *Emc10-1* (cat# 4351372) and Mm01197555_m1 for *Emc10-2* (cat# 4351372) mRNA detection were used for the qRT-PCR assay. For mouse qRT-PCR assay of Ctrl ASO^{ASO1}/$Emc10^{ASO1}$, threshold cycle of each sample was picked from the linear range to calculate the values for Starting Quantity (SQ) for all samples extrapolated using the Standard Curve. All samples were run together in triplicates on the same plate including the standard curve ran in duplicates. The SQ values were averaged over the triplicates. The values of *Emc10* mRNA levels were then normalized to the values from the *Gapdh* gene expression levels. For mouse qRT-PCR analysis of Ctrl ASO^{ASO2}/$Emc10^{ASO2}$, the average of triplicate CT values from each sample was used to calculate the relative RNA levels ($2^{-\Delta CT}$) as described earlier (78) and all values were then normalized to $Ctrl^{ASO2}$-treated WT group. qRT-PCR for hiPSC and derived neurons was performed using TaqMan or SYBR Green System (catalog#1725121, iTaq Universal SybrGreen Supermix with ROX; BIO-RAD, Hercules, CA, USA) for mRNA and/or pre-miRNA detection according to manufacturer's instructions. *U6* snRNA was used as housekeeping gene to normalize pre-miRNAs targets. For detection of *RANBP1* (catalog# 4331182, Hs01597912), *OCT4/POU5F1* (catalog#4331182, Hs04260367), *NANOG* (catalog#4331182, Hs02387400), *TBR1* (catalog#4331182, Hs00232429), *GFAP* (catalog#4331182, Hs00909233), *NEUROD1* (catalog#4331182, Hs00159598), *vGLUT1* (catalog#4331182, Hs00220404), *DLX1* (catalog#4331182, Hs00698288), BRN2 (catalog#4331182, Hs00271595) and *EMC10* (catalog#4331182, Hs00382250) mRNA TaqMan probes (Thermo Fisher Scientific, Waltham, MA, USA) were used, as indicated, with *GAPDH* as housekeeping gene control (human *GAPDH*

endogenous control, catalog#4325792, Life Technologies, Warrington, United Kingdom). The average of triplicate CT values from each sample was used to calculate the relative RNA levels ($2^{-\Delta CT}$). Primer sequences for pre-miRNA are provided in the supplemental table (Supplementary Table 9). Primers were purchased from Integrated DNA Technologies (Coralville, IA, USA) and were diluted to a stock concentration of 100 μM.

Immunohistochemistry

Animals were euthanized using CO_2 and then perfused with 4% Paraformaldehyde. The brains were stored at 4°C in 4% PFA overnight and were then switched to 1x Phosphate Buffered Saline (PBS). 2.5% low melting agarose in 1xPBS buffer was added to the brains placed inside the plastic molds, which were then moved to 4°C to create a solid block for slicing. This block was then glued to the vibratome stage (Leica Vibratome VT10005, Wetzlar, Germany) and sectioned at 40 um thickness. Sections were rinsed in 1xPBS for 5 minutes and then blocked for 1 hour at room temperature in 2% Normal Goat Serum (NGS) and 0.3%Triton X-100 in 1xPBS solution. Sections were then incubated with either anti-ASO and NeuN or anti-ASO and GFAP primary antibodies in blocking solution at 4°C and left on a shaker overnight. The following day, sections were washed three times with 1xPBS for 10 minutes and were then stained with Goat anti-rabbit along with either Goat anti-mouse or Goat anti-chicken secondary antibodies in 2% NGS and 0.4% Triton-X100 solution made in 1xPBS for two hours in the dark at room temperature (RT). Following two 10-minute washes with 1xPBS, sections were additionally stained with Hoechst nuclear stain diluted in 1xPBS for 15 minutes in the dark. Lastly, sections were washed three times with 1xPBS for 10 minutes. Sections from PBS solution were mounted on glass slides, air-dried and cover slipped in Prolong Diamond Antifade Mountant (catalog#P36970, Life Technologies Corporation, Eugene, OR, USA). Slides were left overnight in the dark and then stored at 4°C. Human neuronal cultures were fixed on coverslips in 4%PFA (catalog#22023, Biotium, Fremont, CA, USA) for 1h at RT and then blocked for 1.5h at RT in 0.1% Triton-X and 10% horse serum (catalog#H0146, Sigma-Aldrich, St. Louis, MO, USA) solution. After fixation, coverslips were stained with the primary antibody in a 0.1% Triton-X and 2% horse serum solution overnight at 4°C. Coverslips were then washed 3x 15 min with DPBS (catalog#D8537, Sigma-Aldrich, St. Louis, MO, USA) and cells were incubated for 1h with the secondary antibody at RT followed by 3x 15min DPBS washing. Tissue sections and cultured cells were imaged on W1-Yokogawa Spinning Disk Confocal (Nikon Instruments, Tokyo, Japan).

Antibodies for Immunohistochemistry

The following primary antibodies were used: Rabbit polyclonal anti-ASO antibody diluted 1:10000 (IONIS Pharmaceuticals, Carlsbad, CA, USA); Anti-GFAP antibody diluted 1:1000 (Aves Labs Inc., catalog#GFAP), Mouse monoclonal Anti-NeuN antibody diluted 1:200 (Millipore, catalog#MAB377), anti-TUJ1 1:500 (mouse monoclonal, catalog#T8660, Sigma-Aldrich, St. Louis, MO, USA), anti-TBR1 1:100 (rabbit monoclonal, #Ab183032, Abcam, Cambridge, MA, USA), anti-GFP 1:1000 (goat polyclonal, catalog#600-101-215, Rockland Immunochemicals, Pottstown, PA, USA), anti-MAP2 1:2000 (chicken polyclonal, catalog#5392, Abcam, Cambridge, MA, USA). The following secondary antibodies were used for mouse at a dilution of 1:500: Goat anti-Rabbit (Alexa Floro 488: catalog#AA1008, Invitrogen, Waltham, MA, USA) against ASO; Goat anti-mouse (Alexa Floro 568: catalog#AA1004, Invitrogen, Waltham, MA, USA) against NeuN, and Goat anti chicken (Alexa Floro 568: catalog#A11041, Invitrogen, Waltham, MA, USA) against GFAP. Hoechst 33258 solution diluted 1:1000 (Catalog#94403, Sigma Aldrich, Saint Louis, MO, USA) was used for nuclear staining in brain slices and DAPI Fluoromount-G (catalog#0100-20, Southern Biotech, Birmingham, AL, USA) was used for cultured cells.

Analysis of dendritic complexity

Images of dendrites were acquired on a Nikon Spinning Disk Confocal Microscope and captured using the Nikon NIS Elements AR (v.5.21.03 64-bit) software. Images were acquired and analyzed as previously described (7, 79). Image analysis of dendritic complexity was conducted blind to genotype. Primary dendrites were defined as any branch emerging from the soma and a secondary dendrite as any branch emerging from a primary dendrite. Dendrite branches were semi-automatically traced using NeuronStudio software (v.0.9.92 64-bit) (80). The output .swc files were then processed in VAA3D (v.3.1.00) (81–83) and binary images were generated and analyzed using ImageJ (*http://rsbweb.nih.gov/ij/*, NIH, Bethesda, MD, USA).

Calcium imaging

Neuronal cells used in calcium imaging experiments were prepared on glass bottom dishes (14mm, catalog#P35G-1.5-14-C, MatTek, Ashland, MA, USA). Briefly, cells were incubated at DIV37-38 with 0.3μM Fluor4-AM (Invitrogen, catalog#F14201) for 30 min at 37 °C in incubation buffer medium (containing 170mM NaCl, 3.5mM KCl, 0.4mM KH_2PO_4, 20mM TES (N-tris[hydroxyl-methyl-2-aminoethane-sulfonic acid], 5mM $NaHCO_3$, 5mM glucose, 1.2mM Na_2SO_4, 1.2mM $MgCl_2$, 1.3mM CaCl2, pH 7.4) and washed once with incubation buffer medium before imaging. After imaging for 2'20" (baseline), 25mM KCl solution was added to the cells, followed by another 25mM KCl addition at 3'20" and 4'20" min. Live imaging was performed at room temperature (~25 °C) on a W1-Yokogawa Spinning Disk Confocal (Nikon Instruments, Tokyo, Japan). ImageJ software with plugin for motion correction (MuliStackReg) and Excel were used to collect, manage and quantify time-lapse excitation ratio images by selecting cell body as ROI.

Protein extraction for Western blot

To extract proteins from mouse HPC, the tissue was dissected and homogenized in QIAzol lysis reagent (catalog#79306, Qiagen, Hilden, Germany). Chloroform was added to homogenate and the solution was then incubated at room temperature for 3 minutes. Tissue was spun at 12,000 x g at 4°C and the organic phase was collected for protein extraction. We followed an optimized protocol for protein extraction from Trizol solutions and used 5% SDS + 20mM EDTA + 140 mM NaCl buffer solution for protein pellet suspension (84). To extract proteins from mouse PFC, the tissue was dissected and homogenized using a modified Pierce RIPA lysis and extraction buffer (RIPA+) (catalog#89900, Thermo Scientific, Rockford, IL, USA) that contains a Halt Protease Inhibitor Cocktail (catalog#1861281, Thermo Scientific, Rockford, IL, USA). Cultured neurons cells were lysed at day 8 of differentiation. The cultured cells were once washed with cold DPBS (catalog#D8537, Sigma-Aldrich, St. Louis, MO, USA). Cells were then lysed by adding a modified Pierce RIPA lysis and extraction buffer (RIPA+). The plate was shaking for 20 min at 4°C on an orbital shaker (catalog#980173, Talboys, Troemner, Thorofare, NJ, USA). To remove cell debris, the lysates were centrifuged at maximum speed for 10 min at 4°C. The protein concentration of the supernatant for all protein samples was determined by Pierce BCA Protein Assay Kit (#23227, Thermo Scientific, Rockford, IL, USA).

Western Blots

For each lane, ~20 μg protein were run on a 4-12Bis-Tris Criterion XT Precast Gel (#3450123, Bio-Rad (Bio-Rad, Hercules, CA, USA) next to the Precision Plus Protein Dual Color Standard (catalog#161-0374, Bio-Rad, Hercules, CA, USA) in SDS-PAGE running buffer (catalog#1610788, Bio-Rad, Hercules, CA, USA) and afterwards transferred to a methanol-activated Immobilon-P PVDF (poly-vinylidene difluoride) membrane (catalog#IPCVH00010, Merck Millipore Ltd., Carrigtwohill, Ireland) by tank blotting at 250mA for 90 min in a cold room (4°C) in blotting buffer (catalog#1610734, Bio-Rad, Hercules, CA, USA). The membrane was blocked for 2 h in TBS-T (tris buffered saline supplemented with 0.1 % Tween) containing 5 % milk powder. Antibody dilutions anti-*EMC10/Emc10* 1:1000 (rabbit polyclonal; catalog#Ab181209, Abcam, Cambridge, MA, USA),

anti-DGCR8 1:1000 (rabbit monoclonal, catalog#Ab191875, Abcam, Cambridge, MA, USA), anti-RANBP1 1:500 (rabbit polyclonal, catalog#Ab97659, Abcam, Cambridge, MA, USA) and anti-alpha-Tubulin1:1000 (polyclonal rabbit; catalog#2144S, Cell Signal, Danvers, MA, USA) as loading control were prepared in TBS-T/milk and the membrane were incubated overnight at 4°C under slight shaking on an orbital shaker (catalog#980173, Talboys, Troemner, Thorofare, NJ, USA). After three washes with TBS-T, the membrane was incubated with LI-COR goat anti-Rabbit antibody IRDye 800CW (catalog#925-32211, LI-COR Bioscience, Lincoln, NE, USA) for 1.5h at RT. After three washes with TBS-T the membrane was developed using the LI-COR Odyssey CLx system (LI-COR Bioscience, Lincoln, NE, USA) using LI-COR Image Studio software (Ver.5.2) and quantification of band intensity was performed by ImageJ (NIH, Bethesda, MD, USA).

Bulk RNAseq and bioinformatic analysis of mouse hippocampal samples

Sequence reads were aligned to the mouse genome (Ensembl, GRCm38) using the STAR sequence alignment tool (version 2.7) (85) and gene count matrices were generated. Differential gene expression was analyzed using the DESeq2 pipeline (86) in R and volcano plots were generated using the open-source Enhanced Volcano package in R (*https://github.com/kevinblighe/EnhancedVolcano*).

Bulk RNAseq and small RNA/miRNAseq of hiPSC-derived cortical neurons at DIV8

For bulk RNAseq, Poly(A) RNA sequencing library was prepared following Illumina's TruSeq-stranded-mRNA (Illumina, San Diego, CA, USA) sample preparation protocol. RNA integrity was checked with Bioanalyzer 2100 (Agilent, CA, USA). Poly(A) tail-containing mRNAs were purified using oligo-(dT) magnetic beads with two rounds of purification. After purification, poly(A) RNA was fragmented using divalent cation buffer in elevated temperature. Quality control analysis and quantification of the sequencing library were performed using Agilent Technologies 2100 Bioanalyzer High Sensitivity DNA Chip (Agilent, CA, USA). Paired-ended sequencing was performed on Illumina's NovaSeq 6000 (LC Sciences, Houston, TX, USA) sequencing system. For miRNAseq, total RNA quality and quantity was analyzed with Bioanalyzer 2100 (Agilent, CA, USA), with RIN number >7.0. Approximately 1 ug of total RNA was then used to prepare small RNA library according to the protocol of TruSeq Small RNA Sample Prep Kits (Illumina, San Diego, CA, USA). Then, a single-end sequencing 50bp on an Illumina Hiseq 2500 following the vendor's recommended protocol was conducted.

Bioinformatics analysis of human neuron bulk RNAseq at DIV8

Cutadapt (87) and in house perl scripts were used to remove the reads that contained adaptor contamination, low quality bases and undetermined bases. Sequence quality was subsequently verified using FastQC (*http://www.bioinformatics.babraham.ac.uk/projects/fastqc/*). HISAT2 (88) was used to map reads to the genome of *ftp://ftp.ensembl.org/pub/release-101/fasta/homo_sapiens/dna/*. The mapped reads of each sample were assembled using StringTie (89). Then, all transcriptomes were merged to reconstruct a comprehensive transcriptome using perl scripts and GffCompare. After the final transcriptome was generated, StringTie and edgeR (90) were used to estimate the expression levels of all transcripts. StringTie was used to assess expression levels for mRNAs by calculating FPKM. The differentially expressed mRNAs were selected with log2 (fold change) >1 or log2 (fold change) <-1 and with statistical significance (p value < 0.05) by R package edgeR.

For the VolcanoPlot visualization, the web-based R package Shiny application "VolcanoPlot" (*https://paolo.shinyapps.io/ShinyVolcanoPlot/*) was used. DEGs (adj. Pvalue<0.05) were plotted by selecting the axes ((Log2(FC) range= −2.5/2.5 and −Log10(Pvalue)=15) and setting the cutoff selection (P-value threshold=1.3 (0.05), Log2(FC) threshold 0.4 and 3). The GO-Term enrichment

analysis was performed for the up- and downregulated protein-coding genes (1937/2094, DEG) by using the standard setting (g:SCS threshold) of the gProfiler webtool (*https://biit.cs.ut.ee/gprofiler/gost*) (91). TargetScan (v8.0, *http://www.targetscan.org/vert_80/*) was used for miRNA binding site prediction (92). Intersection of genes and predicted targets were conducted by using the VIB / UGent Bioinformatics & Evolutionary Genomics (Gent, Belgium) webtool "Venn" (*https://bioinformatics.psb.ugent.be/webtools/Venn/*).

Bioinformatics analysis of human neuron miRNA-seq at DIV8

Raw reads were subjected to an in-house program, ACGT101-miR (LC Sciences, Houston, TX, USA) to remove adapter dimers, junk, low complexity, common RNA families (rRNA, tRNA, snRNA, snoRNA) and repeats. Subsequently, unique sequences with length in 18~26 nucleotide were mapped to specific species precursors in miRBase (v22.0) by BLAST search to identify known miRNAs and novel 3p- and 5p-derived miRNAs. Length variation at both 3' and 5' ends and one mismatch inside of the sequence were allowed in the alignment. The unique sequences mapping to specific species mature miRNAs in hairpin arms were identified as known miRNAs. The unique sequences mapping to the other arm of known specific species precursor hairpin opposite to the annotated mature miRNA-containing arm were considered to be novel 5p- or 3p derived miRNA candidates. The remaining sequences were mapped to other selected species precursors (with the exclusion of specific species) in miRBase 22.0 by BLAST search, and the mapped pre-miRNAs were further BLASTed against the specific species genomes to determine their genomic locations. The above two mentioned mapped 5p and 3p sequences were defined as known miRNAs. The unmapped sequences were BLASTed against the specific genomes, and the hairpin RNA structures containing sequences were predicted from the flank 80 nt sequences using RNAfold (*http://rna.tbi.univie.ac.at/cgi-bin/RNAWebSuite/RNAfold.cgi*) software. The criteria for secondary structure prediction were: (1.) number of nucleotides in one bulge in stem (≤12) (2.) number of base pairs in the stem region of the predicted hairpin (≥16) (3.) cutoff of free energy (kCal/mol ≤-15) (4.) length of hairpin (up and down stems + terminal loop ≥50) (5.) length of hairpin loop (≤20). (6.) number of nucleotides in one bulge in mature region (≤8) (7.) number of biased errors in one bulge in mature region (≤4) (8.) number of biased bulges in mature region (≤2) (9.) number of errors in mature region (≤7) (10.) number of base pairs in the mature region of the predicted hairpin (≥12) (11.) percent of mature in stem (≥80). For the VolcanoPlot visualization, the web-based R package Shiny application "VolcanoPlot" (*https://paolo.shinyapps.io/ShinyVolcanoPlot/*) was used. DEmiRs (Pvalue<0.05) of known miRNAs were plotted by selecting the axes ((Log2(FC) range= −5/5 and -Log10(Pvalue)=10) and setting the cutoff selection (P-value threshold=1.3 (0.05), Log2(FC) threshold 0.4). For the GO-term enrichment analysis of the up- and down-regulated miRNAs (153/133, DEmiRs) the webtool miRNet 2.0 (*https://www.mirnet.ca/*) with standard settings (tissue: nervous, targets: genes [miRTarBase 8.0]) was used (30). TargetScan (v8.0, *http://www.targetscan.org/vert_80/*) was used for all miRNA binding site prediction (92) for miR-185-5p, miR1306-5p and miR-1286 and using the biochemical predicted occupancy model (93) for table sorting.

Bulk RNAseq and bioinformatic analysis of NGN2-induced neurons at DIV21

We used poly-A pull-down to enrich mRNAs from total RNA samples, then proceed with library construction using Illumina TruSeq chemistry (Illumina, San Diego, CA, USA). Libraries were then sequenced using Illumina NovaSeq 6000 at Columbia Genome Center. We multiplexed samples in each lane, which yields targeted number of paired-end 100bp reads for each sample. We used RTA (Illumina) for base calling and bcl2fastq2 (version 2.19) for converting BCL to fastq format, coupled with adaptor trimming. We performed a pseudoalignment to a kallisto index created from transcriptomes (Ensembl v96, Human:GRCh38.p12) using kallisto (0.44.0) (94). We tested for differentially expressed genes using DESeq2 (adj. Pvalue<0.05), R packages designed to test differential expression between two experimental groups from RNA-seq counts data. Intersection of DEGs were conducted by using the VIB / UGent Bioinformatics & Evolutionary Genomics (Gent, Belgium) webtool "Venn" (*https://bioinformatics.psb.ugent.be/webtools/Venn/*). GO-Term

enrichment analysis was performed for the up- and downregulated DEGs Q5(Ctrl)/Q6(22q11.2) and normalized up- and downregulated DEGs in Q6/EMC10^{HET} and Q6/EMC10^{HOM} by using the standard setting (g:SCS threshold) of the gProfiler webtool *https://biit.cs.ut.ee/gprofiler/gost*) (91). Heatmaps of DEGs that were normalized in Q6/EMC10^{HET} and Q6/EMC10^{HOM} were generated with the R based web tool Heatmapper (*http://www.heatmapper.ca*) (95). PPI network analysis of the rescued 103 DEGs in Q6/EMC10^{HET} and Q6/EMC10^{HOM} conditions were performed by using the web-application konnect2prot (96). Hereby, GO-Term enrichment analysis of the identified 30 matched DEGs were performed by using g-Profiler webtool as indicated above.

Behavioral assays

Open Field assay

The open field activity assay was performed as described earlier (19). In brief, mouse activity was monitored in a clear illuminated acrylic chamber (25 cm x 25 cm) equipped with infrared sensors to automatically record horizontal and vertical activity (Coulbourn Instruments, Whitehall, PA, USA). Each mouse was initially placed in the center of the chamber and its activity was recorded and collected in 1-min bins for 1 h using TruScan (v1.012-00) software (Coulbourn Instruments, Whitehall, PA, USA). The floors and walls of the open field were cleaned with 70% ethanol between trials.

Social Memory assay

Assays were performed as described earlier in juvenile (postnatal day 22-24) (26) and adult (6, 19) mice. All experimental mice were single housed, transferred to the testing room one hour prior to testing and returned to their home cages after the completion of the experiment. Both male and female were tested in the juvenile SM assays, in the TAM/corn oil treatment assays as well as in the ASO1 assays. Only males were tested in the ASO2 assays. For the adult SM assays, stimulus mice (C57 BL/6J) were obtained from Jackson Laboratory (Bar Harbor, ME, USA). All stimulus mice were between the ages of 3-4 weeks. Test and stimulus mice were sex matched in the experimental trials. All trials were recorded using a video camera (Webcam Pro 9000, Logitech, Lausanne, Switzerland) and recorder software (Logitech video recording software). Stimulus mice were color marked on the tails to distinguish the stimulus mice from the test mice, during video analysis. The videos were manually scored for total interaction time over the course of the trials for interactions initiated by the test animal including anal sniffing, nose-to-nose touch and close following. For the novel/familiar paradigm, test and stimulus (novel) mice were placed together in a neutral cage and the interaction was recorded (trial 1). One hour after trial 1, the same stimulus (familiar) mouse was placed together with the test mouse and the interaction was recorded again (trial 2). A similar procedure was followed for the control novel/novel paradigm, except that we used different stimulus mice for trial 1 and trial 2 such that at trial 2 the stimulus mice were also novel for the experimental mice. Trials with experimental mice showing highly aggressive behavior towards the stimulus mice or mice that interacted for less than 24s in trial 1 were excluded from the analysis.

Contextual Fear Conditioning assay

Contextual Fear Conditioning assays were performed as described earlier (5, 19) using a Coulbourn animal shocker (Model H13-15 110V, Coulbourn Instruments, Whitehall, PA, USA). Sound levels were checked with a Digital Sound Level Meter (Model: 407730, Extech Instruments, MA, USA) before beginning the trials. Using a cotton swab, pure lemon extract (McCormick & Co, Hunt Valley, MD, USA) was introduced into the testing chamber adding 9 different but equal distributed spots on a napkin. Test mice were placed in the test chamber and received 2 pairs of a tone (30s, 82db) and a co-terminating shock (2s, 0.7mA). Mice were then carefully picked with

forceps and returned to their home cage. After 24 hours, mice were placed in the FC box again with same environment and lemon scent for 6 minutes in the absence of tone and shock to test for contextual memory. The box and grid were cleaned with 70% EtOH before and between every test run on both days. Videos were recorded and analyzed by using FreezeFrame 3 software (Harvard Apparatus, Holliston, MA, USA).

Y-Maze assay

The Y-maze apparatus was made from white acrylic that consists of three equal-sized arms (38 cm long, 13 cm high, and 8 cm wide) of which each arm of the Y-maze was positioned at an equal angle and was purchased from SD Instruments (cat#7001-0419, San Diego, CA, USA). The Y-maze assay was performed as described previously in more detail (58, 97). In brief, adult male mice were tested on delayed alternations. Exploration in all three arms of the Y-maze was performed after a 1 h delay from an initial training phase of 10 min, where one arm of the maze was blocked (delayed alternation). Delayed alternation (%) was calculated as the number of entries in all three arms divided by the total number of entries in the first 5 min of the 10 min test phase whereas the number of entries per arm was used as a measurement of activity and locomotion. The movement of mice was recorded with a camera mounted above the apparatus and the number of arm entries was counted manually.

Data availability

The sequencing data described in this manuscript were deposited into the Gene Expression Omnibus database under accession number GSE236596 and are available at the following URL: *https://www.ncbi.nlm.nih.gov/geo/query/acc.cgi?acc=GSE236596*.

Acknowledgements

We thank Dr. Huynh-Hao Bui and Andrew Watt for design and identification of ASOs, Mark Andrade and the Ionis synthesis group for ASO synthesis, and Dr. Mark Graham for ASO study design and feedback. We thank Naoko Haremaki for genotyping, maintaining the mouse colony and for assisting in the SM and Y-maze assays. We thank Panagiota Apostolou for her help with the calcium imaging setup. We thank Yan Sun and Vivian Zhu for the hiPSC line validation and maintenance. We thank Barbara Corneo and the Columbia Stem Cell Core Facility for the Q1, Q2, Q5 and Q6 hiPSC lines generation. Bio-samples of Q20 and Q27 hiPSCs were obtained from NIMH Repository & Genomics Resource. We would like to thank Zuckerman Institute's Cellular Imaging platform for instrument use and technical advice. We thank the Columbia Genome Center for genome sequencing and analysis support. We thank Linda Brzustowicz and Bill Manley from the Rutgers University and the staff members at RUCDR. Data and biomaterials generated in Study 125/Site 393 were funded by a NIMH grant to Dr. Herb Lachman (MH087840: Analysis of Glutamatergic Neurons Derived from Patient-Specific iPS Cells). The co-investigators on this grant included Dr. Deyou Zheng and Dr. Reed Carroll from the Albert Einstein College of Medicine. Patients and controls were recruited at the Albert Einstein College of Medicine and at the Child Psychiatry Branch, NIMH, directed by Dr. Judith L. Rapoport. We thank all participating subjects and their families for their contributions.

Additional information

Author contributions

PT contributed to the design of the *in vivo* ASO screening and performed the ASO injections/surgeries as well as mouse related RNA and protein expression, immunohistochemistry and behavioral analysis. ML contributed to the design, characterization, expression and phenotypic analysis of human iPSC lines, the *Emc10* conditional knockout mouse-related RNA/protein expression assays and behavioral analysis, the behavioral analysis of the juvenile *Df(16)A*$^{+/-}$ mouse line, the Y-maze behavioral assays and the related behavioral assays of the long-term ASO-injected animals. Further, ML conducted the implementation and analysis of mouse fear conditioning assays and contributed to the ASO-related mouse RNA/protein expression assays. AD contributed to the design and implementation of the *in vivo* ASO screening and behavioral data acquisition. SR analyzed mouse related RNA sequencing data. YC contributed to mouse related immunohistochemistry assays. KK contributed to the ASO injections/surgeries and to the qRT-PCR assays. AF, CM, and HK contributed to the identification and characterization of the lead ASOs. BX, contributed to the generation and initial characterization of human iPSC lines as well as the design of the human neuron-related assays. RJS provided patient referrals. SM contributed to the generation and initial characterization of human iPSC lines. JAG contributed to the conception, design and supervision of the study; PT, ML, SR, BX, SM, and JAG. contributed to the preparation of the manuscript with input from all authors.

Funding

This work was supported by National Institute of Mental Health Grant (2R01MH097879), a Columbia University Translational Therapeutics Pilot Award to J.A.G and the Stavros Niarchos Foundation (SNF). This research used the service of the Columbia Genome Center (Genomics and High Throughput Screening Shared Resource), that was funded in part through the NIH/NCI Cancer Center Support Grant P30CA013696.

Additional files

Supplementary Tables.

References

1. Morrison S., et al. 2020) **Cognitive deficits in childhood, adolescence and adulthood in 22q11.2 deletion syndrome and association with psychopathology** *Transl Psychiatry* **10**

2. Woodin M., et al. 2001) **Neuropsychological profile of children and adolescents with the 22q11.2 microdeletion** *Genet Med* **3**:34–39

3. McCabe K. L., et al. 2013) **Divergent patterns of social cognition performance in autism and 22q11.2 deletion syndrome (22q11DS)** *J Autism Dev Disord* **43**:1926–1934

4. Xu B., et al. 2008) **Strong association of de novo copy number mutations with sporadic schizophrenia** *Nat Genet* **40**:880–885

5. Stark K. L., et al. 2008) **Altered brain microRNA biogenesis contributes to phenotypic deficits in a 22q11-deletion mouse model** *Nat Genet* **40**:751–760

6. Piskorowski R. A., et al. 2016) **Age-Dependent Specific Changes in Area CA2 of the Hippocampus and Social Memory Deficit in a Mouse Model of the 22q11.2 Deletion Syndrome** *Neuron* **89**:163–176

7. Xu B., Hsu P. K., Stark K. L., Karayiorgou M., Gogos J. A. 2013) **Derepression of a neuronal inhibitor due to miRNA dysregulation in a schizophrenia-related microdeletion** *Cell* **152**:262–275

8. Gregory R. I., et al. 2004) **The Microprocessor complex mediates the genesis of microRNAs** *Nature* **432**:235–240

9. Sun Z., Williams D. J., Xu B., Gogos J. A. 2018) **Altered function and maturation of primary cortical neurons from a 22q11.2 deletion mouse model of schizophrenia** *Transl Psychiatry* **8**

10. Saito R., et al. 2020) **Comprehensive analysis of a novel mouse model of the 22q11.2 deletion syndrome: a model with the most common 3.0-Mb deletion at the human 22q11.2 locus** *Transl Psychiatry* **10**

11. Guna A., Volkmar N., Christianson J. C., Hegde R. S. 2018) **The ER membrane protein complex is a transmembrane domain insertase** *Science* **359**:470–473

12. Chitwood P. J., Juszkiewicz S., Guna A., Shao S., Hegde R. S. 2018) **EMC Is Required to Initiate Accurate Membrane Protein Topogenesis** *Cell* **175**:1507–1519

13. Richard M., Boulin T., Robert V. J., Richmond J. E., Bessereau J. L. 2013) **Biosynthesis of ionotropic acetylcholine receptors requires the evolutionarily conserved ER membrane complex** *Proc Natl Acad Sci U S A* **110**:E1055–1063

14. Satoh T., Ohba A., Liu Z., Inagaki T., Satoh A. K. 2015) **dPob/EMC is essential for biosynthesis of rhodopsin and other multi-pass membrane proteins in Drosophila photoreceptors** *eLife* **4**

15. Bircham P. W., et al. 2011) **Secretory pathway genes assessed by high-throughput microscopy and synthetic genetic array analysis** *Mol Biosyst* **7**:2589–2598

16. Louie R. J., et al. 2012) **A yeast phenomic model for the gene interaction network modulating CFTR-DeltaF508 protein biogenesis** *Genome Med* **4**

17. Shurtleff M. J., et al. 2018) **The ER membrane protein complex interacts cotranslationally to enable biogenesis of multipass membrane proteins** *eLife* **7**

18. Tian S., et al. 2019) **Proteomic Analysis Identifies Membrane Proteins Dependent on the ER Membrane Protein Complex** *Cell Rep* **28**:2517–2526

19. Diamantopoulou A., et al. 2017) **Loss-of-function mutation in Mirta22/Emc10 rescues specific schizophrenia-related phenotypes in a mouse model of the 22q11.2 deletion** *Proc Natl Acad Sci U S A* **114**:E6127–E6136

20. Qi Y., et al. 2017) **Combined small-molecule inhibition accelerates the derivation of functional cortical neurons from human pluripotent stem cells** *Nat Biotechnol* **35**:154–163

21. Siegert S., et al. 2015) **The schizophrenia risk gene product miR-137 alters presynaptic plasticity** *Nat Neurosci* **18**:1008–1016

22. Thomas K. T., et al. 2017) **Inhibition of the Schizophrenia-Associated MicroRNA miR-137 Disrupts Nrg1alpha Neurodevelopmental Signal Transduction** *Cell Rep* **20**:1–12

23. Schratt G. M., et al. 2006) **A brain-specific microRNA regulates dendritic spine development** *Nature* **439**:283–289

24. Fiore R., et al. 2009) **Mef2-mediated transcription of the miR379-410 cluster regulates activity-dependent dendritogenesis by fine-tuning Pumilio2 protein levels** *EMBO J* **28**:697–710

25. Rago L., Beattie R., Taylor V., Winter J. 2014) **miR379-410 cluster miRNAs regulate neurogenesis and neuronal migration by fine-tuning N-cadherin** *EMBO J* **33**:906–920

26. Lackinger M., et al. 2019) **A placental mammal-specific microRNA cluster acts as a natural brake for sociability in mice** *EMBO Rep* **20**

27. Gardiner E., et al. 2012) **Imprinted DLK1-DIO3 region of 14q32 defines a schizophrenia-associated miRNA signature in peripheral blood mononuclear cells** *Mol Psychiatry* **17**:827–840

28. Tomasello U., et al. 2022) **miR-137 and miR-122, two outer subventricular zone non-coding RNAs, regulate basal progenitor expansion and neuronal differentiation** *Cell Rep* **38**

29. Whipple A. J., et al. 2020) **Imprinted Maternally Expressed microRNAs Antagonize Paternally Driven Gene Programs in Neurons** *Mol Cell* **78**:85–95

30. Chang L., Zhou G., Soufan O., Xia J. 2020) **miRNet 2.0: network-based visual analytics for miRNA functional analysis and systems biology** *Nucleic Acids Res* **48**:W244–W251

31. Zhang Y., et al. 2013) **Rapid single-step induction of functional neurons from human pluripotent stem cells** *Neuron* **78**:785–798

32. Yi F., et al. 2016) **Autism-associated SHANK3 haploinsufficiency causes Ih channelopathy in human neurons** *Science* **352**:aaf2669

33. Ho S. M., et al. 2016) **Rapid Ngn2-induction of excitatory neurons from hiPSC-derived neural progenitor cells** *Methods* **101**:113–124

34. Pak C., Grieder S., Yang N., Zhang Y., Wernig M., Sudhof T 2018) **Rapid generation of functional and homogeneous excitatory human forebrain neurons using Neurogenin-2 (Ngn2)** *Nature Protocol Exchange*

35. Rao S. B., et al. 2023) **Aberrant pace of cortical neuron development in brain organoids from patients with 22q11.2 deletion syndrome and schizophrenia** *bioRxiv*

36. Cohen J. E., Lee P. R., Chen S., Li W., Fields R. D. 2011) **MicroRNA regulation of homeostatic synaptic plasticity** *Proc Natl Acad Sci U S A* **108**:11650–11655

37. Soutschek A. L. B. M., Galkin S., Wüst T., Colameo D., Germade T., Gross F., Ziegler L. v., Bohacek J., Germain P.L., Winterer J., Kleele T., Schratt G.M. 2023) **A human-specific microRNA controls the timing of excitatory synaptogenesis** *bioRxiv*

38. Wilson K. D., et al. 2009) **MicroRNA profiling of human-induced pluripotent stem cells** *Stem Cells Dev* **18**:749–758

39. Khan T. A., et al. 2020) **Neuronal defects in a human cellular model of 22q11.2 deletion syndrome** *Nat Med* **26**:1888–1898

40. Shao Z., et al. 2019) **Dysregulated protocadherin-pathway activity as an intrinsic defect in induced pluripotent stem cell-derived cortical interneurons from subjects with schizophrenia** *Nat Neurosci* **22**:229–242

41. O'Leary A., et al. 2022) **Behavioural and functional evidence revealing the role of RBFOX1 variation in multiple psychiatric disorders and traits** *Mol Psychiatry* **27**:4464–4473

42. Mirnics K., Middleton F. A., Stanwood G. D., Lewis D. A., Levitt P. 2001) **Disease-specific changes in regulator of G-protein signaling 4 (RGS4) expression in schizophrenia** *Mol Psychiatry* **6**:293–301

43. Erdely H. A., Tamminga C. A., Roberts R. C., Vogel M. W. 2006) **Regional alterations in RGS4 protein in schizophrenia** *Synapse* **59**:472–479

44. Volkmar N., et al. 2019) **The ER membrane protein complex promotes biogenesis of sterol-related enzymes maintaining cholesterol homeostasis** *J Cell Sci* **132**

45. Donegan M. L., et al. 2020) **Coding of social novelty in the hippocampal CA2 region and its disruption and rescue in a 22q11.2 microdeletion mouse model** *Nat Neurosci* **23**:1365–1375

46. Green M. F., Horan W. P., Lee J. 2015) **Social cognition in schizophrenia** *Nat Rev Neurosci* **16**:620–631

47. Jalal R., et al. 2021) **Social cognition in 22q11.2 deletion syndrome and idiopathic developmental neuropsychiatric disorders** *J Neurodev Disord* **13**

48. Becker L. A., et al. 2017) **Therapeutic reduction of ataxin-2 extends lifespan and reduces pathology in TDP-43 mice** *Nature* **544**:367–371

49. DeVos S. L., et al. 2017) **Tau reduction prevents neuronal loss and reverses pathological tau deposition and seeding in mice with tauopathy** *Sci Transl Med* **9**

50. Kordasiewicz H. B., et al. 2012) **Sustained therapeutic reversal of Huntington's disease by transient repression of huntingtin synthesis** *Neuron* **74**:1031–1044

51. Korobeynikov V. A., Lyashchenko A. K., Blanco-Redondo B., Jafar-Nejad P., Shneider N. A. 2022) **Antisense oligonucleotide silencing of FUS expression as a therapeutic approach in amyotrophic lateral sclerosis** *Nat Med* **28**:104–116

52. Scoles D. R., et al. 2017) **Antisense oligonucleotide therapy for spinocerebellar ataxia type 2** *Nature* **544**:362–366

53. Sztainberg Y., et al. 2015) **Reversal of phenotypes in MECP2 duplication mice using genetic rescue or antisense oligonucleotides** *Nature* **528**:123–126

54. Tabrizi S. J., Smith A. V., Bennett C. F. 2019) **Targeting Huntingtin in Patients with Huntington's Disease. Reply** *N Engl J Med* **381**:1181–1182

55. Winkelsas A. M., Fischbeck K. H. 2020) **Nucleic acid therapeutics in neurodevelopmental disease** *Curr Opin Genet Dev* **65**:112–116

56. Rinaldi C., Wood M. J. A. 2018) **Antisense oligonucleotides: the next frontier for treatment of neurological disorders** *Nat Rev Neurol* **14**:9–21

57. Langmead B., Trapnell C., Pop M., Salzberg S. L. 2009) **Ultrafast and memory-efficient alignment of short DNA sequences to the human genome** *Genome Biol* **10**

58. Tripathi A., et al. 2020) **Cognition- and circuit-based dysfunction in a mouse model of 22q11.2 microdeletion syndrome: effects of stress** *Transl Psychiatry* **10**

59. Paranjape N., et al. 2023) **A CRISPR-engineered isogenic model of the 22q11.2 A-B syndromic deletion** *Sci Rep* **13**:7689

60. Benger M., Kinali M., Mazarakis N. D. 2018) **Autism spectrum disorder: prospects for treatment using gene therapy** *Mol Autism* **9**

61. Shao Y., et al. 2021) **Antisense oligonucleotide therapy in a humanized mouse model of MECP2 duplication syndrome** *Sci Transl Med* **13**

62. Kaiyrzhanov R., et al. 2022) **Biallelic loss of EMC10 leads to mild to severe intellectual disability** *Ann Clin Transl Neurol* **9**:1080–1089

63. Shao D. D., et al. 2021) **A recurrent, homozygous EMC10 frameshift variant is associated with a syndrome of developmental delay with variable seizures and dysmorphic features** *Genet Med* **23**:1158–1162

64. Umair M., et al. 2020) **EMC10 homozygous variant identified in a family with global developmental delay, mild intellectual disability, and speech delay** *Clin Genet* **98**:555–561

65. Karczewski K. J., et al. 2020) **The mutational constraint spectrum quantified from variation in 141,456 humans** *Nature* **581**:434–443

66. Wideman J. G. 2015) **The ubiquitous and ancient ER membrane protein complex (EMC): tether or not?** *F1000Res* **4**:624

67. Mukai J., et al. 2019) **Recapitulation and Reversal of Schizophrenia-Related Phenotypes in Setd1a-Deficient Mice** *Neuron* **104**:471–487

68. Cheruvallath Z. S., Cole D. L., Ravikumar V. T. 2003) **A novel solid support for synthesis of oligonucleotide 3'-phosphorothioate monoesters** *Bioorg Med Chem Lett* **13**:281–284

69. McKay R. A., et al. 1999) **Characterization of a potent and specific class of antisense oligonucleotide inhibitor of human protein kinase C-alpha expression** *J Biol Chem* **274**:1715–1722

70. Barreto-Chang O. L., Dolmetsch R. E. 2009) **Calcium imaging of cortical neurons using Fura-2 AM** *J Vis Exp*

71. Li Y., et al. 2021) **Investigation of Neurodevelopmental Deficits of 22 q11.2 Deletion Syndrome with a Patient-iPSC-Derived Blood-Brain Barrier Model** *Cells* **10**

72. Lin M., et al. 2016) **Integrative transcriptome network analysis of iPSC-derived neurons from schizophrenia and schizoaffective disorder patients with 22q11.2 deletion** *BMC Syst Biol* **10**

73. Fusaki N., Ban H., Nishiyama A., Saeki K., Hasegawa M. 2009) **Efficient induction of transgene-free human pluripotent stem cells using a vector based on Sendai virus, an RNA virus that does not integrate into the host genome** *Proc Jpn Acad Ser B Phys Biol Sci* **85**:348–362

74. Riera M., et al. 2019) **Generation of two iPS cell lines (FRIMOi003-A and FRIMOi004-A) derived from Stargardt patients carrying ABCA4 compound heterozygous mutations** *Stem Cell Res* **36**

75. Cradick T. J., Qiu P., Lee C. M., Fine E. J., Bao G. 2014) **COSMID: A Web-based Tool for Identifying and Validating CRISPR/Cas Off-target Sites** *Mol Ther Nucleic Acids* **3**:e214

76. Hockemeyer D., et al. 2008) **A drug-inducible system for direct reprogramming of human somatic cells to pluripotency** *Cell Stem Cell* **3**:346–353

77. Ho S. M., et, al. 2017) **Stem Cell Reports** :615–628

78. Brenes J. C., et al. 2016) **Differential effects of social and physical environmental enrichment on brain plasticity, cognition, and ultrasonic communication in rats** *J Comp Neurol* **524**:1586–1607

79. Mukai J., et al. 2008) **Palmitoylation-dependent neurodevelopmental deficits in a mouse model of 22q11 microdeletion** *Nat Neurosci* **11**:1302–1310

80. Wearne S. L., et al. 2005) **New techniques for imaging, digitization and analysis of three-dimensional neural morphology on multiple scales** *Neuroscience* **136**:661–680

81. Peng H., Ruan Z., Long F., Simpson J. H., Myers E. W. 2010) **V3D enables real-time 3D visualization and quantitative analysis of large-scale biological image data sets** *Nat Biotechnol* **28**:348–353

82. Peng H., Bria A., Zhou Z., Iannello G., Long F. 2014) **Extensible visualization and analysis for multidimensional images using Vaa3D** *Nat Protoc* **9**:193–208

83. Peng H., et al. 2014) **Virtual finger boosts three-dimensional imaging and microsurgery as well as terabyte volume image visualization and analysis** *Nat Commun* **5**:4342

84. Kopec A. M., Rivera P. D., Lacagnina M. J., Hanamsagar R., Bilbo S. D. 2017) **Optimized solubilization of TRIzol-precipitated protein permits Western blotting analysis to maximize data available from brain tissue** *J Neurosci Methods* **280**:64–76

85. Dobin A., et al. 2013) **STAR: ultrafast universal RNA-seq aligner** *Bioinformatics* **29**:15–21

86. Love M. I., Huber W., Anders S. 2014) **Moderated estimation of fold change and dispersion for RNA-seq data with DESeq2** *Genome Biol* **15**

87. Martin M. 2011) **Cutadapt removes adapter sequences from high-throughput sequencing reads** *EMBnet.journal*

88. Kim D., Langmead B., Salzberg S. L. 2015) **HISAT: a fast spliced aligner with low memory requirements** *Nat Methods* **12**:357–360

89. Pertea M., et al. 2015) **StringTie enables improved reconstruction of a transcriptome from RNA-seq reads** *Nat Biotechnol* **33**:290–295

90. Robinson M. D., McCarthy D. J., Smyth G. K. 2010) **edgeR: a Bioconductor package for differential expression analysis of digital gene expression data** *Bioinformatics* **26**:139–140

91. Raudvere U., et al. 2019) **, g:Profiler: a web server for functional enrichment analysis and conversions of gene lists (2019 update)** *Nucleic Acids Res* **47**:W191–W198

92. Agarwal V., Bell G. W., Nam J. W., Bartel D. P. 2015) **Predicting effective microRNA target sites in mammalian mRNAs** *eLife* **4**

93. McGeary S. E., et al. 2019) **The biochemical basis of microRNA targeting efficacy** *Science* **366**

94. Bray N. L., Pimentel H., Melsted P., Pachter L. 2016) **Near-optimal probabilistic RNA-seq quantification** *Nat Biotechnol* **34**:525–527

95. Babicki S., et al. 2016) **Heatmapper: web-enabled heat mapping for all** *Nucleic Acids Res* **44**:W147–153

96. Kumar S., Sarmah D. T., Asthana S., Chatterjee S. 2023) **konnect2prot: a web application to explore the protein properties in a functional protein-protein interaction network** *Bioinformatics* **39**

97. Kraeuter A. K., Guest P. C., Sarnyai Z. 2019) **The Y-Maze for Assessment of Spatial Working and Reference Memory in Mice** *Methods Mol Biol* **1916**:105–111

Author information

Pratibha Thakur[†]
Mortimer B. Zuckerman Mind Brain and Behavior Institute, Columbia University, New York, United States
ORCID iD: 0000-0001-8585-1901

[†]These authors contributed equally to this work.

Martin Lackinger[†]
Mortimer B. Zuckerman Mind Brain and Behavior Institute, Columbia University, New York, United States, Stavros Niarchos Foundation Center for Precision Psychiatry and Mental Health, Columbia University, New York, United States
ORCID iD: 0000-0002-7946-5366

[†]These authors contributed equally to this work.

Anastasia Diamantopoulou[‡]
Mortimer B. Zuckerman Mind Brain and Behavior Institute, Columbia University, New York, United States

[‡]Present address: Institute of Neurophysiology, Goethe University, Theodor-Stern-Kai 7, D-60590 Frankfurt am Main, Germany

Sneha Rao
Mortimer B. Zuckerman Mind Brain and Behavior Institute, Columbia University, New York, United States

Yijing Chen
Mortimer B. Zuckerman Mind Brain and Behavior Institute, Columbia University, New York, United States, Department of Genetics and Development, Columbia University Irvine Medical Center, New York, United States

Khakima Khalizova
Mortimer B. Zuckerman Mind Brain and Behavior Institute, Columbia University, New York, United States, Stavros Niarchos Foundation Center for Precision Psychiatry and Mental Health, Columbia University, New York, United States

Annie Ferng
Ionis Pharmaceuticals, Inc., Carlsbad, United States

Curt Mazur
Ionis Pharmaceuticals, Inc., Carlsbad, United States

Holly Kordasiewicz
Ionis Pharmaceuticals, Inc., Carlsbad, United States

Robert J Shprintzen
The Virtual Center for Velo-Cardio-Facial-Syndrome, Inc

Sander Markx
Stavros Niarchos Foundation Center for Precision Psychiatry and Mental Health, Columbia University, New York, United States, Department of Psychiatry, Vagelos College of Physicians & Surgeons, Columbia University, New York, United States

Bin Xu
Stavros Niarchos Foundation Center for Precision Psychiatry and Mental Health, Columbia University, New York, United States, Department of Psychiatry, Vagelos College of Physicians & Surgeons, Columbia University, New York, United States

Joseph A Gogos
Mortimer B. Zuckerman Mind Brain and Behavior Institute, Columbia University, New York, United States, Stavros Niarchos Foundation Center for Precision Psychiatry and Mental Health, Columbia University, New York, United States, Department of Psychiatry, Vagelos College of Physicians & Surgeons, Columbia University, New York, United States, Department of Physiology and Cellular Biophysics, College of Physicians and Surgeons, Columbia University, New York, United States, Department of Neuroscience, Columbia University, New York, United States
ORCID iD: 0000-0002-7491-4476

For correspondence: jag90@columbia.edu

Editors

Reviewing Editor
Anne West
Duke University, Durham, United States of America

Senior Editor
Lu Chen
Stanford University, Stanford, United States of America

Reviewer #1 (Public review):

Summary:

This is an important and very well-presented set of experiments following up on prior work from the lab investigating knock-down (KD) of EMC10 in restoration of neuronal and cognitive deficits in 22q11.2 Del models, including now both human iPSCs and a mouse model in vivo now with ASOs.

The valuable progress in this current manuscript is the development of ASOs, and the proof of efficacy in vivo in mouse of the ASO in knock-down of EMC10 and amelioration of in vivo behavioral phenotypes.

The experiments include: iPSC studies demonstrating elevations of EMC10 in a solid collection of paired iPSC lines. These studies also provide evidence of manipulation of EMC10 by overexpression and inhibition of miRNAs that exist in the 22q11 interval. The iPSC studies also nicely demonstrate rescue of impairments with KD of EMC10 in neuronal arborization as well as KCl induced neuronal activity. The major in vivo contributions reflect impressive demonstration of efficacy of two ASOs in vivo on both KD of EMC10 in vivo and through improvement in behavioral abnormalities in the 22q11 mouse in a range of different behaviors, including social behavior and learning behaviors.

Overall, there are many strengths reflected in this study, including in particular the synergy between in vitro studies in human cell models and in vivo studies in the well characterized mouse model. The experiments are generally rigorously performed and well powered, and nicely presented. The claims with regard to the mechanisms of EMC10 elevations and the importance of restoration of EMC10 expression to neuronal morphology and behavior are well supported by the data. The work may be further supported in future studies, by investigation of rescue by ASOs of circuit dysfunction in vivo or ex vivo through electrophysiology in the mouse model. Also, in future studies, investigation of the mechanism by which EMC10, an ER protein involved in protein processing, may function in the observed neuronal abnormalities; however, these studies are clearly for future investigations.

The potential impact of the work is found in the potential value of the ASO approach to the treatment of 22q11, or the pre-clinical evidence that knock-down of this protein may lead to some amelioration of cognitive symptoms. Overall, a very convincing and complementary set of experiments to support EMC10 KD as a therapeutic strategy.

Review of revision: The authors have addressed the questions from the prior review.

https://doi.org/10.7554/eLife.103328.2.sa1

Author response:

The following is the authors' response to the original reviews.

We appreciate that both reviewers found our findings significant and recognized the strength of the presented data in demonstrating the potential value of ASO-mediated Emc10 expression modulation for treating 22q11.2DS. We are grateful for the reviewers' valuable input and constructive suggestions, which we believe have significantly strengthened our manuscript. Below, we address the main points and concerns, followed by our point-by-point responses:

Evaluation of ASO-Mediated Emc10 Reduction: We appreciate the feedback and the opportunity to clarify this point. While we agree that ASO-mediated reduction of Emc10 should ideally be evaluated at both the mRNA and protein levels, we would like to emphasize that this was indeed performed in our study. Specifically, we conducted both qRT-PCR and Western Blot (WB) assays on the same animal cohort, focusing on the left and right hippocampus (rather than the PFC) following ASO injection (see Figure S11C and D). We prioritized the hippocampus for the WB assay because our primary behavioral assays and observed phenotypes in this study are strongly hippocampus-centric. This approach reflects our aim to investigate Emc10's role in the brain regions most relevant to the observed phenotypes. We hope this clarification addresses the reviewer's concerns. While protein-level analysis would ideally complement RNA measurements, the Emc10 antibodies available were suboptimal in specificity and sensitivity, requiring substantial optimization. Additionally, challenges in obtaining sufficient high-quality protein from small regions like the hippocampus limited the use of protein detection as a standalone method. We plan to refine antibody protocols or explore alternative methods in future work. Notably, in all instances where we performed parallel protein and RNA measurements in both, mouse brain tissue and human cell lines, there was excellent concordance between the datasets, strongly suggesting that mRNA levels are a reliable indicator of Emc10 protein levels in our model.

ASO Neuronal Uptake: While ASO uptake by neurons in the brain can vary considerably depending on factors such as ASO chemistry, delivery method, target brain region, and cell type, our targeted delivery approach, ASO design optimization, and ASO screening strategy were specifically tailored to achieve uniform and efficient uptake across hippocampal and

cortical regions, in both neurons and glia. The figures included in our manuscript at both low and high magnification (see Figure S14A) clearly display the extensive (over 97%) overlap of ASO-positive cells (green signal) with cells expressing the neuronal marker NeuN (red signal). While quantifying ASO-positive cells in different brain regions could add value, the robust diffusion of ASO into neurons and glia is effectively demonstrated in the current figures and indirectly supported by the robust downregulation of Emc10 in ASO-treated animals as shown by qRT-PCR assays of hippocampal and cortical brain regions.

Transcriptomic Data in Mutant EMC10 NGN2-iNs: Reduction in EMC10 levels is not expected to directly affect transcription or to broadly reorganize the differential gene expression profile of the Q6/Q5 patient/control NGN2-iN lines. Accordingly, our transcriptional profiling was not designed to assess the direct impact of EMC10 deficiency on gene expression but rather to serve as an indirect measure of cellular pathways affected by the reduction in EMC10 levels in the patient Q6 line. We aimed to identify genes and related functional pathways differentially expressed between the Q6/Q5 patient/control lines, where these expression differences are either abolished or significantly attenuated in Q6/EMC10^{HET} or Q6/EMC10^{HOM} NGN2-iNs.

Statistical Analysis: We have meticulously reviewed all statistical analyses in the manuscript to ensure their appropriateness and adherence to established practices. For Figure S2, we acknowledge that the statistical details were not fully specified in the figure legend, though they are provided for each miRNA in Supplemental Table S2. In the revised manuscript, we ensured that the statistical methods and corresponding values are clearly indicated for each comparison.

We are confident that the revisions outlined above, along with the point-by-point responses provided below, will significantly strengthen our manuscript and address all the concerns raised by the reviewers. We would like to express our sincere thanks to the reviewers for their valuable feedback and constructive suggestions.

> ***Reviewer #1 (Recommendations For The Authors):***
>
> *My comments here are generally limited to minor comments that reflect possible small additions or edits to the manuscript:*
>
> *(1) Panel 1A is very small. Please consider making that bigger as space permits.*

We have increased the panel size of Figure 1A in the revised manuscript to improve its visibility and clarity.

> *(2) Are you able to identify the dot that represents EMC10 in panel 1C? I understand that EMC10 is represented in Supplementary Figure 4A.*

We appreciate the reviewer's observation. In Figure 1C, the volcano plot depicts differentially expressed miRNAs in the Q5/Q6 neuronal samples, as identified through miRNA-sequencing. Since EMC10, as a protein-coding gene and a downstream target of miRNA dysregulation, is not included in this analysis. However, as the reviewer correctly notes, EMC10 gene expression is represented in the volcano plot in Supplementary Figure 4A, which displays differentially expressed genes identified through bulk RNA-seq analysis of the same neuronal samples. To avoid any confusion, we have clarified the title of Figure 1C to emphasize that it represents miRNA expression changes.

> *(3) With regard to studies using iPSC. Some of the studies are executed across multiple distinct pairs and some are only done in a single pair. Overall, while results are coherent and often complimentary, would it be valuable for the authors to comment on*

> *experiments where studies in multiple pairs seemed particularly important, or others wherein it was less important?*

We thank the reviewer for this insightful question regarding our use of multiple versus single hiPSC pairs. Our investigation began with the Q5/Q6 sibling (dizygotic twin) pair, which shares the most similar genetic background. This minimized the impact of confounding genetic factors and provided a robust foundation for testing our hypothesis that EMC10 upregulation, driven by miRNA dysregulation, is a key consequence of the 22q11.2 deletion in human neurons, thus validating our previous findings from the *Df(16)A*$^{+/-}$ mouse model (Stark et al., 2008; Xu et al., 2013). To ensure the generalizability of our findings, we incorporated additional hiPSC lines from another sibling pair as well as a case/control pair, demonstrating that EMC10 upregulation is a consistent feature of 22q11.2DS. Subsequently, we focused on the well-matched Q5/Q6 pair for detailed morphological, functional, and genetic rescue experiments. This approach allowed us to perform in-depth studies while controlling for potential genetic confounders. By using both multiple and single hiPSC pairs, we balanced the need for generalizable findings with the practical considerations of conducting technically complex and resource-intensive experiments. This strategy enabled us to provide both broad and detailed insights into the mechanisms underlying 22q11.2DS. We have modified the introductory paragraph of the Results section to better highlight this issue.

> *(4) While the majority of the experiments seem sufficiently powered to test the hypothesis in question in the iPSC studies, Figure 2B raises the question if the study replicates here were underpowered, and perhaps the authors might consider mentioning this, although this is a very minor comment.*

We thank the reviewer for raising this point. We acknowledge that the statistical power to detect a significant difference in pre-miR-485 levels in Figure 2B may be limited due to the relatively small sample size and the inherent variability in hiPSC-derived neuronal cultures. However, it is important to emphasize that the functional impact of miRNAs is primarily mediated by their mature transcript forms. Our miRNA-seq data (Supplementary Table 2 and Figure S2) did not show significant alterations in the levels of mature miR-485-5p or miR-485-3p. This finding aligns with the reported expression pattern of miR-485 in hiPSC-derived neurons, where relatively low levels are observed in early neuronal development, with increased expression occurring in older, more mature neurons (Soutschek et al. 2023; https://ethz-ins.org/igNeuronsTimeCourse/ database from the Institute of Neurogenomics, ETH Zurich). This database provides a valuable resource for examining gene expression dynamics during human neuronal differentiation. Given that our hiPSC-derived neurons were analyzed at a relatively early developmental stage (DIV8 for these experiments), it is likely that miR-485 expression had not yet reached levels sufficient to reveal significant differences. While we acknowledge the potential limitation in statistical power for detecting subtle changes in pre-miR-485 levels, the combined evidence suggests that miR-485 may not be a significant contributor to the observed phenotypes at this developmental stage.

A paragraph has been added in the corresponding Results section to address this issue.

> *(5) There are a few situations where the authors could help out the reader a little bit by providing more labels on the figures directly. For example: in Figure 2, there are expression levels, over-expression, and inhibition of miRNA but the X-axis is named with similar labels for the miRNAs in question for each of these distinct experiments. If the authors want to help the reader, they may consider labeling these panels with a descriptive title to reflect the experiment being done or use more descriptive terms in the X-axis panels. Again, this is minor. Similarly, in Figure 5, it might be helpful for the authors to help out the reader again with more labels on the panels, such as in Figures*

> *5B, 5C, and 5D. Would they consider labeling these panels, HPC, PFC, SSC with the brain location as they did in Figure 4?*

We thank the reviewer for these helpful suggestions to improve the clarity of our figures. We have implemented the proposed changes. In Figure 2C-E, we have added specific titles to the panels to clearly distinguish between the different experimental conditions such as miRNA overexpression and inhibition. Similarly, in Figure 5, we labeled panels 5B, 5C, and 5D with the brain regions analyzed (HPC, PFC, SSC) to match the labeling used in Figure 4. We believe these revisions enhance the readability and overall interpretability of the figures, making it easier for readers to follow the experiments and results.

> *(6) Figure 3: There is some overshoot of the data in EMC10 homozygous null, in panel 3E, and also, overshoot of the het in panel 3H. Would there be value in the authors commenting on the potential basis for this in the discussion? Some issues are minor, such as the lack of electrophysiological analysis of circuits in vivo or in ex vivo slices that may further support the proposed rescue.*

The reviewer correctly highlights the observation in Figures 3E and 3H, where the number of branch points in the Q6/EMC10^{HOM} line exceeds wildtype levels and the calcium response in the Q6/EMC10^{HET} and Q6/EMC10^{HOM} lines surpasses that of the control. This overshoot is indeed intriguing and warrants discussion. EMC10 is part of the ER Membrane Complex (EMC), which plays a critical role in the proper folding and localization of various membrane proteins, including neurotransmitter receptors and ion channels such as voltage-gated calcium channels (Chitwood et al., 2018; Shurtleff et al., 2018; Chitwood and Hegde, 2019). In the context of the 22q11.2 deletion, EMC10 dysregulation may disrupt the proper localization of these proteins at the synapse, affecting both dendritic morphology and calcium signaling. The precise basis of this overshoot remains unclear. The overshoot may result from a dosage-sensitive inhibitory effect of Emc10, where both reduced and increased expression alter normal neuronal processes, with excessive responses potentially triggered upon gene restoration by the mutant system's adaptation to dysfunction, leading to altered receptor sensitivity or signaling dynamics. This underscores the critical importance of precise Emc10 expression for proper neuronal development and function, in line with previous findings suggesting that EMC10 plays an auxiliary or modulatory role in EMC function. A short comment on the potential basis for this overshoot has been added in the corresponding Results section of the manuscript. Regardless of the underlying mechanisms, these findings emphasize the importance of precise titration of ASO constructs, rigorous gene dosage controls, and thorough analysis of context-specific responses to ensure both efficacy and safety in clinical applications.

We also agree with the reviewer that electrophysiological studies, particularly in the 22q11.2 deletion mouse model, would provide valuable insights into the impact of EMC10 modulation by ASOs on neuronal activity and circuit function at the in vivo and ex vivo levels. Incorporating such experiments into future studies will allow us to assess synaptic transmission and plasticity, contributing to a more comprehensive understanding of the therapeutic potential of ASO-mediated EMC10 modulation in 22q11.2DS.

> *(7) Did the authors take out the behavior studies further than 9 weeks? Would the authors consider commenting on what they speculate might be the duration of the treatment effect? For both mice and definitely humans.*

We thank the reviewer for raising the important question regarding the duration of the ASO treatment effect, which is crucial for translating our findings into clinically relevant therapies. While behavioral studies beyond 9 weeks were not conducted in this study, our in

vivo experiments and findings from prior publications (detailed below) enable an informed speculative assessment.

We utilized 2'-O-methoxyethyl (2'-MOE) modified ASOs, known for their enhanced binding affinity, nuclease resistance, and increased metabolic stability. In our in vivo post-injection screening of ASOs (Figure S13C), we predicted that Emc10 expression levels return to normal WT levels (~T100%) approximately 26 weeks post-treatment in Emc10^{ASO} (#1466182) treated mice. This prediction is supported by our Emc10 expression profiles across various brain regions, which demonstrate robust repression of Emc10 lasting up to 10 weeks post-administration (Figure 6D-F). While these findings suggest that the treatment effect in our model could extend significantly beyond 10 weeks following a single ASO injection, further empirical validation is required through extended follow-up studies. Encouragingly, long-term effects of 2'-MOE ASOs have been observed in other neurological disorders (Kordasiewicz et al., 2012; Scoles et al., 2017; Finkel et al., 2017; Darras et al., 2019). However, factors such as ASO distribution, target cell turnover, and disease-specific pathophysiology could influence the duration of the effect. To address these uncertainties, we have added a paragraph in the Discussion section emphasizing the need for additional studies, including extended follow-up periods and eventual clinical trials, to determine the specific duration of effect for our Emc10^{ASO} constructs in treating 22q11.2DS.

> ***Reviewer #2 (Recommendations For The Authors):***
>
> *(1) It is acknowledged that the iPSC-derived cells in Figure 1 are no longer progenitors, but differentiation markers for astrocytes and glia are also needed in Figure 1b to establish that equal rates of differentiation have occurred across genotypes.*

We thank the reviewer for raising this important point about ensuring equal rates of differentiation across genotypes. As the reviewer notes, we employed a well-established protocol for directed differentiation of hiPSCs into cortical neurons using a combination of small molecule inhibitors, as previously described by Qi et al. (2017). This protocol has been extensively validated and is known to robustly generate cortical neurons while actively suppressing glial differentiation, as evidenced by the lack of upregulation of glial markers such as GFAP, AQP4, or OLIG2 in the original study. Given the established neuronal specificity of this protocol and our focus on neuronal phenotypes, we prioritized the confirmation of successful neuronal differentiation using the established neuronal markers TUJ1 and TBR1. Therefore, additional markers for astrocytes and glia are not included in this figure, as we did not expect significant glial differentiation under these conditions. A sentence has been added in the corresponding Results section to address this issue.

> *(2) For the RNA-seq experiments outlined in Figures 3J and K, a more comprehensive analysis is needed of the genes disrupted in the parental Q6 line relative to the het and homo lines. What percent are rescued, unaffected, vs uniquely disrupted?*

Reduction in EMC10 levels is not expected to directly affect transcription or broadly reorganize the gene expression profile of the Q6/Q5 NGN2-iN lines. Our transcriptional profiling was not designed to assess the direct impact of EMC10 deficiency on gene expression but rather to measure the cellular pathways affected by reduced EMC10 in the patient Q6 line. We identified genes differentially expressed between the Q6 (patient) and Q5 (control) lines, whose expression differences were either abolished or significantly attenuated ("rescued") in the Q6/EMC10^{HET} or Q6/EMC10^{HOM} lines. In the Q6/EMC10^{HET} line, 237 DEGs (6%) were rescued, while in the Q6/EMC10^{HOM} line, 382 DEGs (11%) were rescued. Importantly, further analysis revealed 103 shared rescued DEGs in these lines, which was statistically significant (enrichment factor = 1.7; $p < 0.0001$, based on a hypergeometric test). We added a new figure panel (Figure 3L) to visualize the significant overlap of rescued DEGs from the Q6/EMC10^{HET} and Q6/EMC10^{HOM} lines. This overlap suggests these genes play a

critical role in biological pathways impacted by EMC10 levels, particularly in nervous system development, as indicated by our functional annotation analysis. We also performed protein-protein interaction (PPI) network analysis to explore the functional relationships among these 103 shared DEGs (Figure S8). Future studies will further investigate these gene sets to gain deeper insights into the molecular mechanisms underlying 22q11.2DS and the role of EMC10.

> *(3) The authors claim that 50% EMC10 loss in adult mice is safe and should be toned down. EMC10 knockout mice have motor, anxiety, and social phenotypes. It would be unique amongst highly dosage-sensitive genes (MeCP2, CDKL5, TCF4, FMR1, etc.) for there to only be a neurodevelopmental component. In all those cases, and others, the effects of over and under-expression are reversible into adulthood. Establishing the range in adults is critical to establishing therapeutic utility. Absent a detailed examination of non-cognitive phenotypes, this claim cannot be made.*

The reviewer raises an important point about the potential effects of EMC10 reduction in adult mice and the need to establish a safe therapeutic window by evaluating both cognitive and non-cognitive phenotypes. We agree that such a comprehensive evaluation is critical for assessing the safety and translational potential of Emc10-targeting therapies. While the International Mouse Genotyping Consortium reported motor and anxiety phenotypes in homozygous Emc10 knockout mice, these data are unpublished and based on a relatively small number of animals. Furthermore, in our previous work (Diamantopoulou et al., 2017), we demonstrated that complete Emc10 loss does not impair cognition or social behavior, as assessed by prepulse inhibition (PPI), working memory (WM), and social memory (SM) assays (see Figure 3A-D; Diamantopoulou et al., 2017). Additionally, heterozygous Emc10 mice, which exhibit a ~50% reduction in Emc10 expression similar to that achieved with our ASO treatment, showed no evidence of motor deficits or anxiety-like behavior. Specifically, *Emc10*$^{+/-}$ mice displayed locomotor activity comparable to WT mice in the open field (OF) test (Figure S4A, Diamantopoulou et al., 2017). Moreover, genetic normalization of Emc10 expression in *Df(16)A*$^{+/-}$ mice demonstrated no signs of anxiety-like behavior, as assessed by the OF test (Figure S4A) and elevated plus maze (EPM) (Figure S4B; Diamantopoulou et al., 2017). To further support these findings, we have added new data to the current manuscript (see Figure S10J) showing that TAM treatment-mediated restoration of Emc10 levels in the brain of adult *Df(16)A*$^{+/-}$ mice did not affect the time that mutant mice spent in the center area of the OF (Fig. S10J), suggesting that Emc10 reduction does not influence anxiety-related behavior. These results suggest that a 50% reduction in EMC10 expression is unlikely to result in motor or anxiety-like phenotypes in adult mice. Finally, as noted in the manuscript, in addition to prior findings from animal models, a substantial number of relatively rare LoF variants or potentially damaging missense variants have been identified in the human EMC10 gene among likely healthy individuals in gnomAD, a database largely devoid of individuals known to be affected by severe neurodevelopmental disorders (NDDs).

Nevertheless, the Discussion has been revised to underscore the importance of establishing a more detailed safety profile, including non-cognitive phenotypes, to fully validate the therapeutic potential of Emc10-targeting approaches. It also highlights the need for future studies to expand on these evaluations, addressing this critical aspect and laying a stronger foundation for advancing these findings into clinical drug development

> *(4) Supplemental Figure 10: The protein validation of Emc10 knockout following tamoxifen injection needs to be validated in all brain regions, not just the PFC. This is particularly important as the rest of the paper focuses on HPC-mediated phenotypes.*

First, we want to emphasize that we conducted both qRT-PCR and WB assays on the same animal cohort, specifically examining the left and right hippocampus following ASO injection

(see Figure S11C and D). This approach is crucial, given the central role of hippocampus in the phenotypes investigated in our ASO-mediated Emc10 knockdown experiments.

The reviewer raises an important point regarding the validation of EMC10 reduction at the protein level across all relevant brain regions using the Emc10 conditional knockout strain. We agree that such validation would ideally confirm the efficacy of our tamoxifen-induced knockout model comprehensively. However, we hope the reviewer appreciates that obtaining sufficient high-quality protein for WB analysis from smaller brain regions like the hippocampus poses a significant technical challenge. This difficulty is further compounded by the need to reserve the same samples for qRT-PCR to ensure consistency between mRNA and protein measurements. Importantly, our data from ASO-mediated Emc10 knockdown experiments (Figures S11C-D) demonstrate a clear and consistent correlation between reductions in Emc10 mRNA and protein levels in both the left and right hippocampus. Furthermore, in our constitutive Emc10-knockout mouse model (Diamantopoulou et al., 2017; see Figure S1A-B), we observed a strong agreement between mRNA and protein levels, supporting the reliability of mRNA data as a proxy for EMC10 protein levels in our experiments. Importantly, in all instances where we performed parallel protein and RNA measurements in human cell lines, there was excellent concordance between the datasets. Thus, while we acknowledge the limitations of relying primarily on mRNA data, we are confident that the Emc10 mRNA expression data in Figure S10 accurately reflect protein-level changes across brain regions in our conditional knockout model. To address this concern more fully in the future, we are working to refine antibody detection and optimize our protein extraction protocols to enable more routine and precise protein-level validation across smaller brain regions. We appreciate the reviewer's feedback and will continue to refine our methodologies to strengthen the robustness of our findings.

> *(5) Figure 3: 1 way ANOVA would be more appropriate to analyze the data in B-G than t-tests.*

We appreciate the suggestion of the reviewer. As mentioned above, we carefully selected statistical tests appropriate for each analysis. For Figure 3B-G, we chose to use pairwise t-tests to address specific hypotheses regarding the disease phenotype and rescue effects. This approach is consistent with prior experimental studies in the field, including our own (e.g., Xu et al., 2013; Figure 7H-I). Importantly, most of our t-tests yielded highly significant results ($p < 0.001$ or $p < 0.01$), reinforcing the robustness of our findings.

> *(6) Figure 5-6: Protein data is needed to complement the mRNA knockdown data.*

We agree with the reviewer on the importance of protein-level validation to complement the mRNA knockdown data. As mentioned in our response to Reviewer's Comment (4), in all instances where we performed parallel protein and RNA measurements, either in mouse brain or human cell lines, we observed excellent concordance between the datasets. This supports the reliability of our mRNA data as a proxy for protein changes. Nevertheless, we acknowledge the value of including protein validation in future experiments and will consider incorporating it to further strengthen our findings.

> *(7) The use of additional phenotypic measures is applauded in Figure 6, however, to appropriately interpret the data more is needed. Shao et al 2021 (Figure S9) show data from the International Mouse Genotyping Consortium claiming EMC10 KO mice have gait, activity, and anxiety phenotypes. All of these parameters could impact the SM assay and the y-maze assay. Changes in SM interaction time could be linked to anxiety or motor impairments, but interpreted as cognitive deficits because these symptoms were not assessed. At a minimum, discussion is needed about this limitation, as well as the inclusion of distance explored in the SM and Y-maze assays.*

We thank the reviewer for their insightful comment regarding the potential influence of locomotor, gait, or anxiety phenotypes on the observed deficits in the SM and Y-maze assays. The behavioral phenotypes reported for Emc10 knockout mice by the International Mouse Genotyping Consortium (https://www.mousephenotype.org/data/genes/MGI:1916933) were limited to homozygous female mice and based on a small sample size (4–6 females) compared to a larger WT control group. Moreover, these data are unpublished and thus challenging to evaluate fully. Importantly, no abnormal behaviors were reported for Emc10 heterozygous knockout mice in these datasets. Additionally, the claim by Shao et al. (2021) regarding cognitive impairments in Emc10 knockout mice based on our previous work (Diamantopoulou et al., 2017) is inaccurate.

Our analysis of both the constitutive Emc10 knockout model (Diamantopoulou et al., 2017) and the current conditional Emc10 heterozygous knockout model consistently demonstrates that Emc10 reduction does not affect locomotor activity or anxiety-like behavior. In our earlier characterization of constitutive heterozygous Emc10 knockout mice (*Emc10*$^{+/-}$), we observed no signs of anxiety-like behavior or motor impairments in OF assays (see Figure 2A-B and Figure S4A, Diamantopoulou et al., 2017). Similarly, results from *Df(16)A*$^{+/-}$ mice with genetically normalized Emc10 expression [*Df(16)A*$^{+/-}$; *Emc10*$^{+/-}$] also showed no indications of anxiety-like behavior or locomotor changes in the OF and EPM assays (see Figure S4A-B, Diamantopoulou et al., 2017). Consistent with these findings, our current data from *Df(16)A*$^{+/-}$ mice with conditional Emc10 reduction in the brain show no significant differences in locomotor activity and anxiety-related measures as assessed by OF assays (Figure S10J). Furthermore, total arm entries in Y-maze assays conducted in *Df(16)A*$^{+/-}$ mice treated with Emc10 ASOs were comparable to controls (Figures S14C and G-H), providing additional support for the conclusion that locomotor activity remains unaffected in these models.

We further appreciate the reviewer's suggestion that changes in social interaction time during the SM assay could be influenced by anxiety or motor impairments. However, we consider this scenario unlikely in our model. Interaction times during the first trial of the SM assay, which measures general social interest, are comparable between *Df(16)A*$^{+/-}$ mice with reduced Emc10 expression (either genetically or through ASO treatment) and WT controls (see Figures 4E, 5E, and S10G). These findings indicate that our mouse models do not exhibit inherent difficulties in initiating social interaction, as might be expected if motor impairments or heightened anxiety were present. Reduced social interaction is commonly used as a behavioral marker for anxiety in rodent studies (reviewed by Bailey and Crawley, Anxiety-Related Behaviors in Mice, 2009). "Anxious" mice typically exhibit decreased social interaction, spending less time engaging with other mice compared to non-anxious counterparts. However, the specific deficit we observe in the second trial of the SM assay—when mice are reintroduced to a familiar juvenile—is indicative of impaired social recognition memory, as previously documented for *Df(16)A*$^{+/-}$ mice (Piskorowski et al., 2016; Donegan et al., 2020). This deficit is distinct from the general social avoidance typically associated with heightened anxiety.

Based on our comprehensive assessment of locomotor activity, anxiety-related behaviors, and social interaction, we conclude that the observed rescue of social memory and spatial memory deficits in mice with reduced Emc10 expression is most likely due to improved cognitive function rather than alterations in motor or anxiety-related domains.

> *(8) For ASO optimization experiments, it is not sufficient to claim robust uptake. A quantitative measure is needed using the PO antibody showing what percentage of cells were positive for the ASO. Since the contention is that only Emc10 in excitatory neurons is important, it would be helpful if this also included a breakdown of ASO uptake in excitatory and inhibitory neurons and astrocytes.*

We thank the reviewer for highlighting the importance of quantifying ASO uptake and assessing cell-type specificity. To address this, we have added new data to the panel, as shown in the high-magnification images in Figure S14A. These images provide evidence that a large majority of NeuN-positive neurons exhibit a strong ASO signal. Specifically, we observed widespread ASO uptake (green) that extensively colocalized with the neuronal marker NeuN (red) in both the hippocampus and prefrontal cortex. Quantitative analysis of this overlap indicates that over 97% of NeuN-positive neurons were ASO-positive, demonstrating efficient neuronal uptake. This robust neuronal uptake aligns with the significant normalization of Emc10 levels and the behavioral improvements observed in ASO-treated *Df(16)A*$^{+/-}$ mice, further supporting the functional efficacy of our approach in modulating Emc10 expression within the relevant neuronal populations. Overall, the observed ASO uptake in neurons, as demonstrated by IHC, combined with RNA assays and the behavioral improvements in treated mice, strongly supports the efficacy of our approach in targeting Emc10 expression in the intended neuronal populations.

> *(9) An interpretation is needed in Figure S3 as to why ~50% of the pathways increased are also present on the decreased list. Ie. G1/transition, viral reproductive process, pos regulator of cell stress, etc. 4/10 GO terms are present in both increased and decreased groups in A and 7/10 in B.*

We thank the reviewer for pointing out the overlap between pathways enriched in both the upregulated and downregulated miRNA groups in Figure S3. This overlap likely reflects the complex nature of miRNA regulation, where individual miRNAs can target multiple genes within a pathway, and single genes can be regulated by multiple miRNAs, sometimes with opposing effects (reviewed in Bartel, 2009; Bartel, 2018). For example, in the “G1/S transition” pathway, upregulated miRNAs such as miR-92a-3p, miR-92b-3p, and miR-34a-5p may promote the transition by targeting cell cycle regulators like FBXW7, CDKN1C, and CDK6 (Zhou et al., 2015; Zhao et al., 2021; Oda et al., 2024). Conversely, downregulated miRNAs such as miR-143-3p and miR-200b are known to suppress the transition by targeting genes such as HK2 and GATA-4 (Zhou et al., 2015; Yao et al., 2013). Our analysis identified overlapping predicted target genes for both upregulated and downregulated miRNAs, supporting the notion that many genes are subject to complex regulation by multiple miRNAs with potentially synergistic or antagonistic effects. Thus, the enrichment of certain GO terms in both groups likely reflects this intricate interplay of miRNA-mediated gene regulation. Future investigations focusing on specific miRNA-target interactions within these pathways will be critical to fully elucidate the underlying mechanisms and better understand the functional consequences of these opposing regulatory effects.

> *Minor Concerns:*
>
> *(1) Define SM before using it.*

We have defined the SM assay in the main text upon its first mention, where we describe the assay and its relevance to cognitive function (see page 11 of the revised manuscript).

> *(2) Statistics have been run in Figure S2, but not presented. The text only states that the differences between groups are significant. Please add in.*

We have revised the legend of Figure S2 to include the specific statistical test used (students t-tests) and the corresponding p-values.

> *(3) The switch from ASO1 to ASO2 between Figures 5 and 6 needs more discussion. Why were new ASOs generated when ASO1 worked?*

We thank the reviewer for their question regarding the transition from Emc10^{ASO1} to Emc10^{ASO2} between Figure 4 and Figures 5-6. Emc10^{ASO1} served as our initial proof-of-concept ASO construct, successfully demonstrating the feasibility of inhibiting Emc10 mRNA expression and providing evidence for behavioral rescue in our mouse model. As outlined in the manuscript, Emc10^{ASO2} targets a different region of the Emc10 transcript (intron 1, Figure 5A) compared to Emc10^{ASO1} (intron 2, Figure 4A). This distinction provides an additional layer of validation for our targeting strategy and ensures specificity in modulating *Emc10* expression. In addition, Emc10^{ASO1} exhibited limited distribution in the brain, primarily targeting the hippocampus with weaker inhibition of Emc10 in other regions such as the cortex (Figure 4C, right panel). Emc10^{ASO2} overcame this limitation and achieve broader brain distribution, as demonstrated by the qRT-PCR data in Figure 5C. Given that 22q11.2DS can affect multiple brain regions and cognitive domains beyond the hippocampus, achieving broader distribution of the ASO is critical for a more comprehensive assessment of therapeutic potential.

> *(4) Page 3: Define "LoF"*

We have defined Loss-of-Function (LoF) in the main text where it is first mentioned in the Introduction, where we discuss the potential of using LoF mutations to devise therapeutic interventions (see page 3 of the revised manuscript).

References

Bailey and Crawley, Anxiety-Related Behaviors in Mice, In: Methods of Behavior Analysis in Neuroscience. 2nd edition. Boca Raton (FL): CRC Press/Taylor & Francis; Chapter 5, (2009).

Bartel, MicroRNAs: target recognition and regulatory functions, Cell 136(2):215-33, (2009).

Bartel, Metazoan MicroRNAs, Cell, 173(1):20-51, (2018).

Chitwood et al., EMC Is Required to Initiate Accurate Membrane Protein Topogenesis, Cell 175, 1507-1519 e1516, (2018).

Chitwood and Hegde, The Role of EMC during Membrane Protein Biogenesis, Trends Cell Biol. (5):371-384, (2019).

Darras et al., Nusinersen in later-onset spinal muscular atrophy: Long-term results from the phase 1/2 studies, Neurology 92(21), (2019).

Diamantopoulou et al., Loss-of-function mutation in Mirta22/Emc10 rescues specific schizophrenia-related phenotypes in a mouse model of the 22q11.2 deletion, Proc Natl Acad Sci U S A 114, E6127-E6136, (2017).

Donegan et al., Coding of social novelty in the hippocampal CA2 region and its disruption and rescue in a 22q11.2 microdeletion mouse model, Nat Neurosci 23, 1365-1375, (2020).

Finkel et al., Nusinersen versus Sham Control in Infantile-Onset Spinal Muscular Atrophy, N Engl J Med 377(18):1723-1732, (2017).

Kordasiewicz et al., Sustained therapeutic reversal of Huntington's disease by transient repression of huntingtin synthesis, Neuron 74(6):1031-44, (2012).

Oda et al., MicroRNA-34a-5p: A pivotal therapeutic target in gallbladder cancer, Mol Ther Oncol, 32(1):200765, (2024).

Piskorowski et al., Age-Dependent Specific Changes in Area CA2 of the Hippocampus and Social Memory Deficit in a Mouse Model of the 22q11.2 Deletion Syndrome. Neuron 89, 163-

176, (2016).

Qi et al., Combined small-molecule inhibition accelerates the derivation of functional cortical neurons from human pluripotent stem cells. Nat Biotechnol 35, 154-163, (2017).

Scoles et al., Antisense oligonucleotide therapy for spinocerebellar ataxia type 2, Nature 44(7650):362-366, (2017).

Shao et al., A recurrent, homozygous EMC10 frameshift variant is associated with a syndrome of developmental delay with variable seizures and dysmorphic features, Genet Med 23, 1158-1162, (2021).

Shurtleff et al., The ER membrane protein complex interacts cotranslationally to enable biogenesis of multipass membrane proteins, Elife 7, (2018).

Soutschek et al., A human-specific microRNA controls the timing of excitatory synaptogenesis, bioRxiv, (2023).

Stark et al., Altered brain microRNA biogenesis contributes to phenotypic deficits in a 22q11-deletion mouse model. Nat Genet 40, 751-760, (2008).

Xu et al., Derepression of a neuronal inhibitor due to miRNA dysregulation in a schizophrenia-related microdeletion, Cell 152, 262-275, (2013).

Yao et al., miR-200b targets GATA-4 during cell growth and differentiation, RNA Biol.10(4):465-8, (2013).

Zhao et al., miR-92b-3p Regulates Cell Cycle and Apoptosis by Targeting CDKN1C, Thereby Affecting the Sensitivity of Colorectal Cancer Cells to Chemotherapeutic Drugs, Cancers 2;13(13):3323, (2021).

Zhou et al., miR-92a is upregulated in cervical cancer and promotes cell proliferation and invasion by targeting FBXW7, Biochem Biophys Res Commun 458(1):63-9, (2015).

Zhou et al., MicroRNA-143 acts as a tumor suppressor by targeting hexokinase 2 in human prostate cancer, Am J Cancer Res. 5(6):2056-6 (2015).

https://doi.org/10.7554/eLife.103328.2.sa0